5-2017

Diffusion-weighted magnetic resonance imaging in diagnosing graft dysfunction : a non-invasive alternative to renal biopsy.

Elizabeth Marie Hollis
University of Louisville

DIFFUSION-WEIGHTED MAGNETIC RESONANCE IMAGING IN DIAGNOSING GRAFT DYSFUCNTION: A NON-INVASIVE ALTERNATIVE TO RENAL BIOPSY

By

Elizabeth Marie Hollis

B.A., Hanover College, 2014

A Thesis

Submitted to the Faculty of the

School of Medicine of the University of Louisville

in partial Fulfillment of the requirements for the Degree of

Master of Science

in Pharmacology/Toxicology

Department of Pharmacology and Toxicology

University of Louisville

Louisville, Kentucky

May 2017

DIFFUSION-WEIGHTED MAGNETIC RESONANCE IMAGING IN DIAGNOSING GRAFT DYSFUCNTION: A NON-INVASIVE ALTERNATIVE TO RENAL BIOPSY

By

Elizabeth Marie Hollis

B.A., Hanover College, 2014

A Thesis Approved on

April 6, 2017

By the following Thesis Committee:

_____

Ayman El-Baz, Ph.D., Thesis Director

_____

Michael Merchant, Ph.D.

_____

LaCreis Kidd, Ph.D.

DEDICATION

This thesis is dedicated to my parents

Mr. Thomas Charles Hollis

And

Mrs. Sheila McAlpin Hollis

My sister

Ms. Sarah Ruth Hollis

My Pets

Mr. Demon Dog Hollis

Ms. Noel Fuzz-Bucket “Twitster-Twit” Pigmy-Puff Hobbit Hollis

Mr. Bohdi “Blohdie” Fat Dog III Hollis

Mr. Killer Spuds Mackenzie Hollis

Mrs. Blimp Stroke Kitty Hollis

And

Ms. Pumpkin Hollis

My best friend

Mr. Ramchand JN M.S.

And all my friends and family who without their love and support this would not have been possible.

In Memory of

Dr. Walter Herbert “Doc” Hollis M.D.

1921-2017

ACKNOWLEDGMENTS

I would like to express my deepest gratitude to my mentor Dr. Ayman El-Baz, for his patience and guidance. I would also like to thank the rest of my committee members, Dr. Merchant and Dr. Kidd, for their assistance and comments during this process. Thanks are given to all the co-authors including but not limited to; Mr. Andy Switala, Mohamed Shehata, M.S., and Fahmi Khalifa, Ph.D., who I collaborated with on co-authoring peer-reviewed publications. I am especially grateful for all of the Nephrologist at the Veterans' Affair Hospital in Louisville, Kentucky, for letting me shadow to gain a better understanding on what patients with kidney disorders go through. Additional thanks should be given to all the patients that were included in these studies, without them this would not have been possible. Finally, I would like to thank my friends and family who have supported me through this whole process and I know that they will support me in my next step in life.

ABSTRACT

DIFFUSION-WEIGHTED MAGNETIC RESONANCE IMAGING IN DIGNOSING GRAFT DYSFUCNTION: A NON-INVASIVE ALTERNITAVE TO RENAL BIOPSIES

Elizabeth Marie Hollis

April 6, 2017

The thesis is divided into three parts. The first part focuses on background information including how the kidney functions, diseases, and available kidney disease treatment strategies. In addition, the thesis provides information on imaging instruments and how they can be used to diagnose renal graft dysfunction. The second part focuses on elucidating the parameters linked with highly accurate diagnosis of rejection. Four parameters categories were tested: clinical biomarkers alone, individual mean apparent diffusion coefficient (ADC) at 11-different b- values, mean ADCs of certain groups of b-value, and fusion of clinical biomarkers and all b-values. The most accurate model was found to be when the b-value of b=100 s/mm^2 and b=700 s/mm^2 were fused. The third part of this thesis focuses on a study that uses Diffusion-Weighted MRI to diagnose and differentiate two types of renal rejection. The system was found to correctly differentiate the two types of rejection with a 98% accuracy. The last part of this thesis concludes the work that has been done and states the possible trends and future avenues.

TABLE OF CONTENTS

LIST OF TABLES

TABLE PAGE

LIST OF FIGURES

FIGURE PAGE

CHAPTER I

TOWARDS NON-INVASIVE DIAGNOSTIC TECHNIQUES FOR EARLY DETECTION OF ACUTE RENAL TRANSPLANT REJECTION: A REVIEW

A. Overview

The kidney is an essential yet complicated filtering organ of the body. When the kidney reaches stage 5 chronic kidney disease, end stage renal failure, the preeminent therapy is renal transplantation. Although renal transplants are the superior treatment, there is a lack of kidney donors which has proven challenging. Therefore, all efforts should be employed to prolong the survival rate of the transplanted kidney. However, renal graft dysfunction (i.e., acute renal rejection) is one of the serious barriers to long term kidney transplant survival. Currently, graft dysfunction's gold standard of diagnosis is renal biopsy. Although renal biopsy is helpful, it is not preferred due to its invasive nature, high morbidity rates, and high economic cost. Therefore, noninvasive imaging techniques have become the subject of extensive research and intense interest, giving strong promise to replace, or at least to decrease, biopsy usage in diagnosing graft dysfunction. This survey will discuss not only the current diagnosis and treatment of graft dysfunction but also the state-of -the-art imaging techniques in detecting acute renal transplant rejection.

B. Introduction

The kidney is a very important organ. It is the main filtration organ in the human body, keeping the nutrients that the body needs in and expelling the waste that can become toxic. Maintaining the health of this organ is very important. There are diseases that can cause the kidney to decrease in function such as diabetes, hypertension, glomerular disease, and polycystic kidney disease [1]. These can result in a gradual loss of kidney function leading to waste build up in the body and cause the patient to develop chronic kidney disease (CKD).

Chronic kidney disease affects about 26 million people with 17,000 transplants being performed each year in the U.S. [2, 3]. Although transplants have greatly improved the outcome of patients diagnosed with stage 5 CKD, complications can still arise. One of the main concerns is graft dysfunction. Routine post-transplantation clinical evaluation of kidney function is of immense importance to prevent the graft loss. The diagnostic technique currently recommended by the National Kidney Foundation (NKF) to measure overall kidney function is estimated Glomerular Filtration Rate (eGFR), which is based on measuring the serum creatinine level. However, this test has low sensitivity and is a late marker for renal graft dysfunction. Unfortunately, a significant change in serum creatinine level is detectable only after the loss of 60% of renal function [4]. The needle biopsy is the current gold standard for diagnosing different types of renal dysfunction. [4]. However, needle biopsies are difficult to perform, costly, and time-consuming. More over renal biopsy can lead to complications such as infections, bleeding, and, at times, death. With Fthe evolution of computer aided diagnostic systems, we hope to diagnose different types of graft dysfunction, saving time and money. Thus, there is a great need for new

noninvasive techniques with the capability to provide accurate diagnosis of kidney dysfunction is of countless clinical significance.

The main purpose of this chapter is to present an overview of current clinical techniques for renal transplant function evaluation as well as an examination of new ways to improve the detection of graft dysfunction using image-based technology.

The rest of this chapter is organized as follows. “Kidney Anatomy and Function,” provides a brief overview of the treatment options for people who develop stage 5 CKD, concentrating on transplantation as a definitive therapy. “Renal Problems/ Disease/Symptoms,” focuses on follow-up post transplantation care, which includes possible complications that could arise with a concentration on graft dysfunction. “Treatment,” concentrates on tests used to detect graft dysfunctions including the traditional methods such as blood, urine, and renal biopsy. This is followed by the image based techniques such as magnetic resonance imaging (MRI), and ultrasound.

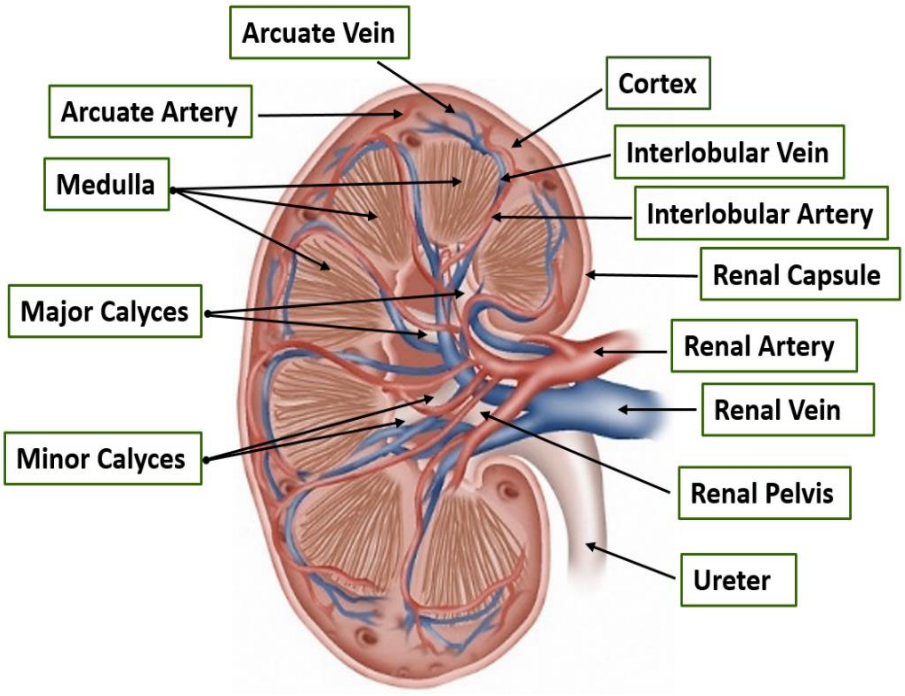

Figure 1. Coronal cross-section of a normal kidney with labeled anatomy.

C. Kidney Anatomy and Function

As stated before, kidneys are the main filtration system in the body. Kidneys are able to keep needed nutrients like salts, sugar, and protein in. Conversely the kidney also expels excess nutrients, water, and waste such as urea, and ammonia out of the body. Kidneys help the body to maintain homeostasis as well by regulating blood pH, blood pressure, and osmolality. Osmolality is the amount of particles of solutes that are dissociated in a solvent [5]. Each kidney is shaped like a bean and is about the size of a fist [6] and weighs about 150 g [7]. They are located in the lower back below the rib cage. As shown in Figure 1, the kidney is composed of an outer "shell" (renal cortex), an inner layer (renal medulla), and a hollow area where the urine is collected, (renal pelvis) [7] . Inside the cortex and medulla are the filtration units known as the nephrons (see Figure. 2),

which are then made up of smaller subunits such as the glomerulus, vasa recta, and loop of Henle [7]. Since the kidneys filter the blood it must be connected to veins and arteries. The kidneys are connected to the renal artery and vein which is connected to the iliac artery and vein, respectively. That is the general overview of the kidney anatomy, now this paper will trace the filtration pathway of the blood. The blood enters the kidney by way of the renal artery. Once there, the blood moves to the nephrons of the cortex where the blood then enters the afferent arteriole which allows the blood to move through in the glomerulus. The glomerulus is then able to filter out waste by leveraging blood pressure. Waste is filtered into the Bowman's capsule, to the lumen of the proximal tubule, then to the Loop of Henle and thin segment, which can be found in the medulla. At these places in the nephron more selective reabsorption can be done. From this, waste moves to the distal tubule and then collecting tubule finally ends up in the renal pelvis. The waste that ends up in the renal pelvis will then move out through the ureter to the bladder and then out of the body by way of the urethra. The clean blood exits the glomerulus by way of the efferent arteriole. Once blood reaches the efferent arteriole additional filtration takes place in the Peritubular capillaries where the blood could also move down the Vasa recta in the medulla, nutrients that were filtered out by the loop of Henle and thin segment can be reabsorbed there. The blood then exits through the venules and then through the arcuate veins, finally leaves the kidney through the renal vein. The clean blood then moves back to the heart [7]. As one can see this organ is very complex and with this complexity many problems can arise. In the next section this article will discuss what can go wrong as well risk associated with increased changes of developing these complications.

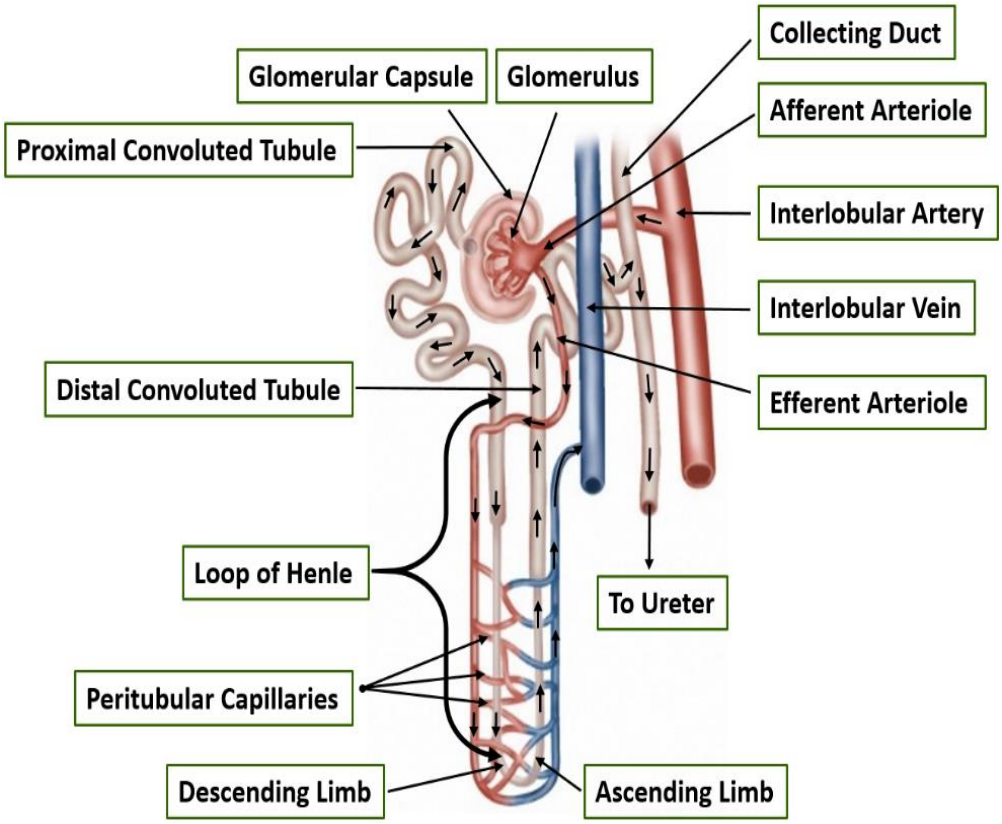

Figure 2. A nephron structure with labeled anatomy and pathway of filtration.

D. Renal Problems/ Disease/ Symptoms

The renal system is a very complex system, in which various complications and diseases can arise. There are multiple conditions and/or diseases that can arise in the kidney such as kidney stones, injury, infections, and cancer. The focus of this chapter will be on CKD, the 9th leading cause of death in America [8]. CKD is a gradual loss of function of the kidney, where the nephrons become compromised [2]. To date, 26 million people in the U.S. are living with CKD [2]. The risk of developing CKD could be increased due to a few different factors such as; pre-existing conditions, diseases, age, race, lifestyles and family history. Conditions that increase the likelihood of developing CKD include diabetes, high blood pressure, heart disease, and high cholesterol [9]. People with the following diseases are at increased risk of CKD, they include; Human Immunodeficiency Virus

(HIV), Hepatitis C, Metabolic syndrome, cancer, and sickle cell trait [10]. When an individual is 65 years or older they are more at risk. African Americans tend to also have a greater risk compared to the rest of the population [9] Lifestyles that increase risk include people that are obese [11] or people that smoke [9] or exposed to second hand smoke. In terms of family history of CKD, that if a patient has a parent or family member with CKD they have a greater chance of developing CKD [9].

People with the aforementioned risk factors should inform their doctors if they experience CKD-related symptoms, summarized below become present. In early stage CKD the patient may be asymptomatic but as the disease progresses symptoms may arise. Symptoms can include change in urination whether it changes in frequency, feeling, color, or texture. The urine can also start to contain blood [12]. Apart from the change in urination symptoms such as limb swelling, iron build up that can cause nose bleeds and bad breath [12]. As the disease progresses infection like symptoms can arise [13]. CKD can also have an effect not only on the body but also on mental state and activity level. These symptoms can include fatigue, generalized weakness, decreased libido, change in memory [13], and compromised mental function [12]. Other rare yet, more serious, symptoms include rash, generalized pain, chest pain, and shortness of breath [12-15]. Patients with any of these last symptoms should seek immediate medical attention. Every patient is different and there is no set relationship between symptoms and stage of kidney disease [13]. If left untreated symptoms should worsen and lead to stage 5 CKD/ kidney failure. If the patient remains untreated in stage 5 CKD, toxins will build up in the body and cause death. To prevent this from happening the patient should be treated with dialysis or transplantation. The next

section will inspect treatment options for patients at stage 5 CKD, concentrating mostly on transplantation.

E. Treatment

Luckily, treatments for patients with stage 5 renal failure include blood dialysis or renal transplantation. Blood dialysis is when one's blood is filtered of waste or excess water, either with use of a machine outside the body (hemodialysis) or chemically inside the body (peritoneal dialysis) [16]. Although dialysis is a helpful treatment, kidney transplantation constitutes a longer term treatment Kidney translation involves the surgical insertion of a donor's kidney into the CKD patient. The new kidney should improve filtration for the patient. Since transplantation is the definitive therapy for End-Stage Renal Disease (ESRD), the following describes in more details the kidney transplantation procedure and associated complications and diseases.

1. Transplantation

Renal transplantation does not mean nephrectomy (i.e. removal of the malfunctioned kidney) is performed on the patient with CKD. The CKD patient usually keeps both of the kidneys, unless those kidneys are causing pain or other complications [17]. This means the patient will have three kidneys after the procedure. The donated kidney also has its own ureter, renal artery, and vein intact. The donated kidney is placed distal (below) the native kidneys with the donated ureter connecting to the bladder, and the renal artery and vein connecting to the iliac artery and vein of the patient, respectively [18]. Figure 3 demonstrates the entire anatomy of a patient’s renal system after transplantation.

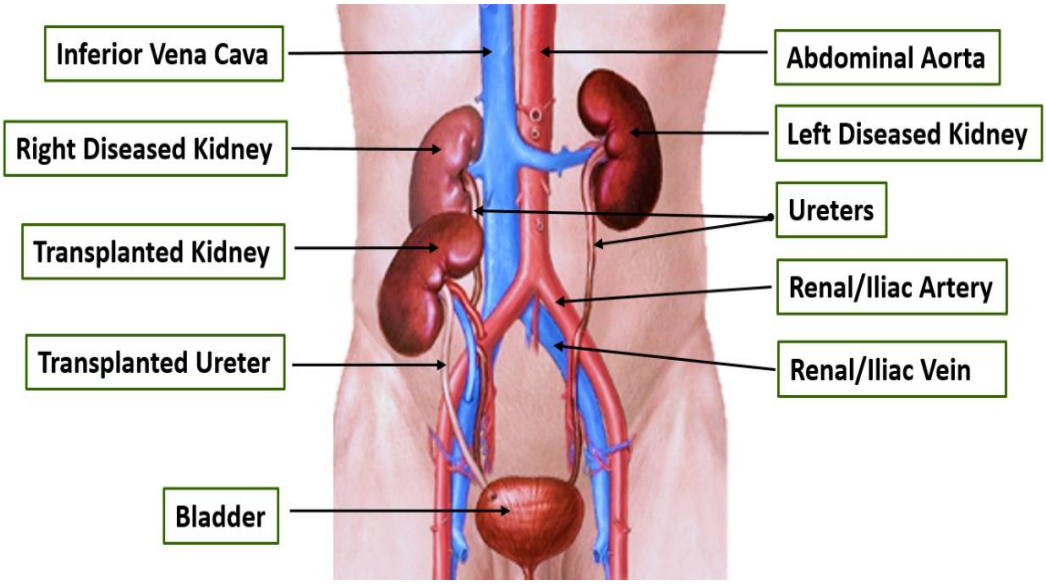

Figure 3. Anatomy of renal system of a patient after kidney transplant.

This procedure seems fairly simple in concept. However, the process to find that donor can be fairly complicated medically, logistically, and legally. There are two different types of renal transplantation donors namely cadaver and living donors. Only one-third of the transplantations are from living donors; whereas the remaining two-thirds are from cadaver donors [19]. The type of donor is often the first decision the physician and the CKD patient must make. Often a more desirable choice would be to have a living donor give one of their kidneys. However, this is not without its complications. The donor must meet all criteria such as being HLA (+ or -) and/or ABO compatible, in good physical health, and in no way coerced against their will to donate [19, 20]. This means the donors can back out at any time. Therefore, even if there is a willing live donor the physician may persuade the patient to get on the United Network of Organ Sharing (UNOS) [21]. Based on where the patient is on the list determines if and when they will receive a donated kidney. The donated kidneys from this list are from cadaver donors. In order for the

cadaver's kidney to be viable the kidney must be functioning before death and undamaged. Also, the time and location of death may play a part since the kidney must not decompose before the kidney can be donated [19]. In the U.S., the living donors must be willing to donate their kidney and cadaver donors must also make it clear that they are willing to be a donor after death.

With all of these criteria, it is clear why there are still over 100,800 people wating for a kidney, despite 17,000 kidney transplants are performed annually in the United States. With this in mind, it is very important that the transplanted kidney is kept viable as long as possible to avoid nephrectomy and repeat transplantation [3]. In the following section, we shall overview what happens during post-transplantation care, which should improve the organ viability following surgery. This includes follow up procedures and the complications that arise for transplant patients.

F. Post-Transplant Follow-Ups and Complications

Just as with any medical procedure, complications can arise, such as infection and bleeding so one must remain under the constant care of one's physician. They must continue follow ups to ensure that the new kidney is functioning and that new complications do not arise. To prevent new complications from arising, the patient should follow the instructions of their physician by taking their anti-rejection medications and visiting their physician as directed [22]. The frequency at which a patient has to visit their physician will decrease as time after transplantation increases. Once the patient has reached 210 days post-operatively, they should be seeing their physician monthly or if abnormalities arise [23]. During those clinical visits, various tests such as examining the patient's weight, blood pressure, and temperature will be done to assess both the overall

health of the patient and the health of the kidney. The urine and blood lab test will be discussed later in this article. If these tests appear abnormal, the physician may order a renal biopsy and/or scans [24]; both will be discussed in greater detail later in the article. For now, this article will concentrate on the complications that can arise during these tests, specifically those complications that are associated with renal transplants. This section will take a look at those types and concentrate specifically on graft dysfunction. First, this article will explain different types of complications other than graft dysfunction.

1. Types of Complications

There are six categories of complications including: urological complications, vascular complications, fluid collection, recurrent native renal disease, graft dysfunction, and neoplasms. This section will take a short look at the first five complications, then the next section will go a little more in depth for graft dysfunctions. Urological complications are simply when organs involved in the urinary system (e.g, bladder, urethra and ureter) become obstructed or permit urine leakage [25, 26]. Vascular complications involving the renal or iliac artery/vein may include narrowing, blockage or formations of holes in the vascular system [27]. Fluid collection is closely related to urological and/or vascular complication in which blood or urine will collect in unwanted areas. This residual collection of blood or urine may result in urinomas, hematomas, abscesses, or lymphoceles [26-28]. Neoplasms are abnormal growth such as tumors that grow on the renal system and other areas. This is said to be caused by the prolonged exposure to immune suppressing drugs [27, 29, 30]. Lastly, recurrent native renal disease is when the disease that caused the patient to develop CKD, such as diabetes, is now affecting the donated kidney [31, 32]. Unfortunately, patients may develop a combination of the previously mentioned health

complications. It is critical to diagnose and treat these complications, as soon as possible. Most of these complications are typically easier to detect when compared to graft dysfunction. This is because these complications can be detected using various imaging techniques such as ultrasounds and MRIs [33]. These imaging techniques will be discussed later in the paper, but the concentration will be more on graft dysfunction. The complication and cause that is more challenging to diagnose is graft dysfunction, which shall be examined next.

2. Graft Dysfunctions

Graft dysfunction is defined as a newly transplanted organ that longer functions. As a consequence, toxins build up, and the body rejects the transplanted organ [27]. It was calculated that within the first 5 years post transplantation, 15% of patients will experience graft dysfunction [34]. There are three classes of graft dysfunction: hyperacute, acute, and chronic. The type of graft dysfunction is differentiated by the mechanism and in part time of dysfunction onset [35]. Currently, hyperacute rejection is relatively rare nowadays. This class of rejection is caused by antibodies attacking the donated organ due to the donated organ having the wrong HLA (+ or -) and/or ABO blood antigens. Hyperacute rejection generally presents itself within in minutes or hours after transplantation [20]. There is no cure for hyperacute rejection [36]. Chronic kidney rejection's mechanism is not well understood but appears to present itself after 5 years post-transplant [20]. This article will concentrate on acute kidney rejection (AKR). Just as there are different types of complications in renal transplant, there are different causes of graft dysfunction. This can provide somewhat of a challenge in diagnosis and treatment. This is due to the fact that there is a different treatment for each cause of graft dysfunction. There are four different

causes of graft dysfunction; they include: acute tubular necrosis antibody-mediated rejection (ATN), T-cell mediated rejection, immunosuppressive toxicity (IT), and viral infection (VI). ATN is when the antibodies of the patient recognize and elicit an immune-response against the newly donated kidney as a foreign body, which ultimately causes the tissue to become necrotic and die. ATN is treated with a drug therapy regimen that may include plasmapheresis, mycophenolate mofetil, and tacrolimus [37-39]. T-cell mediated rejection is when killer T-cells attack the donated organ causing apoptosis in the tissue [40]. T-cell mediated rejection may be treated with corticosteroids, antithymocyte globulin, and immunosuppression therapy. Patients who experience antibody-mediated rejection may not respond to the T-cell mediated rejection treatment [41-43]. Immunosuppressive toxicity arise when immunosuppressive drugs (e.g., cyclosporine and tacrolimus), used to prevent kidney transplantation rejection, actually causes renal failure due to the nephrotoxic nature Nephrotoxicity may be treated by stopping, changing, or altering the does or type of drug. [44-46]. Another cause of graft dysfunction includes VI which is caused by Cytomegalovirus or Herpes simplex virus entering the body and damage the kidney [47]. Patients with these viral injections may receive immunosuppressant and/or antiviral treatments [37]. The causes of AKR can be presented singularly or in combination, which can add to the difficulty in diagnosing the cause of AKR. How the cause of these graft dysfunctions isdiagnosed will be discussed in the next section of this chapter.

G. Detection/Assessment of Renal Rejection

It is important the patient keeps regular visits with their physician to ensure their newly transplanted organ functions properly. The main focus of the post-transplantation

follow-up is to keep the graft viable for as long as possible. If the patient continues regular follow-ups and notifies the physician of any symptoms that arise, it is feasible to detect complications early and save the donated organ. This section will give an overview of the existing techniques/methods for diagnosing graft dysfunction, including traditional non-imaged-based and new techniques underdevelopment, as detailed below

1. Traditional Methods

Traditionally, blood and urine analysis are implemented during a routine follow-up. Abnormal blood or urine test may prompt the physician to order a renal biopsy for a definitive diagnosis. This diagnosis should also tell the physician what is causing the kidney malfunction. These next sections will show how these diagnoses are determined. First, this article will discuss urine testing.

a. Urine Tests

A simple and non-invasive urine assessment can test for multiple substances. Based on the patient's urine, the physician measures a number of biomarkers to determine eGFR. Most often the biomarker used to calculate eGFR is serum creatinine. To calculate eGFR, the concentration of creatinine found in the urine sample is placed into an equation which has constants that change based on sex, race, and age. Using the calculated eGFR, one may determine what stage of function the kidney(s) are in, 0 being at an increased risk and 5 being end stage renal failure [48, 49]. This diagnostic technique is presently suggested by the National Kidney Foundation (NKF) to measure overall kidney function [4]. However, this test has low sensitivity and is a late stage marker of renal dysfunction (a significant change in serum creatinine level is detectable only after the loss of 60% of renal function),

and it does not assess the function of individual kidneys [4]. The next test that shall be discussed will be a blood test.

b. Blood Test/Works

This method is similar to urine analysis in that it measures estimated eGFR using serum creatinine. However, since it does pierce the skin when obtaining the blood, this test is slightly more invasive than urine analysis. A complete blood count and differential count (CBC and diff) [50] measures more substances than urine samples, including detecting the presence of burred blood cells which can be present in patients with CKD. Burr cells are blood cells that appear almost gear like. They appear when there is an excess amount of waste in the body, which is likely to happen in patients with CKD [51, 52]. Although blood analysis has a few more benefits than a urine test, it has the similar setback in that the test has low sensitivity and is a late marker of renal dysfunction and it does not assess the function of individual kidneys [4]. The last traditional method that shall be discussed is a renal biopsy.

c. Biopsy ("Gold Standard")

Renal biopsy is the gold standard for the graft function assessment; however, it is by far the most invasive. For this procedure, a renal biopsy needle is guided by a camera, ultrasound or x-ray and is inserted into the patient's back and kidney, as shown in Figure 4 [50]. The tissue obtained is evaluated under a microscope [53]. The patient is fully conscious and told not to move [50]. If the patient moves, they run the risk of perching other organs, excessive bleeding and infections. Patients who use blood thinners particularly have and increased risk for excessive bleeding. Biopsy-associated infection may in part be related to the fact the patients are on an immunosuppressive therapy regimen

to prevent renal transplantation rejection [34, 54]. These complications can lead to nephrectomy or even death; both occur in 1 in every 1,000 renal biopsies [34].

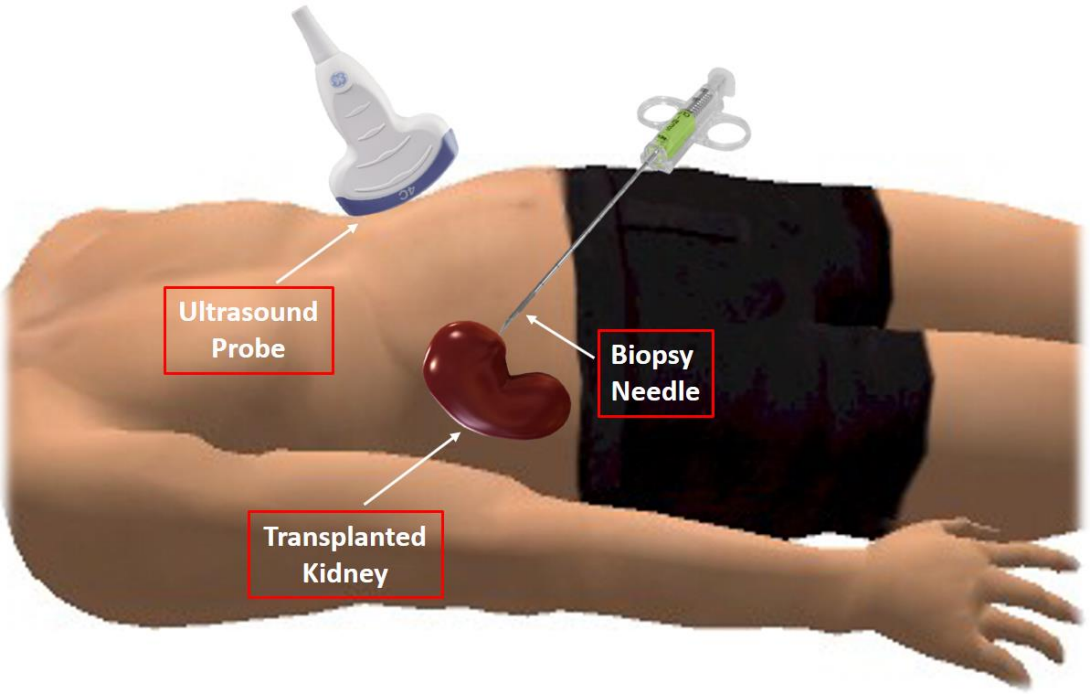

Figure 4. Example of renal biopsy procedure guided with Ultrasound.

Along with the invasiveness of the procedure, there are multiple setbacks that are associated with this procedure. Renal biopsies, although a useful tool, have the tendency to give a missed diagnosis or inaccurately estimate the extent of the problem. This is because it is only sampling a small portion of the kidney. So if the needle is even slightly off target, the biopsy needle can miss an effective portion of the kidney, resulting in a false negative. As a consequence, the patient may have to undergo another biopsy, which may cause the patient additional pain and precious time lost to save the graft. On the subject of time, it takes up to two weeks to obtain renal biopsy results [55]. That time that could be used for treatment is wasted and can result in failure of the donated kidney. On top of these

setbacks, the financial cost of the procedure can reach over $20,000 [56]. In essence, renal failure can cause both physical pain and a financial burden.

Though these tests have been routinely used for transplant assessment and have helped in improving graft survival, new methods are needed to diagnose and differentiate the cause of graft dysfunction. Additionally, existing techniques, i.e. eGFR and biopsy, for diagnosis of renal rejection are late biomarkers. Moreover, renal biopsy has significant morbidity, is very expensive, takes up to two weeks to get the final report, and can result in over- or under-estimates of problems by only sampling small areas of the kidney. Therefore, the development of non-invasive tests to monitor kidney transplant rejection will permit early intervention prevent rejection and associated damages, which will improve long-term outcomes.

The following section will overview existing non-invasive imaging techniques and their possible use for renal function assessments and graft dysfunction diagnoses. The imaging techniques that are included in this article are ultrasound and MRI.

2. Image-Based Techniques for Renal Transplant Evaluation

The progress of computer-aided diagnosis (CAD) systems for renal transplant assessment using diverse imaging modalities is a current area of amplified research. Non-invasive imaging-based techniques have been clinically used to assess transplanted kidneys with the advantage of providing information on each kidney separately. For example, radionuclide imaging (also termed scintigraphy), the traditional technique in renal imaging, is an admirable modality for gauging graft function, both qualitatively and quantitatively, while also assessing for common complications [57]. However, this procedure appears to miss the mark in presenting accurate anatomical information due to its narrow spatial

resolution. Therefore, functional idiosyncrasies inside different areas of the kidney (such as cortex and medulla) cannot be differentiated precisely [58]. Additionally, radionuclide imaging contains radiation exposure [59], thus restraining the range of its applications, particularly in monitoring diseases such as Acute Tubular Necrosis or cyclosporine [60]. Computed tomography (CT) is a commonly accessible equipment that uses contrast agents that permits accurate evaluation of numerous diseases and complications in renal transplantation and at a lower cost than magnetic resonance imaging (MRI) [61]. Conversely, data gathered by CT to sense renal acute rejection lacks specificity and the contrast agents used are currently nephrotoxic. Therefore, currently CT scans are typically restricted to the detection of acute renal rejection [62]. In contrast to these radionuclides and CTs, ultrasound (US) and magnetic resonance imaging (MRI) are the most popular imaging modalities used for the diagnosis of kidney diseases, as described in the upcoming sections.

a. Ultrasound (US) Imaging

Typically, ultrasound (US) imaging is used for the assessment of renal allografts functionality during the early phases of postoperative period as well long-term follow-up. This imaging modality is preferred over some of the others because it is easy to perform and repeat, inexpensive, and repeated, inexpensive, and is non-toxic to the kidneys[63]. Pulsatility index (PI) and resistance index (RI) are the most common measurements to assess renal functionality using US. Below, we will discuss some recent studies that assessed renal transplants using different forms of ultrasound (e.g., power Doppler (PD), color Doppler (CD), contrast enhanced (CE), etc.) as shown in Figure 5.

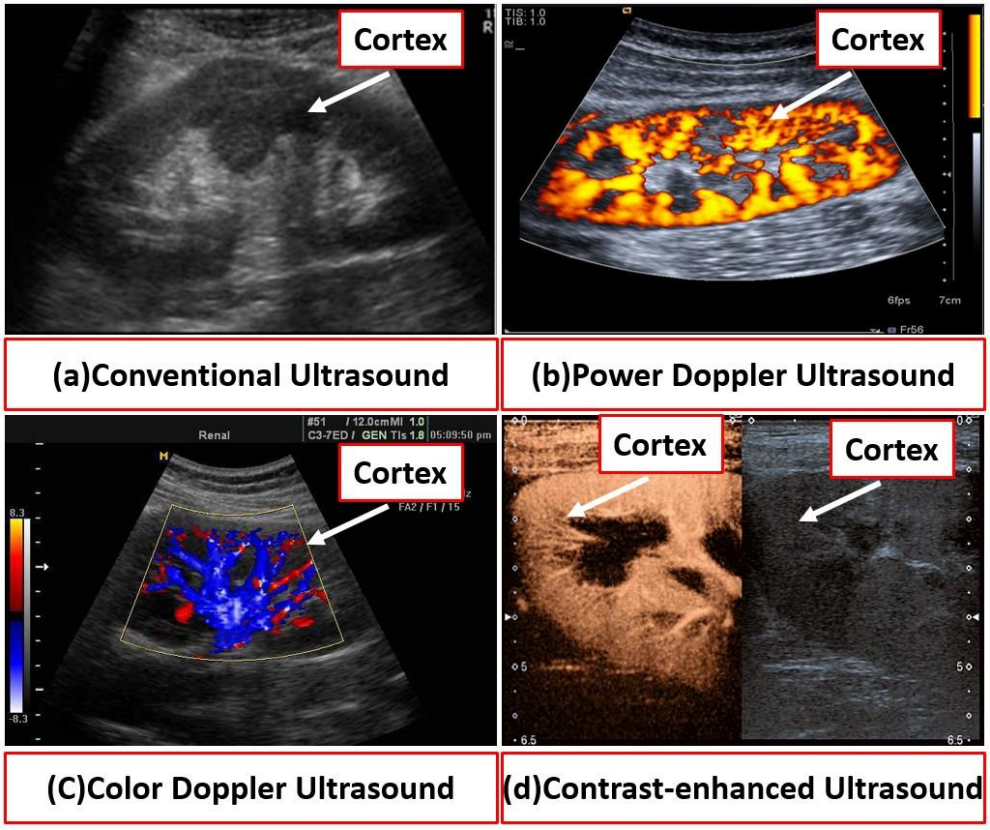

Figure 5. Example of different Ultrasounds.

In an investigation to illustrate the factors that impact Pulsatility index and resistance index in patients with immediate (IGF), slow (SGF), or delayed (DGF) kidney graft function, Chudek et al. [64] observed that ischemic injury, which occurred chiefly prior to organ harvesting, played an overriding role in defining intra-renal resistance in the early post-transplant period. Saracino et al. [65] investigated whether the long-term renal functionality could be predicted using resistance index measurements obtained soon after renal transplantation. On the other hand, Kramann et al. [66] evaluated whether resistance index measurements could to predict renal allograft survival. They concluded long-term allograft survival predictions would require attainment of, resistance index measurements 12-18 month post-transplantation. Krejvci et al. [67] utilized a CD imaging, PD imaging,

and composite gray-scale to examine the power of US for early detection of a subclinical acute rejection. A significant difference between the different groups mentioned before in their study was found. In another study by Damasio et al. [68], the ability of Doppler US to differentiate between dual and single kidney transplantation (DKT and SKT, respectively) was exploited. After the measurement of resistance index parameters for both dual kidney transplantation and single kidney transplantation groups, they concluded that those patients with dual kidney transplantation had lower kidney volumes and higher resistance index than those with single kidney transplantation.

A study by Shebel et al. [69] investigated the ability of PD in the differentiation between acute tubular necrosis and acute rejection (AR). Their study included 67 renal transplant recipients in the early post-transplantation period. After a manual placement of region of interests, cortical perfusion (CP) and resistance index were measured for all recipients and CP was tested with respect to resistance index and serum creatinine (SCr). Upon their own CP grading scale system, they found a statistical significant relationship between their SCr and CP grading ($P < 0.01$) and between resistance index and CP grading ($P < 0.05$). They concluded that the power Doppler using cortical perfusion grading is more sensitive in the detection of early AR compared to resistance index and cross-sectional measurements.

Fischer et al. [70] demonstrated ultrasound contrast media (USCM) was more effective than ultrasound imaging that uses the resistance index indicator in the diagnosis of early stage allograft dysfunction. Additionally, Benozzi et al. [71] discovered that both contrast enhanced US and US could identify grafts with early stage dysfunction, but only some contrast enhanced US derived parameters could discriminate between AR and ATN.

Schwenger et al. [72] exploited the power of CE sonography (CES) in early prediction of long-term renal transplant functionality compared to color doppler ultrasonography (CDUS). In their study, 68 renal transplants were investigated using both CES and CDUS one week after transplantation. Renal blood flow (RBF) and resistance index were measured for all transplant recipients. These measurements were evaluated in relation to the recipients' clinical data represented by glomerular filtration rate (GFR) in a post-transplantation period, ranging from one week to one year. Based on their data they concluded RBF measurements using CES was significantly corresponded with kidney functionality in the aforementioned period after transplantation period. However, resistance index measurements using CDUS did not track with kidney functionality. In another study Gocze et al. [73] differentiated between acute kidney injury (AKI) stages using contrast enhanced US based on the quantification of blood perfusion. Instead of generating time-intensity curves (TIC), they used another quantification method called arrival time parametric imaging (ATPI). Their study included 10 patients who underwent contrast enhanced US of which 4 patients had no evidence of AKI, 1 with stage 1 AKI, and 5 with stage 2 or 3 AKI. Color-maps based on inflow time (IT) of the contrast agent were generated using the contrast enhanced US-ATPI quantification method and were divided into six major categories based on their values. Then, these ITs were assessed for different poles of kidney cortex (i.e. lower, middle, and upper) and the total IT was the sum of all arrival times of these three poles for each kidney. They observed that patients with stage 2 or 3 AKI have more delayed ITs than those of the other groups. They concluded that contrast enhanced US-ATPI technique may help in detecting different stages of AKI. Recently, Jin et al. [74] assessed renal allografts using contrast enhanced US. In their study,

57 renal transplant patients underwent contrast enhanced US. Then, they were divided into three groups: 23 patients with AR (group 1), 10 patients with ATN (group 2), and 24 patients with normal allografts (group 3). After a manual placement of region of interests, a new index to detect AR called rising time (RT) was measured instead of arrival time (AT). In addition, time to peak (TTP) and delta time among region of interests (ΔRT and ΔTTP) were measured, analyzed, and correlated with clinical data (e.g., GFR). They found that RT, TIP, and (ΔRT and ΔTTP) were significantly higher in group 1 compared to those in group 2 and group 3.

Although several studies utilized US to evaluate and assess renal functionality pre- and post-transplantation by evaluating conventional ultrasound parameters, for instance the Pulsatility index and RI, two contradictory studies [75, 76] concluded that resistance index is not an exact sign of renal graft dysfunction, and it could only offer a predictive marker of the graft. Moreover, Doppler US may give high resistance index and Pulsatility index values (>0.8), which is an indication comparable to those of ATN [66, 77]. These contradictions led researchers and investigators to examine a different imaging modality to assess renal functionality (e.g., MRI). In the next section, we will discuss up-to-date studies utilizing different MR imaging modalities.

b. Magnetic Resonance Imaging (MRI)

MR imaging is a non-ionizing technique that has become the most important non-invasive diagnostic tool in many clinical applications [78]. MRI not only provides excellent morphological information but also possesses the ability to offer the best soft tissue contrast compared to all imaging techniques (e.g., US and CT), which allows advanced analysis of different aspects of renal function. There are various specific types of MRI scans. While

some of these types provide only structural but not functional information, other MRI modalities, such as dynamic MRI, BOLD MRI and diffusion MRI are frequently used for renal function evaluation. Next, we overview the recent studies utilizing these MRI modalities for renal transplant assessment.

i. Dynamic Contrast-Enhanced (DCE) MRI

Renal dynamic MRI is an emerging imaging technique for assessing kidney function. The technique is based on repeated imaging of the organ-of-interest before and after administration of a contrast-gent. Figure 6 shows a typical example of DCE-MRI of the kidney. In recent years, several studies have exploited DCE-MRI to non-invasively analyze kidney function in both native and transplanted kidneys. This imaging modality has the ability to non-invasively characterize important functional parameters (e.g., RBF, GFR, and renal plasma flow (RPF)) as well as tissue-specific functional changes.

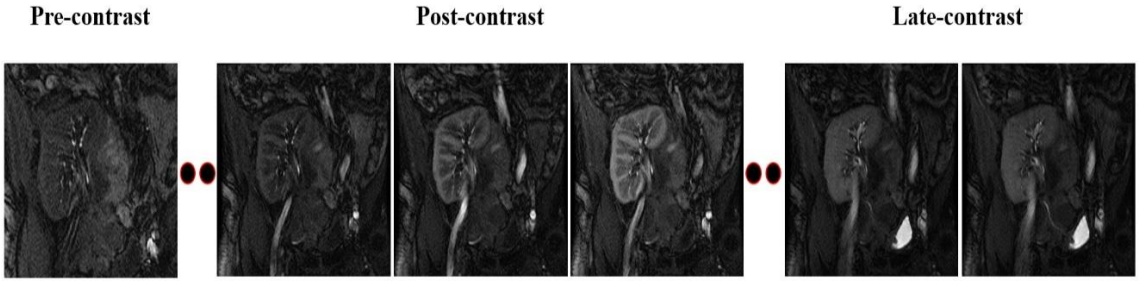

Figure 6. Example of an DCE-MRI sequence with Pre -, Post-, and Late- contrast images

In particular, a study by de Priester et al. [79] utilized dynamic MR enhancement curves to qualitatively evaluate diseased (27 patients) and non-diseased (8 patients) renal transplants. Cortical and the medullary enhancement parameters were obtained from a physiological model that was fitted to the raw data. Cortical arterial blood volume and medullary wash-out rates were found as the main discriminatory parameters between diseased and non-diseased patients. Yuksel [80] introduced a DCE-MRI-based CAD

system for the evaluation of transplant function, which employed deformable image segmentation, kidney registration, and cortical perfusion construction. After kidney segmentation, a manual cortical region of interest is used to construct the perfusion curve from the co-aligned images and the kidney function is evaluated visually based on the pattern of the constructed curves. Several studies [81-84] have been developed for early diagnosis of acute transplant rejection and included automated kidney segmentation, local kidney alignment, and classification of the allograft status. Empirical (nonparametric) cortical parameters were employed for the evaluation of kidney status using: the peak signal intensity, the time-to-peak, the wash-in slope (slope between the peak and the first minimum), and the wash-out slope (peak and the signal measured from the last image in the sequence). A supervised Bayesian classifier was employed and the system classified 13 out 15 and 15 out of 15 correctly for both training and testing, respectively. Similar approaches were proposed in [85-87]. The studies utilized a global alignment step of the MR images, the whole kidney perfusion curves were analyzed rather than the cortical one as in [81-84], and the systems were evaluated on a 100 patient cohort and achieved a 94% diagnostic accuracy using Bayesian supervised classifier. Functional evaluation of cortical and medullary regions by Rusinek et al. [88] exploited rigid alignment, graph-cut segmentation, and compartmental modeling. Their framework was tested on 22 clinical data sets and the study concluded that the accuracy and precision in RPF and GFR are acceptable for clinical use.

A semi-automated framework was proposed by Zikic et al. [89] to evaluate kidney kinetic parameters. Their framework employed manually segmenting the kidney and applying motion correction steps using template-matching based registration to correct for

image motion. Functional parameters (plasma volume and tubular flow) evaluation, however; was performed visually by trained physicians for 10 data sets of healthy volunteers. De Senneville [90] conducted a similar study to evaluate renal function for healthy volunteers and transplant patients. Their framework performs sequentially rigid-body registration, manual cortex segmentation, and the GFR estimation using Patlak-Rutland model. Compared to the transplanted kidneys, a significant uncertainty reduction on the computed GFR for native kidneys was observed. Aslan et al. [91] developed an automated CAD system to classify normal kidney function from kidney rejection using DCE-MRI. Following kidney segmentation, three classification methods (least square support vector machines (LS-SVM), Mahalanobis distance, and the Euclidean distance) were compared to assess transplant status based on medullary perfusion curves. On a cohort of 55 clinical data sets, they achieved a diagnostic accuracy, sensitivity, and specificity of 84%, 75%, and 96%, respectively using the Mahalanobis distance-based classifier. A trace kinetic modeling-based framework was proposed by Anderlik et al. [92] for quantitative assessment of kidney function. The GFR was estimated from the time-intensity curves for 11 data sets after motion correction using Sourbron et al. [93] compartment model. A framework by Zollner et al. [94] employed a k-means clustering [95] method to extracted regional functional kidney parameters. Only four dynamic MRI data sets were used and qualitative evaluation of the mean signal intensity time courses of kidney regions was performed. Wentland et al. [96] utilized MRI-based intrarenal perfusion measurement to differentiate between normal-functioning kidney allografts and allografts with ATN or acute rejection (AR) on a cohort of 24 biopsy proven patients. The study concluded that the cortical and medullary blood flow is significantly reduced in grafts experiencing AR,

as compared with normal grafts. Additionally, AR patients demonstrated medullary blood flow reduction as compared with ATN patients.

Recently, a study by Abou El-Ghar et al. [97] explored the feasibility of DCEMRI in evaluation of renal allograft dysfunction. Their CAD system employed computer based techniques for motion correction and creation of renographic curves. Functional evaluation on 55 patients using the mean medullary intensity achieved sensitivity, specificity and accuracy of 75%, 96% and 84%, respectively, to separate normal kidneys from impaired ones. Yamamoto et al. [98] utilized dynamic MRI to prospectively assess its ability to identify the cause of acute graft dysfunction. Their study employed 60 patients, 31 of which had normal function and 29 had acute dysfunction due to AR. Their study employed a multicompartmental tracer kinetic model to estimate the GFR and mean transit time (MTT) at different compartments of the kidney. The study documented differences in the fractional MTT values between normal grafts and grafts undergoing AR or ATN; however, substantial overlaps among these groups and with normal kidneys were observed. Hodneland et al. [99] developed a framework for the estimation of kidney indexes. Their approach combined viscous fluid model for motion correction of the kidney and semi-automated kidney segmentation with the nearest neighbor approach. Two healthy volunteers were enrolled in the study with a total of four data sets for evaluation. The study reported a slight underestimation of GFR values compared with the creatinine reference values. A study by Positano et al. [100] included a two-step rigid registration and adaptive prediction of kidney position for the estimation for renal parameters. Perfusion curves were constructed for both automatically and manually registered data sets. Then, four functional indices (peak signal intensity, MTT, initial up-slope, and time to peak) were extracted. The

study concluded that for both curves the perfusion parameters were similar. A framework by Khalifa et al. [101, 102] was proposed for automated classification of kidney transplant status. The system included kidney segmentation and the local kidney motion correction using by a Laplace partial differential equation-based method [103, 104]. Their initial study [101] included only 26 data sets, a K-nearest neighbor classifier, and two empirical parameters (the time-to-peak and wash-out slope) for evaluation. Their system achieved a 92.31% correct classification using the whole kidney perfusion curves. Their framework was extended in [102] by using four augmented cortical empirical parameters (peak intensity value, time-to-peak, up-slope and average plateau) by the genetic algorithm [105]. Unlike [101], the system was tested on 50 patients, and the overall diagnostic accuracy increased to 96%. Another study [95] extended the work in [101, 102] and employed the gamma-variate analytical function-based model to fit agent cortical kinetic curves. Both functional model parameters and the time-to-peak and average plateau were used to assess the transplant status in a cohort of 50 patients.

Although DCE-MRI has been employed as a widespread imaging technique to develop several CAD systems for renal transplants assessment purpose, the contrast agents may implicate nephrogenic systemic fibrosis; thus, many medical centers are reluctant in applying the DCE-MRI to patients with renal disease [99]. In order to circumvent this major drawback, DW-MRI and BOLD-MRI have been recently exploited to assess renal transplants as they do not involve any use of contrast agents, like DCE-MRI. Below, we will briefly discuss some recent renal transplant assessment studies using BOLD-MRI. This is followed by a short discussion on other studies that utilized DW-MRI to assess renal transplants.

ii. Blood Oxygen Level Dependent (BOLD) MRI

In addition to DCE-MRI, another imaging technique, called BOLD-MRI, has been utilized to study renal rejection using the amount of oxygen diffused blood (i.e. oxygen bioavailability) in the kidney determine if it is functioning properly. Specifically, the amount of deoxyhemoglobin is measured by the apparent relaxation rate (R2*) parameter [107].

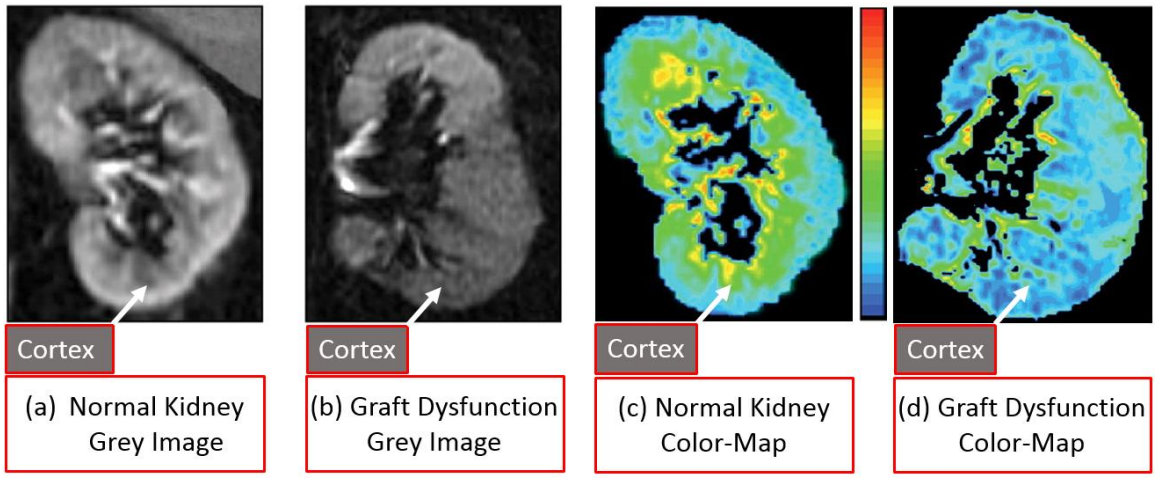

Figure 7. BOLD-MRI grey scale images (a) normal kidney and (b) kidney with graft dysfunction and R2* color-maps images (c) normal kidney and (d) kidney with graft dysfunction.

In particular, Djamali et al. [108] investigated the ability of BOLD-MRI to assess renal allografts. In their study, 23 patients underwent BOLD-MRI scans, of which 5 were normal allografts and 18 had acute allograft dysfunction (5 with ATN and 13 with AR). Medullary and cortical region of interests were placed, and mean cortical (CR2*), medullary (MR2*), and medullary to cortical (MCR2*) were calculated. They found that MR2* and MCR2* values of patients with ATN and AR were significantly decreased more than those with normal allografts. However, no differences in CR2* values between the different groups were observed. In a similar study by Han et al. [109], BOLD-MRI was

conducted to differentiate between patients with AR and ATN after transplantation. Their study included 110 patients; 82 with normal allografts (group 1) and 28 with kidney dysfunction, including 21 with AR (group 2) and 7 with ATN (group 3). Group 2 was divided into two subgroups: 13 patients with T-cell-mediated rejection (TMR) and 8 patients with antibody-mediated rejection (AMR). Manual region of interests were placed in the cortical and medullary regions, and CR2*, MR2*, and MCR2* were compared between different groups. They performed a statistical analysis, and they found that values of CR2*, MR2*, and MCR2* of group 2 were reduced compared to those of the other two groups. Contradictory to Djamali et al. [108] study, they found that values of MR2* of group 3 were higher than those of group 1. However, no significant difference was observed between the TMR and AMR subgroups.

Sadowski et al. [110] employed BOLD-MRI to assess kidney transplants. Manual cortical and medullary region of interests were placed on 17 patients who underwent BOLD-MRI scans, and these patients were divided into three groups: 5 patients with normal allografts (group 1), 4 with ATN (group 2), and 8 with AR (group 3). The MR2* and CR2* were calculated in the same way as their previous study [108], and compared between the different groups. Specifically, MR2* values of group 3 allografts were decreased compared to those of group 1 and group 2, while no significant difference was observed in MR2* values between group 1 and group 2. However, no difference was detected in CR2* values among the three groups. Another interesting study by Liu et al.[107] was investigated to detect renal allograft rejection using BOLD-MRI. A total number of 50 patients with renal allografts were included and divided into three groups as 35 patients with normal allografts (group 1), 10 patients with AR (group 2), and 5 patients

with ATN (group 3). After cortical and medullary region of interests placement, CR2* and MR2* were measured to assess the three groups. Group 2 had the lowest MR2*, while no significant difference was detected in CR2* values among the three groups.

Although BOLD-MRI is a valuable imaging technique that has been investigated by some researchers in detecting renal allografts dysfunction, BOLD-MRI remains challenging, not only because of the low of signal-to-noise ratio (SNR) and the weakness of the electromagnetic fields [111], but also the limited applicability of renal BOLD-MRI due to kidney motions and susceptibility induced by bowel gas which may lead to impaired image quality [112].

iii. Diffusion-Weighted (DW) MRI:

Recently, DW-MRI has become a subject of extensive research as an emerging imaging modality for renal function assessment thanks to DW-MRI's ability to provide both anatomical and functional information, while avoiding radiation exposures (like CT) and contras agents' administration (like DCE-MRI). For DW-MRI, its functional parameter, called apparent diffusion coefficient (ADC), is estimated from different gradient field strengths and duration (b-values), as shown in Figure 8, to describe the unique tissue characteristics of inner spatial water behavior [112]. Therefore, several studies have utilized DW-MRI to assess renal functionality by measuring the ADC values, but the results have varied [107].

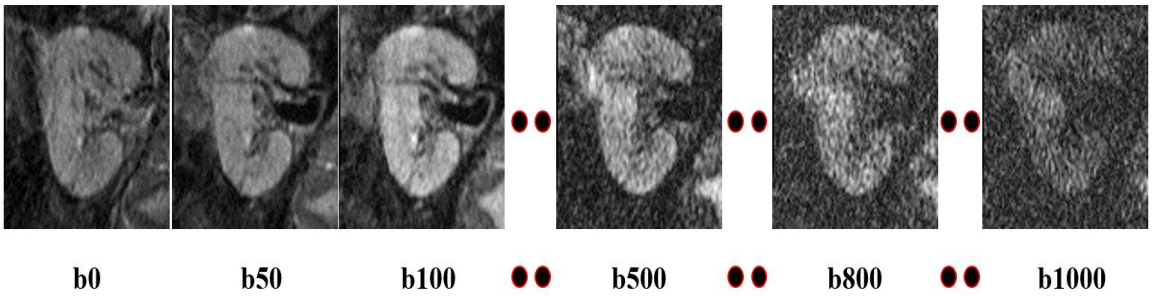

Figure 8. Example of an DW-MRI sequence at different b-values.

A study by Eisenberger et al. [113] was conducted to assess renal allografts functionality. They started with a manual placement of region of interests in the upper, middle, and lower poles of the cortex and medulla on several slices to cover large regions of the allograft. Then, they calculated the means and standard deviations of the ADCs from all b-values, which combines both the perfusion free ADC and microcirculation parameters, quantified with perfusion fraction, Fp. A significant reduction in these parameters was observed in the cortex and the medulla for the AR and ATN patients, and the aforementioned parameters were correlated with the creatinine clearance (CrCl) values. Similarly, a recent study by Hueper et al. [114] included 64 patients with renal allografts, of which 33 were patients with initial graft function (IGF) and 31 were patients with DGF. These patients underwent DW-MRI scans at two b-values (0 and 600 s/mm2). After placement of manual region of interests and estimation of renal diffusion parameters, including ADC and Fp, they concluded that renal diffusion parameters were significantly reduced in patients with DGF and their values well correlated with renal function and renal allograft fibrosis in biopsy specimens. Xu et al. [115] investigated the power of DW-MRI to diagnose AR renal allografts on 26 biopsy-proven rejection and 43 non-rejection patients. Higher ADC values were obtained from the normal allografts than those from AR allografts. The ROC curve was constructed and demonstrated the best sensitivity and

specificity at the b-value of 800 s/mm2. The functionality of 21 renal allografts was assessed by Palmucci et al. [116]. Patients were divided into three groups by their CrCl values and their ADCs and true diffusion (TD) were estimated with renal function indices. Manual region of interests of the transplanted kidney for the three groups were placed and the cortical ADC and TD were evaluated. A moderate positive correlation between the CrCl and both the ADC and TD, as well as no difference between the ADC and TD values for the contiguous groups have been found. The subsequent extension [117] of these evaluations to 35 patients revealed a slightly smaller positive correlation than the previously reported one [116]. However, acute rejection responses after transplantation could not be detected.

Vermathen et al. [118] investigated the determination of long-term (3 years) stability and potential changes for renal allograft recipients. Cortical and medullary region of interests were selected and the ADC values were measured from all b-values. A significant correlation between different ADC components was demonstrated in the case of normal transplants. However, the Fp values were the highest, and the medullary Fp had the greatest changes in the case of reduced transplants. Possible relations between the selected laboratory results and diffusion parameters in the early period after kidney transplantation was explored by Katarzyna et al. [119]. To overcome the DW-MRI T2-"shine-through" [120], additional exponential ADCs were measured. These measurements were conducted in the kidney's cortex and medulla over multiple user-defined region of interests at the b-values of 600 and 1000 s/mm2. They obtained the best-quality AD measurement in the renal cortex at the b-value of 1000 s/mm2 because of the relative variability of results and SNR. In addition, strong dependencies were observed between

the ADC and exponential ADC, measured in the renal cortex at b1000 s/mm2, and the estimated GFR. Kaul et al. [121] investigated renal dysfunction assessment using cortical and medullary ADC maps. A significant decrease in ADC values of medullas compared to those cortexes in normal donor kidneys and normal allografts was reported. Both the medulla and cortex ADCs decreased or increased significantly for a rejection or the recovery from the rejection itself, respectively. Abou-El-Ghar et al. [122] assessed renal functionality for 70 renal allograft patients. DW-MRI scans at two b-values of 0 and 800 s/mm2 were performed for 49 patients with normal renal allografts (group 1) and 21 patients with acute graft impairment (group 2: 10 acute cellular rejection (ACR), 7 ATN, and 4 immunosuppressive toxicity (IT) rejection types). In a single cross-section, a user-defined region of interest was placed at the middle of the kidney and a pixel-wise ADC was calculated. Results shown that the ADC values of group 2 were significantly lower than those of group 1, and no overlap was detected between the ADCs of group 1 and the ATN patients of group 2. However, the minimal overlap was observed between the ADCs of group 1 and the patients with the ACR and IT of group 2.

Detection of early renal allograft dysfunction caused by AR and ATN was exploited by Liu et al. [107] using DW-MRI. With manually selected cortical and medullary region of interests, lower ADC values of the AR group than those of the control groups were revealed, whereas no difference in the ADC values between the AR and ATN groups was detected. A similar earlier study was conducted by Thoeny et al. [123]. A recent study to distinguish between rejection and non-rejection renal transplants was made by Shehata et al. [124]. Their study included 36 renal transplants of which 6 were non-rejection and 30 were rejection. After DW-MRI data motion correction using a 2D B-splines approach, they

segmented the largest coronal cross-section of the kidney using a fully automated level sets segmentation approach. Then, they calculated the ADCs at different b-values from the segmented coronal cross-section for each subject. By using a leave-one-subject-out scenario along with a K Star classifier, they got an 87% total classification accuracy. In addition, they depicted color-maps from the calculated ADCs for the visualization purpose at different b-values. In a more recent study, Shehata et al. [125] determined renal rejection type after transplantation using DW-MRI. In their study, 39 renal rejection transplants of which 31 were TMR and 8 were ATN-AMR. Firstly, DW-MRI data co-alignment using a 3D B-splines approach, followed by kidney segmentation using geometric deformable models were performed. Then, they calculated 3D cumulative distribution functions (CDFs) from ADCs for the entire segmented kidney at different low and high b-values of (10, 20, 30, 40, 50, 100) and (200 and 300) s/mm2, respectively. To account for blood perfusion and water diffusion of the kidney, they fused the CDFs at low and high b-values together. Finally, a 98% classification accuracy was obtained using a stacked non-negativity constrained autoencoder (SNCAE) classifier along with a leave-one-subject-out scenario.

iv. MRI with specific contrast agent (Ultra small Superparamagnetic Particles of Iron Oxide "USPIO")"

Ultra small Superparamagnetic Particles of Iron Oxide (USPIO) is a contrast agent used in MRI that may one day be another tool that could be used to diagnose renal rejection [126-132]. USPIO is said to be able to detect the amount of macrophage that is present in the kidney and therefore tell whether the kidney is under stress and becoming rejected [126-132]. The more macrophages that are present to absorb the particles through endocytosis,

the weaker the USPIO signal will show on the MRI [126-129, 131, 132]. This technique has not been used in human kidney transplant studies and is still in its infancy and more studies should be performed. The present studies, which were done on rat models in vivo, show some promise in diagnosing preclinical renal rejection [126, 127, 129, 131, 132]. Though there is some promise, USPIO at present lacks specificity, which means the signal could be weakened by other conditions or substances that are found in the body other than the presence of macrophage. Another reason why USPIO lacks specificity is that it cannot determine why the macrophages are present at this time [126-132]. Even with some of these downsides there are enough possible positive aspects of USPIO that more research should be conducted. The next step for research of USPIO could be larger animal studies whose kidneys are more closely related to humans. Once USPIO is proven relatively safe and effective in large animal studies, human studies should be considered.

H. Conclusion

Though the treatment of chronic kidney disease has improved greatly with the use of transplants, there are still challenges such as graft dysfunction that provide a challenge in maintaining survival of the new organ. In the future, the use of image-based diagnosis will be improved and implemented in the diagnosis of both pre- and post-transplantation. It is hoped that by having these improved imaged based CAD systems that diagnosis of graft dysfunction will be less invasive, more accurate, time saving, and inexpensive compared to renal biopsies and other traditional methods of diagnosis. By having all of these advantages it is expected that graft survival will improve in cases of graft dysfunction.

I. Thesis Organization

This thesis is presented in four chapter. The chapters are summarized as followed

1. Chapter I

This chapter was an over view of the function of the kidney, what disorder can arise in the kidney mainly CKD. It then discusses how CKD stage 5 is traditionally treated. Transplantation provides the best outcome for patients however complications can arise and the thesis discusses how graft dysfunction is presently diagnosed and the risk associated with renal biopsies. Finally, we discussed the potential alternatives for diagnosing graft dysfunction, mainly image based techniques such as DW MRI, BOLD MRI, CE US, Ultrasound PD US, DCE MRI.

2. Chapter II

This chapter investigates which perimeters will proved the most accurate outcome when diagnosing graft dysfunction while using the CAD system and a DW- MRI.

3. Chapter III

This chapter investigates the ability of the CAD system using DW-MRI to differentiate between the ATN and T-celled mediated rejection.

4. Chapter IV

This chapter provides a conclusion for this thesis and mentions future plans for this CAD system. This chapter also describes other applications other than its use in assessing kidney function. CAD systems can be used for assessing and/or diagnosing prostate cancer, lung injury, dyslexia and autism. .

CHAPTER II
INVESTIGATING POSSIBLE SIGNIFICANT DIFFERENCES BETWEEN REJECTION AN NON-REJECTED RENAL ALLOGRAFTS USING DIFFUSION-WEIGHTED MRI

A. Overview

The main goal of this study was to determine which parameters were correlated with a more accurate diagnosis of renal rejection in patients who have undergone kidney transplantation, using 4D (3D+b-value) diffusion-weighted MRI (DW-MRI).

The study included 16 patients with stable renal allograft function (Group 1) and 37 patients with rejected allografts (Group 2), determined by renal biopsy post transplantation. All patients' kidneys were evaluated using diffusion-weighted magnetic resonance imaging (DW-MRI) coupled with a computer aided diagnostic (CAD) system, which integrates both clinical and MRI-derived biomarkers. In order to extract the MRI-based biomarkers, the developed CAD system performs multiple image processing steps, including MRI data alignment to handle the motion effects coming from breathing and heartbeat, kidney segmentation using a geometric (level-set based) deformable model, and estimation of image-based functional biomarkers called apparent diffusion coefficients (ADCs) for the segmented kidney at different gradient field strengths and durations (i.e. b-values of 50 and from 100 to 1000 with a step of 100 s/mm2). Kidneys were studied for any areas of diffusion restriction. Radiologists interpreted the images of the DW-MRI without prior knowledge of the results of the renal biopsy. Statistical

analyses were performed to investigate possible correlations between renal allograft biomarkers and the biopsy diagnosis. The statistical analysis examined four categories of parameters: (i) clinical biomarkers (i.e. plasma creatinine (SPCr) and creatinine clearance (CrCl)) alone, (ii) the mean apparent diffusion coefficient (ADC) at 11 different individual b-values (b50 , and b100 to b1000 with step of 100 s/mm2), (iii) all possible combinations of the mean ADCs of individual b-values (i.e. 2^{11}sub-models), and (iv) the fusion of the clinical biomarkers with the mean ADC of fused b-values (the full model) .

By using ANOVA along with the likelihood ratio ($\chi 2$) tests, SPCr and CrCl were found to have a significant effect on the likelihood of acute rejection, as did the mean ADC for individual b-values of 500, 600, 700, and 900 s/mm2. However, patient age, sex, and mean ADC at other b-values were not statistically significant. The reduced model incorporating only ADC at b-values of 100 and 700 s/mm2 together had the lowest Akaike information criterion (AIC) of 58.6, and mean ADC at those same two b-values were the most informative predictors of acute rejection according to their Akaike weighting. For comparison, the top 10 sub-models and the full model were reported.

Preliminary findings suggest that the most statistical significant individual b-values are b-values of 500, 600, 700, and 900 s/mm2. On the other hand, the most informative model for diagnosing acute renal rejection using DW-MRI was the model that combines only the mean ADCs at b-values of 100 and 700 s/mm2 together along with the clinical biomarkers.

B. Introduction

The kidney is a significant organ playing vital roles in the maintenance of electrolytes, acid-base balance, and blood pressure. It is the primary filtration organ in the

human body, keeping in the nutrients that the body needs and expelling out the unwanted toxic wastes. A reduction of kidney function can occur naturally as a result of age or as a result of acute kidney injury or chronic disease (CKD). The primary causes of CKD can be attributed to diabetes and hypertension. However other genetic (polycystic kidney disease or APOL1 nephropathy) or autoimmune (lupus nephritis or primary glomerular nephritis) diseases [1]. While the primary insult may influence the rate of CKD progression, the net effect of the unremitting accelerated loss of the kidney function is the build-up of uremic toxins in the body. The complete or near-complete loss of the kidney's ability to ultrafilter the blood and product urine is referred to as end-stage kidney disease (ESKD). Treatment of ESKD to address the deadly build-up of toxins is achieved thru renal replacement therapy- dialysis or transplantation. Both of these approaches have inherent life altering complications. Hence preserving the health of this organ is of the utmost importance.

The prevalence in the United States (2010-2014) of CKD was about 14.8% of the adult population and 680,000 cases of ESKD. Due to a limitation in available transplantable kidneys only approximately 17,000 yearly transplants were performed during this time [2, 3]. Though this has immensely improved the outcome of patients diagnosed with stage 5 CKD (ESKD), there are still complications that can occur. One of the main concerns is graft dysfunction. Routine post-transplantation clinical evaluation of kidney function is of great importance to prevent the graft loss. The diagnostic technique presently recommended by the National Kidney Foundation (NKF) to measure overall kidney function is glomerular filtration rate (GFR), which is based on measuring the serum creatinine level. However, this test has low sensitivity and is a late biomarker for renal

dysfunction (a significant change in serum creatinine level is detectable only after the loss of 60% of renal function), and it does not assess the function of individual kidneys [4]. The current gold standard for acute rejection (AR) diagnosis is a renal needle biopsy. However, it is invasive, difficult to perform, costly, and a time-consuming procedure. It can also result in over- or under-estimates of AR by only sampling small kidney areas. Thus, the need for new noninvasive techniques to assess renal transplant status with the capability to provide accurate and early diagnosis of AR is of great clinical importance. A promising methodology to diagnose graft dysfunction, without complications, is to utilize imaging techniques such as diffusion-weighted magnetic resonance imaging (DW-MRI) with the assistance of computer aided diagnostic (CAD) systems.

In recent years, developing noninvasive image-based CAD systems for renal transplant assessment has been an area of increased research. For example, scintigraphy or radionuclide, the traditional methods in renal imaging, has been clinically used to qualitatively and quantitatively evaluate graft function [57]. However, due to its limited spatial resolution, it fails in showing accurate anatomical details, so functional abnormalities inside different parts of the kidney (such as cortex and medulla) cannot be discriminated precisely [58]. Furthermore, radionuclide imaging includes radiation exposure [59], thus limiting the range of its applications [60]. Computed tomography (CT) is a commonly available technology that uses contrast agents and allows accurate evaluation of various diseases in renal transplantation [61]. However, information gathered by CT to detect acute rejection (AR) is unspecific and the contrast agents used are still nephrotoxic. Therefore, CT currently has a limited role in diagnosing AR [62]. The aforementioned shortcomings make these imaging techniques impractical for clinical use,

which has led to the use of alternative imaging techniques to assess renal transplant functionality, namely the ultrasound (US) and MRIs.

In contrast to radionuclides and CTs, US is a safer imaging technique for the diagnosis of kidney diseases. However, US suffers from low signal-to-noise ratios (SNRs), shadowing artifacts, and speckles that greatly decrease image quality and diagnostic confidence. Moreover, conventional US parameters are not exact indicators of renal graft dysfunction, and it could only provide a prognostic marker of the graft [75, 76] or even a similar indication like other diagnostic possibilities, such as acute tubular necrosis [66, 77]. These shortcomings have been circumvented recently by evaluating kidney functions with MRI, which allows advanced analysis of different aspects of renal function. There are various types of MRI scans that are used for renal transplant assessment. While some of them provide only anatomical information, other MRI modalities, such as dynamic contrast-enhanced (DCE) and diffusion-weighted (DW) MRI, provide both anatomical and functional kidney information. Clinically, nephrologists recommend the use of DCE-MRI if the eGFR is greater than 30 ml/min only, because the contrast agent may be nephrotoxic for those patients with a eGFR less than 30 ml/min. To account for all eGFR variability and to cover all those kinds of patients, DW-MRI is recommended. Therefore, we focused our study on the use of DW-MRIs as a diagnostic tool. Briefly, we will review some of the existing studies that used DW-MRI in diagnosing acute renal transplant rejection.

Lately, DW-MRI has become a subject of extensive research as an emerging imaging modality for renal function assessment thanks to DW-MRI's ability to provide both anatomical and functional information. For DW-MRI, its functional parameter, called apparent diffusion coefficient (ADC), is estimated from different gradient field strengths

and durations (b-values) to describe the unique tissue characteristics of inner spatial water behavior [112]. Therefore, multiple studies have utilized DW-MRI to assess renal functionality by measuring the ADC values, however the results have been mixed [107].

The aim of this study is to determine which parameters are correlated with a more accurate diagnosis of renal rejection in patients who have undergone kidney transplantation, using 4D (3D+b-value) DW-MRI.

C. Materials

The Institutional Review Boards of the University of Louisville approved the study protocol (IRB protocol # XY.ABCD). A total of 53 patients undergoing kidney transplantation provided consent to participate in this study with all scans and biopsies preformed from July 2014 to June 2015. All kidney transplants were performed at University of Mansoura, Egypt and the donated kidneys were from live donors. Patient characteristics including sex (44 males and 9 females); mean age (26.26 +/- 9.87 years (range, 12-54 years). Patients were divided into these groups (group 1 and group 2). Group 1 (19 patients) included patients with healthy graft function as indicated by their renal biopsies. In Group 1 three patients were excluded from the study due to technical problems yielding total of 16 non-rejection renal transplants. All patients were evaluated by renal biopsy after DW-MRI

Group 2 (41patients) included patients with acute renal rejection, based on renal biopsy histology. In group 2 a total of 4 patients were excluded from the study due to technical problems, yielding a total of 37 patients with rejection allografts. All patients underwent DW-MRI and renal biopsy which were performed together, respectively. Both DW-MRI and biopsy were included in the final analysis and examined by a nephrologist

and a radiologist. Details of DW-MRI demographics and statistics are documented in Table 1.

Table 1

Demographics statistics of the DW-MRI data for the 53 renal transplant patient included in the study.

(N=53)	Overall	Non-Rejected	Rejected
Age in years Mean (SD)	26.26415094 (9.87)	25.125 (10.07)	26.75675676 (9.89)
Gender N (%)			
Male	44 (83)	12 (75)	32 (86)
Female	9 (17)	4 (25)	5 (14)
Age category N (%)			
10-19	15 (28)	5 (31)	10 (27)
20-29	19 (36)	7 (44)	12 (32)
30-39	14 (26)	2 (13)	12 (32)
40-49	4 (7)	2 (13)	2 (5)
50-59	1 (2)	0 (0)	1 (3)
Serum Creatinine Clearance (%)			
10-19	3 (6)	1 (6)	2 (5)
20-29	4 (8)	0 (0)	2 (5)
30-39	4 (8)	1 (6)	3 (8)
40-49	3 (6)	1 (6)	2 (5)
50-59	6 (11)	0 (0)	6 (16)
60-69	9 (17)	0 (0)	9 (24)
70-79	13 (25)	7 (44)	6 (16)
80-89	6 (11)	2 (4)	4 (11)
90-99	2 (4)	1 (6)	1 (3)
100-109	2 (4)	1 (6)	1 (3)

110-119	2 (4)	2 (4)	0 (0)
Plasma Creatinine (%)			
0.0-0.9	4 (8)	3 (19)	1 (3)
1.0-1.9	37 (70)	10 (63)	27 (73)
2.0-2.9	8 (15)	2 (13)	6 (16)
3.0-3.9	1 (2)	0 (0)	1 (3)
4.0-4.9	2 (4)	0 (0)	2 (5)
5.0-5.9	1 (2)	1 (6)	0 (0)

1. MRI Protocol

The MRI study was performed using a 1.5T scanner (SIGNA horizon, General Electric Medical systems, Milwaukee, WI). DW-MR images were obtained by using a body coil and a gradient multi-shot spin-echo echo-planar sequence (TR/TE, 8000/61.2; bandwidth, 142 kHz; matrix, 1.25×1.25 mm2; section thickness, 4 mm; intersection gap, 0 mm; FOV, 32 cm; signals acquired, 7; water signals acquired at different b-values of (b0, b50, b100, b200, b300, b400, b500, b600, b700, b800, b900, and b1000) s/mm2. Approximately 50 sections have been obtained in 60 - 120 s to cover the whole kidney.

D. Methods

The ultimate goal of this study is to determine which parameters are correlated with a more accurate diagnosis of AR in patients who have undergone kidney transplantation, using 4D (3D+b-value) DW-MRI. To move towards this goal, all patients' kidneys were evaluated using DW-MRI coupled with a CAD system, which integrates both clinical biomarkers (e.g., serum plasma creatinine (SPCr) and creatinine clearance (CrCl) and DW-MRI physiological biomarkers; namely, apparent diffusion coefficients (ADCs). Then, statistical analysis was performed to investigate possible correlations between renal

allograft biomarkers and the biopsy diagnosis of either AR or non-rejection (NR) renal transplant. Details are outlined below.

1. DW-MRI Image Analysis

An important and significant advantage of DW-MRI is the ability to interrelate local blood diffusion characteristics with the transplant status. This advantage is achieved through the DW-MRIs ability to measure unique tissue characteristics of inner spatial water behavior called apparent diffusion coefficient (ADC) [133], which can be used to assess the transplant status. In order to obtain accurate estimation of the DW-MRI-derived markers, namely ADCs, the developed CAD system [124, 134] performs multiple image processing steps. First, in this study the noise effects and image inhomogeneity was reduced first for a given DW-MRI data by applying an intensity histogram equalization and the nonparametric bias correction technique [135]. This was followed by a 3D B-splines based non-rigid registration [136] to handle kidney motion to reduce the DW-MRI data variability across subjects. Then, the kidney as segmented using a geometric (level-set based) deformable model [137-139]. After segmenting kidneys, the ADCs [140] were estimated at different gradient field strengths and durations (b-values, in our case 11 b-values) [134]. Furthermore, our CAD system was also designed to demonstrate the local voxel-wise diffusion of the segmented DW-MRI data as color maps. These regional display mappings will be of great importance for the radiologists to help investigate which region of the kidney needs attention and follow-up with appropriate treatment. Figures 9&10 demonstrates the voxel-wise parametric maps for the diffusion of the transplanted kidney for a NR case and an AR case, respectively. The data in Figures 9&10 reveals the expected relation of the DW-MRI parameters for NR versus AR status.

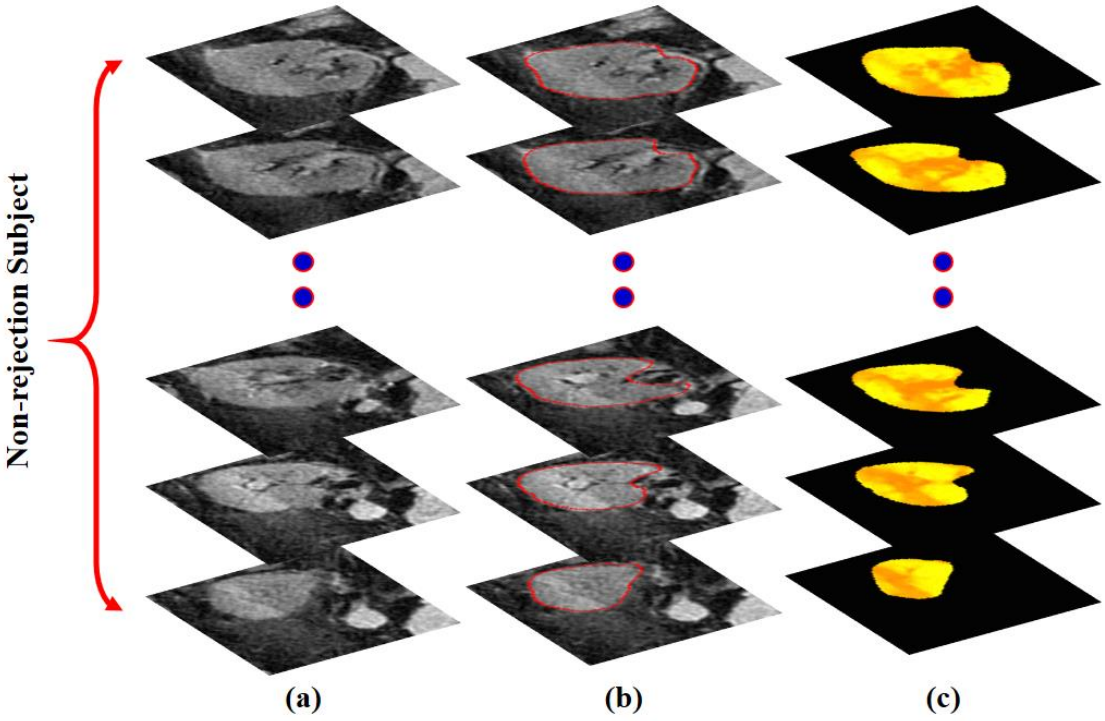

Figure 9. Illustration sample for a non-rejection subject, where (a) the raw data at the b-value of 0 s/mm^2, (b) the segmented kidney object at the b0 s/mm^2, and (c) the average voxel-wise diffusion parametric maps across the subject.

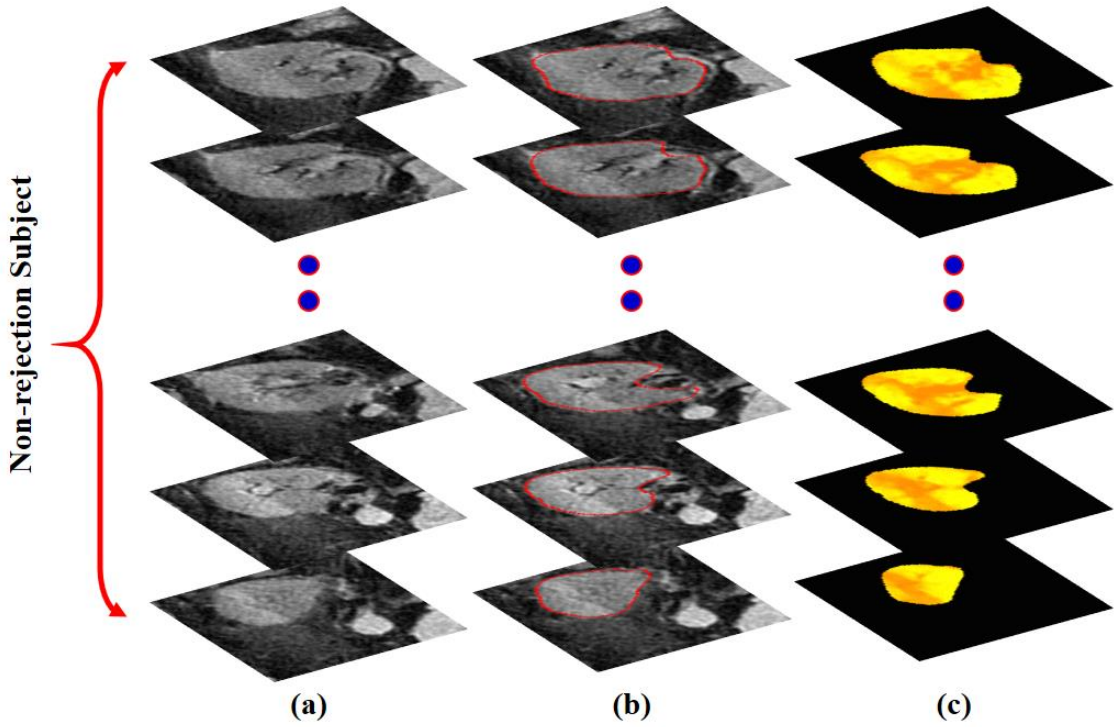

Figure 10. Illustration sample for a rejection subject, where (a) the raw data at the b-value of 0 s/mm^2, (b) the segmented kidney object at the b0 s/mm^2, and (c) the average voxel-wise diffusion parametric maps across the subject.

2. Statistical Analysis

After the DW-MRI-derived markers were estimated (i.e. ADCs), statistical analysis was performed to investigate possible correlations between renal allograft biomarkers and the biopsy diagnosis. The statistical analysis examined four categories of parameters: (i) clinical biomarkers (i.e. serum plasma creatinine (SPCr) and creatinine clearance (CrCl)) alone, (ii) the mean apparent diffusion coefficient (ADC) at 11 different individual b-values (b50, and b100 to b1000 with step of 100 s/mm2), (iii) all possible combinations of the mean ADCs of individual b-values (i.e. 2^{11}sub-models), and (iv) the fusion of the clinical biomarkers with the mean ADC of fused b-values (the full model).

Statistical calculations were performed using R version 3.1.1. The relationship of graft tolerance to ADC was tested using logistic regression of biopsy result (acute rejection or non-rejection) against demographic, laboratory, and imaging parameters. The full model included age and sex, SPCr and CrCl, and mean ADC at each b-value. Statistical significance of each parameter was assessed using likelihood ratio ($\chi 2$) tests. Variable subset selection was performed using the Akaike information criterion (AIC). All 2^{11} models were tested, considering all possible subsets of mean ADC, and the model yielding the lowest AIC was selected as the most informative. However, some questions have to be answered regarding the statistical significant difference between the non-rejection (NR) and the early rejection (ER) renal transplants using: (i) the clinical biomarkers (i.e. SPCr and CrCl) alone, (ii) the mean ADCs at different individual 11 b-values from (b50 to b1000). In addition, two more questions need to be answered regarding how informative the built model is using: (i) the mean ADCs of a certain group of individual b-values (sub-model), and (ii) the fusion of the clinical biomarkers with the mean ADCs of fused b-values (the full model).

E. Results

ANOVA found that SPCr ($\chi 2 = 10.1$, $p = 0.002$) and CrCl ($\chi 2 = 14.1$, $p = 0.0002$) had a significant effect on the likelihood of acute rejection, as did the mean ADC for b = 500 s/mm2 ($\chi 2 = 3.98$, $p = 0.0461$), b = 600 s/mm2 ($\chi 2 = 5.81$, $p = 0.0159$), b = 700 s/mm2 ($\chi 2 = 5.65$, $p = 0.0174$), and b = 900 s/mm2 ($\chi 2 = 4.94$, $p = 0.0262$). Patient age, sex, and mean ADC at other b-values were not statistically significant, as shown in Table 2. The reduced model incorporating only ADC at b = 100 s/mm2 and at b = 700 s/mm2 had the lowest AIC = 58.6, as shown in Table 3, and mean ADC at these same two b-values were

the most informative predictors of acute rejection according to their Akaike weighting (see Figure 11). For comparison, the full model AIC = 65.0.

Table 2.

Results of analysis of covariance on the logistic regression model for acute rejection. ADC*n*: mean ADC at $b = n$; SPCr: serum plasma creatinine; CrCl: creatinine clearance.

Variable	χ^2	*p*-value
ADC_{50}	2.618	0.106
ADC_{100}	3.791	0.0515
ADC_{200}	0.610	0.435
ADC_{300}	1.242	0.265
ADC_{400}	0.016	0.899
ADC_{500}	3.978	0.0461
ADC_{600}	5.813	0.0159
ADC_{700}	5.654	0.0174
ADC_{800}	1.446	0.229
ADC_{900}	4.944	0.0262
ADC_{1000}	0.087	0.769
Age	0.846	0.358
Sex	2.291	0.130
SPCr	14.068	0.000176
CrCl	10.070	0.00151

Table 3

Mean ADC included in the models with the 10 lowest AIC values. The full model and the model with demographics only and lab results are shown for comparison. Δ = AIC − min AIC.

Δ	Predictor variables (*b*-value)										
	50	100	200	300	400	500	600	700	800	900	1000
0		■						■			
0.04		■				■					
0.57				■		■	■	■			
0.96		■					■	■			
1.04	■	■		■		■	■	■	■	■	
1.14		■				■	■	■			
1.16		■				■	■				
1.20		■			■						
1.28	■	■						■			
1.39		■						■	■		
3.29											
6.40	■	■	■	■	■	■	■	■	■	■	■

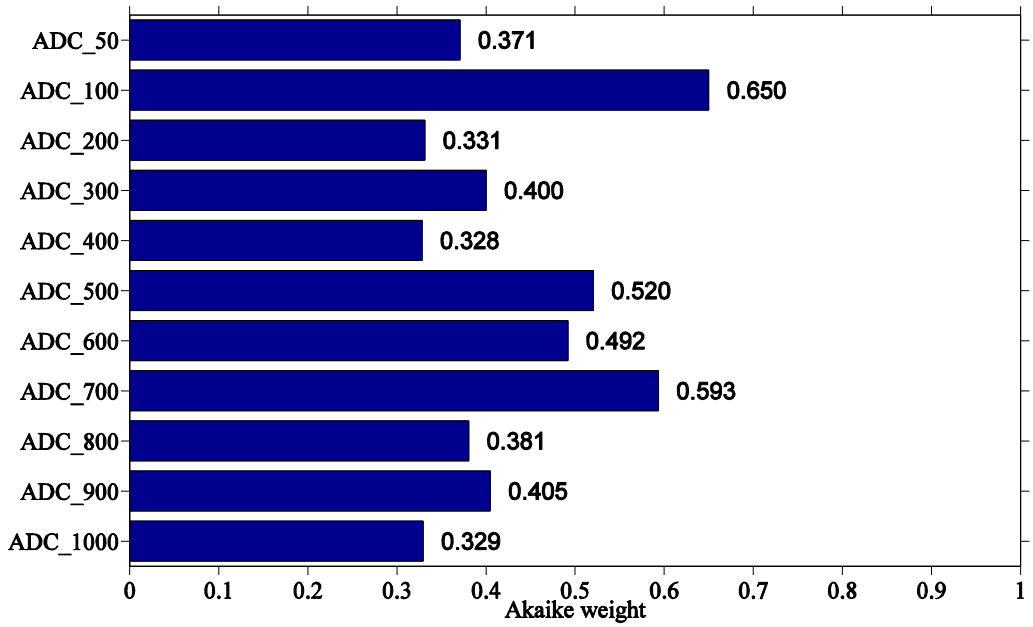

Figure 11. The Akaike weighting criterion versus the sub-models at different b-values, reflects how much informative each sub-model is.

F. Discussion and Conclusions

Using 4D (3D+b-value) diffusion-weighted MRI (DW-MRI) we determined the statistical significance of measured parameters (biomarkers, mean ADC at different individual b-values (b50 to b1000), sub-models, and full model) that correlated with renal rejection in patients who had undergone kidney transplantation. We hypothesized the most accurate parameters for diagnosing would be the full model, due the fact that all the mean ADC of each b-value would have been fused giving all the information of the scan and therefore giving the whole picture. To the best of our knowledge, this is the first time the full model and sub model parameters have been implemented. Based on the AIC the most accurate parameters would be the sub model which fuses b=100 s/mm2 and b=700 s/mm2. All other parameter's accuracy lies in between sub-model fused b=100 s/mm2 and b=700 s/mm2 and full model. A study by Liu et al. [107] explored the detection of early renal

allograft dysfunction caused by AR using DW-MRI. With manually selected medullary and cortical regions of interests (ROIs), lower ADC values of the AR group than those of the control groups were revealed. A similar earlier study was conducted by Thoeny et al. [123] Xu et al. [115] investigated the potential power of DW-MRI to diagnose AR renal allografts on 26 biopsy-proven rejection and 43 non-rejection patients. They found that higher ADC values were obtained from the normal allografts compared to those from AR allografts. The receiver operating characteristic (ROC) curve was constructed and demonstrated the best sensitivity and specificity at the b-value of 800 s/mm2

A study by Hueper et al. [114] was conducted to assess renal allografts functionality included 64 patients with renal allografts, of which 33 were patients with initial graft function (IGF) and 31 were patients with delayed graft function (DGF). These patients underwent DW-MRI scans at two b-values (0 and 600 s/mm2). After placement of manual region of interests in the lower, middle, and upper poles of the medulla and cortex on several portions to cover large regions of the allograft and estimation of renal diffusion parameters, including ADC, they concluded that renal diffusion parameters were significantly reduced in patients with DGF and their values well correlated with renal function in biopsy specimens. Likewise, a recent study by Eisenberger et al. [113] was also conducted to evaluate renal allograft functionality. They began with a manual placement of region of interests. Then they calculated the means and standard deviations of the ADCs from all b-values. A significant reduction in these parameters was observed in the cortex and the medulla for the AR patients, and the previously stated parameters were correlated with the creatinine clearance (CrCl) values. Kaul et al. [121] examined renal dysfunction assessment using cortical and medullary ADC maps. They found a significant decrease in

ADC values of medullas compared to those cortexes in normal donor kidneys and normal allografts. Both the cortex and medulla ADCs decreased or increased significantly for the recovery from the rejection itself or a rejection, respectively. Abou-El-Ghar et al. [122] assessed renal functionality for 70 renal allograft patients. DW-MRI scans at two b-values of 0 s/mm2 and 800 s/mm2 were performed for 49 patients with normal renal allografts (group 1) and 21 patients with acute graft impairment (group 2). In a single cross-section, a user-defined region of interest was placed in the middle of the kidney and a pixel-wise ADC was calculated. Results show that the ADC values of group 2 were significantly lower than those of group 1. Possible relations between the selected laboratory results and diffusion parameters in the early period post kidney transplantation was explored by Katarzyna et al. [119]. These measurements were conducted in the kidney's cortex and medulla over multiple user-defined region of interests at the b-values of 600 and 1000 s/mm2. They obtained the best-quality ADC measurement in the renal cortex at the b-value of 1000 s/mm2 because of the relative variability of results and signal-to-noise ratio (SNR). In addition, strong dependencies were observed between the ADC and exponential ADC, measured in the renal cortex at b1000 s/mm2, and the estimated GFR. Vermathen et al. [118] inspected the determination of long-term (3 years) stability and potential changes for renal allograft recipients. Cortical and medullary region of interests were designated and the ADC values were measured from all b-values. A significant correlation between different ADC components was demonstrated in the case of normal transplants.

In conclusion, our study demonstrated that by fusing specific b-values one can get a more accurate picture than if one were to use a single b-value or that of fusing all b-values together. Our analysis has also shown that our CAD system utilizing DW-MR images,

holds a promise as a reliable non-invasive diagnostic tool. In the future, we plan to test the proposed CAD system on a larger and more diverse cohort of patients to confirm the accuracy and robustness of the proposed technique. In addition, new data set with lower b-values will be included to investigate whether these lower b-values will be more helpful in finding more significant differences between non-rejection and rejection transplants. Furthermore, the ability of the developed technique needs to be examined in diagnosing different types of rejection for proper treatment administration

CHAPTER III

A NEW NON-INVASIVE APPROACH FOR EARLY CLASSIFICATION OF RENAL REJECTION TYPES USING DIFFUSION-WEIGHTED MRI

A. Overview

Although renal biopsy remains the gold standard for diagnosing the type of renal rejection, it is not preferred due to its invasiveness, recovery time (1-2 weeks), and potential for complications, e.g., bleeding and/or infection. Therefore, there is an urgent need to explore a non-invasive technique that can early classify renal rejection types. In this chapter, we develop a computer-aided diagnostic (CAD) system that can classify acute renal transplant rejection (ARTR) types early via the analysis of apparent diffusion coefficients (ADCs) extracted from diffusion-weighted (DW) MRI data acquired at low- (accounting for perfusion) and high- (accounting for diffusion) bvalues. The developed framework mainly consists of three steps: (i) data co-alignment using a 3D B-spline-based approach (to handle local deviations due to breathing and heart beat motions) and segmentation of kidney tissue with an evolving geometric (level-set based) deformable model guided by a voxel-wise stochastic speed function, which follows a joint kidney-background Markov-Gibbs random field model accounting for an adaptive kidney shape prior and visual kidney-background appearances of DW-MRI data (image intensities and spatial interactions); (ii) construction of a cumulative empirical distribution of ADC at low and high b-values of the segmented kidney accounting for blood perfusion and water diffusion, respectively, to be our discriminatory ARTR types feature; and (iii)

classification of ARTR types (acute tubular necrosis (ATN) anti-body- and T-cell-mediated rejection) based on deep learning of a non-negative constrained stacked autoencoder. Results show that 98% of the subjects were correctly classified in our "leave-onesubject-out" experiments on 39 subjects (namely, 8 out of 8 of the ATN group and 30 out of 31 of the T-cell group). Thus, the proposed approach holds promise as a reliable non-invasive diagnostic tool.

B. Introduction

Acute renal rejection, i.e. the immunological response of the body to a foreign kidney, is the most serious cause of renal dysfunction [141]. Medicine has come very far in the treatment of CKD and renal failure with the evolution of kidney transplants, which has significantly improved patient outcomes and quality of life. In the U.S., approximately 17,000 renal transplants are performed annually, and given the limited number of donors, the salvage of a transplanted kidney is very important [141]. Although transplants can improve a patient's well-being, there is a potential risk of kidney rejection by the patient leading to a loss of graft function, and, if not treated in a timely manner, even death [142, 143]. Therefore, early determination of the type of renal rejection is crucial for the identification of proper treatment to administer. As a reminder, the different types of renal rejection include: (i) acute tubular necrosis (ATN) anti-body mediated rejection; (ii) T-cell mediated rejection; (iii) immunosuppressive toxicity (IT); and (iv) viral infection (VI). Each of these rejection types has its own specific treatment procedure and the existence of two types of rejection at the same time further complicates and slows down the treatment process [41].

Currently, renal biopsy is the most definitive technique for diagnosing renal rejection type. However, there are a number of significant drawbacks to this method; specifically, this procedure is invasive and expensive, increases the potential morbidity rate, prolongs recovery time (one to two weeks), and has a high probability for over- or under- estimating the extent of inflammation in the entire graft [141]. Hence, a non-invasive imaging technique coupled with computer-aided diagnostic (CAD) techniques holds a lot of promise due to its ability to simultaneously provide information on each kidney separately, speed of analysis, and decrease in patient morbidity, healthcare costs, and patient recovery time.

A number of different methodologies are being implemented to assess kidney function. In particular, diffusion-weighted (DW) MRI is an emerging imaging technology that is based on the measurement of water molecules inside soft tissue [112]. The main advantage of DW-MRI is its ability to provide both anatomical and functional information, while avoiding radiation exposures and contrast agents administration. Several studies have utilized DW-MRI for functional renal assessment by measuring the cortical apparent diffusion coef- ficient (CADC) and medullary ADC (MADC), but the results have varied [144]. As a result, none of the studies appear to indicate any difference between the types of renal impairment except for the study by Abou-El-Ghar et al. [122] which showed a distinctive pattern. Their study consists of 21 patients with acute graft impairment with 10 Tcell, 7 ATN, and 4 IT rejection types. A region of interest (ROI) is placed at the middle of the kidney in a single cross-section including the entire renal parenchyma, but excluding the renal sinus. For kidney images with an abnormal focal area and high signal intensity, another region of interest is selected separately. On a pixel-by-pixel basis, the ADC values

for the patients are calculated from the three groups, which demonstrate that the ADC of ATN appears as heterogeneous, a mosaic pattern with a tiger stripe appearance. The investigators conclude that under low b-values, ADC values are influenced by both diffusion and blood perfusion, while under high b-values, the influence of blood perfusion is avoided. Another study by Eisenberger et al. [113] investigates manually placing the region of interests in the upper, mid, and lower poles of the cortex and medulla on several slices to cover large regions of the allograft. Then, all individual region of interests are merged to yield one region of interest for the cortex and one for the medulla. Mean and standard deviations of ADCs are calculated for the five patients, four of which have AR and one has ATN. However, due to the lack of patients with transplant dysfunction, the investigators proposed that the trend indirectly indicates possible differences between the AR and the ATN groups. Two additional studies [145, 110] conclude that perfusion MRI demonstrates a significant decrement in renal perfusion of AR allografts, but not in ATN allografts. While other studies [122, 113] support the premise that both the levels of water diffusion and blood perfusion are impaired in AR allografts, whereas only the level of water diffusion is impaired in the ATN allografts.

In addition to DW-MRI, another imaging technique blood Oxygen level-dependant (BOLD) MRI has been utilized to study renal rejection, using the amount of oxygen diffused blood in the kidney to examine the proper functionality of the kidney. Namely, the amount of deoxyhemoglobin is measured by the apparent relaxation rate (ARR) parameter [144]. Some studies find that the ATN kidneys have higher medullary ARR values than those of AR [144, 108–110], while others have discovered that kidneys with ATN have higher cortical ARR values than those with AR [109]. Nonetheless, the general

consensus appears to be one in which higher ARR values. All of the aforementioned clinical statistical analysis studies have some limitations. For example, the methods employ a manual delineation of the kidney using a 2D region of interest, which makes this delineation subjective. In addition, the methods are unable to compensate for the motion of the kidney since the methods did not account for the whole kidney. Furthermore, several of the studies performed only a statistical analysis to investigate the significant difference between pairs at certain b-values. Finally, the studies mentioned above did not investigate the fusion of ADC at multiple low and high b-values.

Therefore, to overcome these limitations, we are developing a fully automated CAD system, shown in Figure 12, with the ability to: (i) delineate the whole kidney and handle its motion; and (ii) implement a stacked autoencoder to fuse the ADC values that have been calculated from the segmented DW-MRI data at low and high b-values. Experimental results, shown in, "Experimental Results," hold promise of the developed CAD system as a reliable non-invasive diagnostic tool. To the best of our knowledge, this is the first CAD system of its kind to distinguish between different types of ARTR.

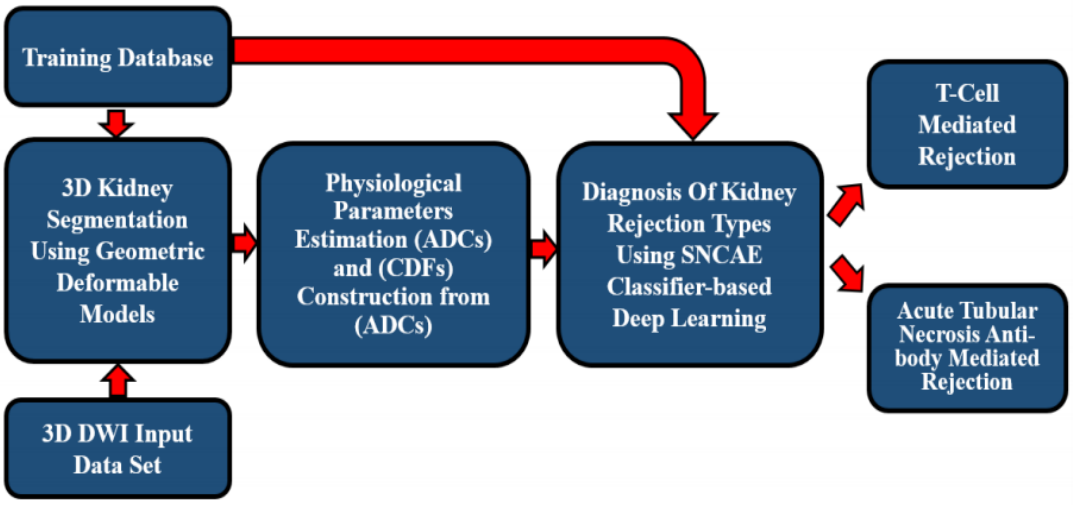

Figure 12. Block-diagram of the proposed framework for kidney rejection types classification from diffusion weighted MRI

C. Methods

Starting from a given input DW-MRI data, our CAD system classifies T-Cell from ATN mediated rejection kidneys in the following three steps: (i) segmenting kidney tissues from surrounding abdominal structures ("Preprocessing, Co-Aligment, and 3D Kidney Segmentation); (ii) estimating voxel-wise physiological parameters (ADC) to form a 3D parametric map for detecting the type of rejected kidney ("Estimating and Depicting Diffusion Parameters"); and (iii) classifying T-Cell from ATN rejection kidney status to evaluate the proposed CAD system as a diagnostic test ("Autoencoding and Deep Learning-Based Classifier").

1. Preprocessing, Co-alignment, and 3D Kidney Segmentation

Initially, we reduce noise effects and DW-MRI heterogeneity by applying an intensity histogram equalization and the nonparametric bias correction method proposed in [135] on each DW-MRI sequence. Then, a 3D B-splines based transformation [136]

using the sum of square difference (SSD) as a similarity metric is applied to handle kidney motions, and thus get more accurate segmentation. Finally, we used the 3D kidney segmentation approach proposed in [137] using level-sets from DW-MRI. To provide the voxel-wise guidance of the level-sets, three features are integrated into a joint MGRF model [146], namely, regional appearance [147, 148], shape, and spatial DW-MRI features as shown in Figure 13. More details about our segmentation approach can be found in [137, 124].

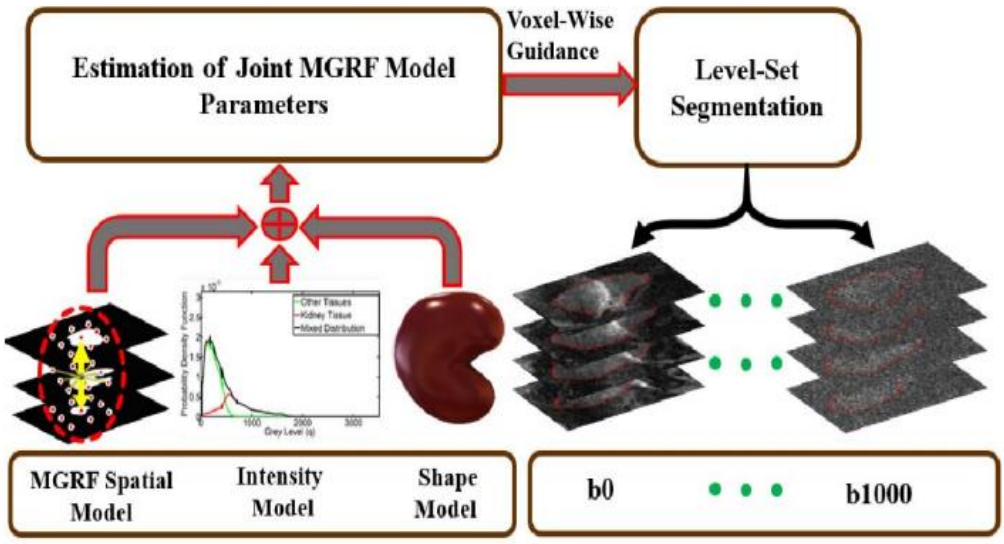

Figure 13. Illustration of Joint MGRF estimation guiding the level-set segmentation technique

2. Estimating and Depicting Diffusion Parameters

After segmenting the kidneys, their discriminatory physiological features are estimated from the images and used to distinguish between ATN and T-cell of ARTR types. This paper uses the ADC defined by Le Bihan [140] as a rejection transplant status feature: $ADC_p = \frac{1}{b_0 - b} \ln\left(\frac{gb:p}{g0:p}\right) = \frac{\ln gb:p - \ln g0:p}{b_0 - b}$ where p = (x, y, z) denotes a voxel at position

with discrete Cartesian coordinates (x, y, z), and the segmented DW-MR images g0 and gb were acquired with the b0 and a given different b-value, respectively.

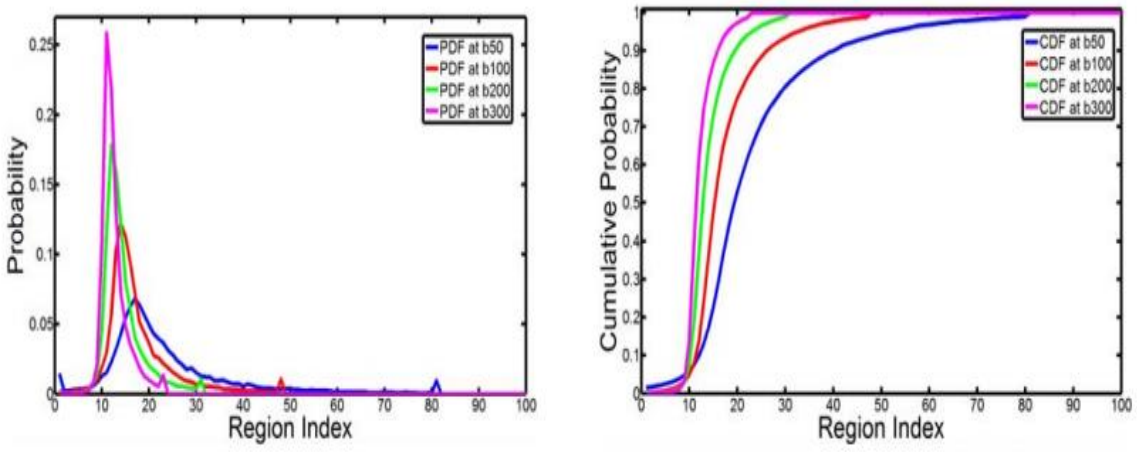

Figure 14. Empirical ADC distributions and their CDFs for one rejection subject at different b-values of (b50, b100, b200, and b300) s/mm^2.

In order to reduce data dimensionality for the rejection transplant status classification, we characterize the entire 3D ADC maps, collected for each subject at the different b-values, by the CDFs of the ADCs, as shown in Figure 14. Differentiation between rejection types can be obtained using DW-MRI acquired at low and high b-values. In this paper, we constructed the CDFs at low and high b-values of (b10, b20, b30, b40, b50, b100) and (b200 and b300), respectively, to classify the type of rejection. The training CDFs are used for deep learning of a stacked non-negativity constrained autoencoder (SNCAE) classifier detailed in, "Autoencoding and Deep Learning-Based Classifier."

3. Autoencoding and Deep Learning-Based Classifier

To classify the rejection transplant status, our CAD system employs a deep neural network with a stack of autoencoders (AE) before the output layer that computes a softmax regression, generalizing the common logistic regression to more than two classes. Each AE

compresses its input data to capture the most prominent variations and is built separately by greedy unsupervised pre-training [149]. The softmax output layer facilitates the subsequent supervised backpropagation-based fine tuning of the entire classifier by minimizing the total loss (negative log-likelihood) for given training labeled data. Using the AEs with a non-negativity constraint (NCAE) [150] yields both more reasonable data codes (features) during its unsupervised pre-training and better classification performance after the supervised refinement.

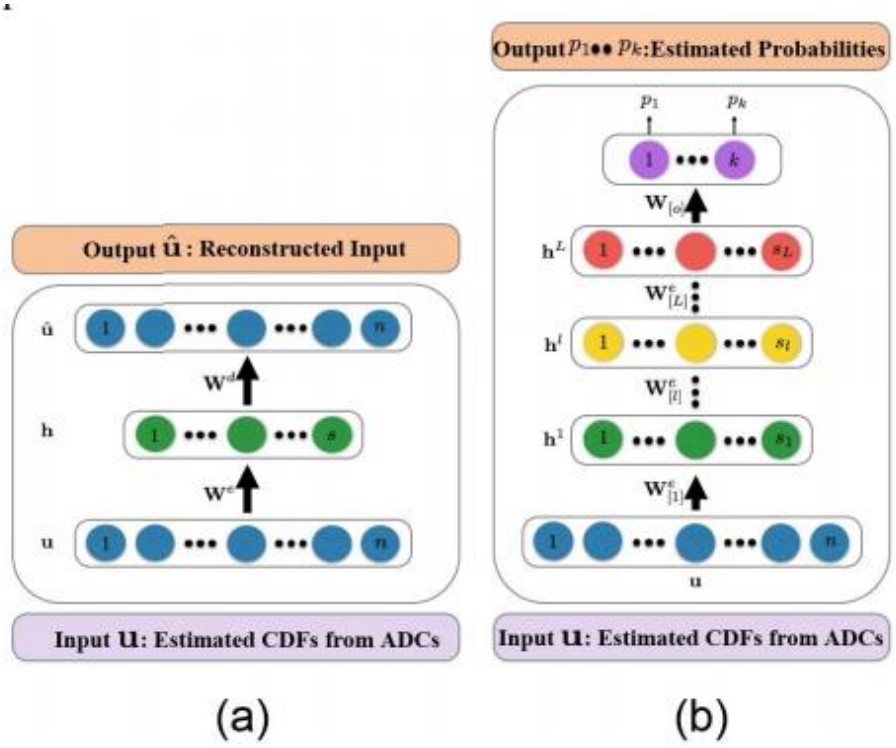

Figure 15: Block-diagram of an NCAE (a) and SNCAE (b) classifier

Let W = {We j ,Wd i : j = 1,...,s; i = 1,...,n} denote a set of column vectors of weights for encoding (e) and decoding (d) layers of a single AE in Figure 15. Let T denote vector transposition. The AE converts an n-dimensional column vector u = [u1,...,un] T of input signals into an s-dimensional column vector h = [h1,...,hs] T of hidden codes (features, or activations), such that s n, by a uniform nonlinear transformation of s weighted

linear combinations of signals: $h_j = \sigma((W_j^e)^T u) \equiv \sigma(\sum_{i=1}^{n} w_{j:i}^e u_i)$where σ(...) is a certain sigmoid, i.e. a differentiable monotone scalar function with values in the range [0, 1] . Unsupervised pretraining of the AE minimizes total deviations between each given training input vector uk; k = 1,...,K, and the same-dimensional vector, uW:k reconstructed from its code, or activation vector, hk (Figure 15(a)). The total reconstruction error of applying such AE to compress and decompress the K training input vectors integrates the 2-norms of the deviations:$J_{AE}(W) = \frac{1}{2K}\sum_{k=1}^{K}\|\hat{u}w: k - u_k\|^2$ To reduce the number of negative weights and enforce sparsity of the NCAE, the reconstruction error of Eq. (2) is appended, respectively, with quadratic negative weight penalties, f(wi) = (min{0, wi}) 2 ; i = 1,...,n, and Kullback-Leibler (KL) divergence, JKL(hWe ; γ), of activations, hWe , obtained with the encoding weights We for the training data, from a fixed small positive average value, γ, near 0: $J_{NCAE}(W) = J_{AE}(W) + \alpha\sum_{j=1}^{s}\sum_{i=1}^{n} f(w_{j:i}) + \beta J_{KL}(h_{w^e;\gamma})$Here, the factors α ≥ 0 and β ≥ 0 specify relative contributions of the non-negativity and sparsity constraints to the overall loss, JNCAE(W), and $J_{KL}(hw^e: jlog\left(\frac{h_{w^e:j}}{\gamma}\right) + (1 - hw^e: j)\log(\frac{1-hw^e:j}{1-\gamma})$

The classifier is built by stacking the NCAE layers with an output softmax layer, as shown in Figure 15(b). Each NCAE is pre-trained separately in the unsupervised mode by using the activation vector of a lower layer as the input to the upper layer. In our case, the initial input data consisted of the 8 CDFs, each of size 100, i.e. n = 800. We calculated the minimum ADC value, the maximum ADC value, and the minimum increment value; thus, we have the step value. Then, we constructed each CDF as 100 regions based on the calculations using the aforementioned parameters in order to not waste any information from the ADCs and, thus, making our data well presented. The bottom NCAE compresses

the input vector to s1 first-level activators, compressed by the next NCAE to s2 second-level activators, which are reduced in turn by the output softmax layer to s◦ values.

Separate pre-training of the first and second layers by minimizing the loss of Eq. (3) reduces the total reconstruction error, as well as increases sparsity of the extracted activations and numbers of the non-negative weights. The activations of the second NCAE layer, h[2] = σ(We [2] Th[1]), are inputs of the softmax classification layer, as sketched in Figure 14(b) to compute a plausibility of a decision in favor of each particular output class, c = 1, 2: $p(c; w_{o:c}) = \frac{\exp(W_{o:c}^T h^{[2]})}{\exp(W_{o:1}^T h^{[2]}) + \exp(W_{o:2}^T h^{[2]})}; and\ c = 1,2;\ \sum_{c=1}^{2} p\left(c; W_{o:c}; h^{[2]}\right) = 1$.Its separate pre-training minimizes the total negative log-likelihood J◦(W◦) of the known training classes, appended with the negative weight penalties:$J_\circ = (W^\circ) = -\frac{1}{K}\sum_{k=1}^{K} logp(c_k; W_{o:c}) + \alpha \sum_{c=1}^{2}\sum_{j=1}^{s2} wo{:}\, c{:}\, j$

Finally, the entire stacked NCAE classifier (SNCAE) is finetuned on the labeled training data by the conventional error backpropagation through the network and penalizing only the negative weights of the softmax layer. In our experiments, we trained our network and tested it based on a leave-one-subject-out scenario 39 times (number of data sets) until we reached the best average accuracy over the entirety of the testing process. At this point, we considered s1 = 25, s2 = 5, s◦ = 2, α = 0.03, β = 3, and γ = 0.5 as the optimum settings for giving the best accuracy. It is worth noting that more conventional classification methods that deal directly with the voxel-wise ADCs of the entire kidney volume as discriminative features encounter two difficulties: (i) varying input data size requires either data truncation for larger kidney volumes or zero padding for smaller ones and (ii) large data volumes lead to considerable time expenditures for training and classification. Our SNCAE classifier exploits only the 100-component CDFs for the 3D

ADC maps estimated at the b-values of (b10, b20, b30, b40, b50, b100, b200, and b300). Fixing the input data size to 8 for such CDFs helps to overcome the above challenges for arbitrary sizes of the original ADCs and notably accelerates the classification.

D. Experimental Results

The proposed CAD system has been tested on a 39 biopsy-proven cohort of which 8 are ATN and 31 are T-cell renal rejection transplants. The DW-MRI data of these patients has been acquired at different b-values ranging from b0 to b1000 using a SIGNA Horizon Scanner (General Electric Medical Systems), with the following parameters: TR = 8000 ms; FOV = 32 cm; in-plan resolution of 1.25 × 1.25 mm2; slice thickness = 4 mm; inter-slice gap = 0 mm; and two excitations. Since the segmentation is an essential step in developing any CAD system for renal rejection types classification, we tested the performance of our segmentation approach on the aforementioned DW-MRI data. Figure 16 shows some coronal segmentation results for one subject acquired at different b-values. The accuracy of the proposed segmentation method has been evaluated using the percentage Dice similarity coefficient (DSC%) [151], the 95-percentile modified Hausdorff distance (MHD) [152], and the percentage of the absolute kidney volume difference (AKVD%). Metrics were computed by comparing the ground truth segmentation to results obtained by the developed segmentation technique. The ground truth segmentations were manually created by an MR expert. The DSC%, MHD mm, and AKVD% statistics obtained for all test data sets for our segmentation approach of the kidney are 92.37±2.34%, 6.87±2.37 mm, and 14.1±4%, respectively, which confirms high accuracy and robustness of the presented segmentation method, even at the higher b-values.

For more details about the kidney segmentation evaluation metrics and kidney segmentation results, see [138].

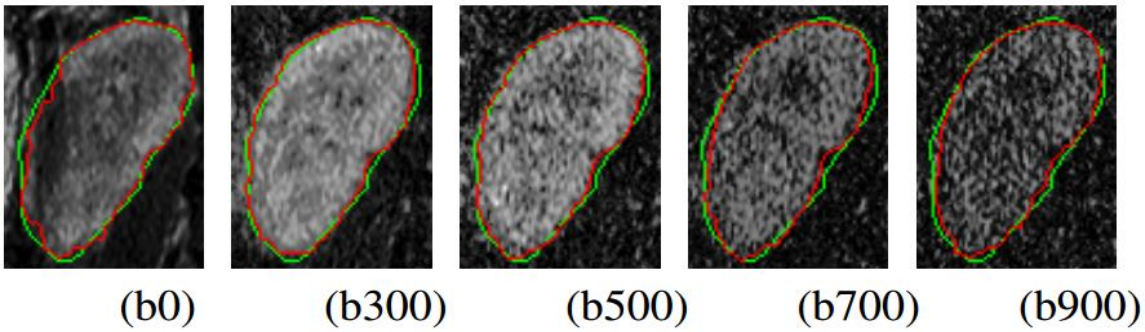

Figure 16. A sample coronal cross-sectional segmentation results of our segmentation technique for one subject using DW-MRI data at b-values of (e.g., b0, b300, b500, b700, and b900) s/mm^2.

Following kidney segmentation, our CAD system classifies the rejection transplants types. Figure 17 shows a sample of CDFs constructed for an ATN rejection subject vs. a T-cell rejection one at b-values of (b50, b100, b200, and b300). Obviously, the CDFs of the two different groups are completely separable; thus, those CDFs could be used as discriminatory features for classification between the two kidney transplant rejection groups. By using a SNCAE-based classifier and the previously constructed 8 CDFs along with a leave-one-subject-out classification scenario, our approach has

correctly classified 98% of the data, namely, 8 out of 8 of ATN and 30 out of 31 of T-cell rejection kidney transplants.

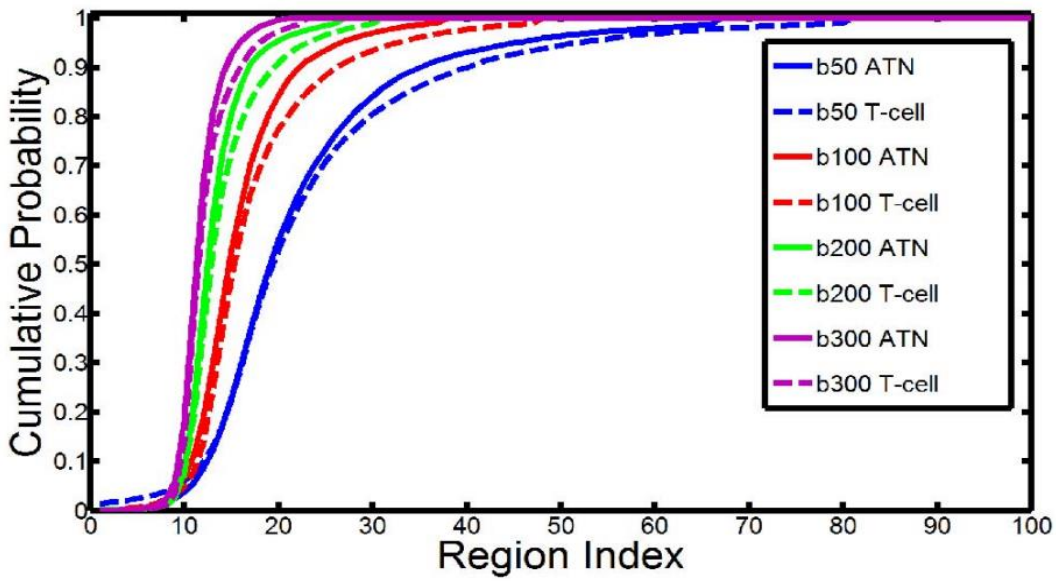

Figure 17. A sample of CDFs for two rejection subjects (ATN in solid lines and T-cell in dashed lines) at b-values of (b50, b100, b200, and b300) s/mm2.

To validate our results, we compared the results obtained from the developed SNCAE classifier with ten other well-known classi- fiers provided by the Weka tool [153]: MultiClassClassifier (MCC), HyperPipes (HPs), IB1, K-nearest IBK, NNge, Logistic (Lg), END, J48, RandomTree (RT), and RandomForest (RF). Table 4 compares our classifier to these ten classifiers in terms of the number of ATN rejection subjects that have been correctly classified (ATN/8), the number of T-cell rejection subjects that have been correctly classi- fied (T-cell/31), and the total classification accuracy (Accuracy%). As shown in Table 4, our classifier provides the best diagnostic accuracy of 98%, which confirms the robustness and the accuracy of the developed classifier. These initial

diagnostic results hold promise of the proposed CAD system as a reliable non-invasive diagnostic tool.

Table 4

Diagnostic accuracy of our CAD system using SNCAE classifier and different classifiers from Weka tool [150].

	Different Types of Weka tool classifiers										
	MCC	HPs	IB1	IBK	NNge	Lg	END	J48	RT	RF	**SNCAE**
ATN/8	8	5	8	8	4	8	7	7	6	7	**8**
T-cell/31	25	31	27	27	31	25	28	28	24	30	**30**
Accuracy %	85	92	90	90	90	85	90	90	77	95	**98**

E. Conclusions

The CAD system presented here has been demonstrated to be capable of early diagnosis and classification of renal transplant rejection types from 4D DW-MRI data. The CAD system combines existing and new techniques for non-rigid image alignment, kidney segmentation with a deformable boundary, estimation of spatial diffusion parameters (ADCs), and an SNCAE classification of the rejection transplanted kidney status using CDFs of the ADCs as integral status descriptions. In a test on a biopsy-proven cohort of 39 participants, our system showed an overall accuracy of 98% in detecting ATN and T-cell rejection kidneys. These experimental results make the proposed framework a reliable non-invasive diagnostic tool for the early identification of renal rejection type. As a future avenue, we intend to increase the test data-sets of both ATN and T-cell rejection kidney transplant groups in order to further validate the accuracy and robustness of our framework in both segmentation of the DW-MRI and diagnosis. In addition, we intend to account for other different causes of rejection such as drug toxicity and viral infection, thus increasing

the number of rejection groups to four, and then explore the ability of our framework to distinguish between those four types of renal rejection.

CHAPTER IV

CONCLUSION AND FUTURE WORK

This thesis focused on why it is important that an alternative to renal biopsies needs to be developed that is non-invasive, less expensive economically, and saves time in diagnosing. The computer aided diagnostic system is that alternative. The second part also provide which parameters were the best for diagnosing. The third part of this thesis demonstrated that not only can the CAD system diagnose between rejected and non-rejected but it shows a high level of accuracy in differentiating between ATN and T-cell mediated rejection. With this thesis, it is clear to see that the CAD system using DW-MRI will one day be an alternative in diagnosing renal graft dysfunction.

As already stated before some future steps that will be taken for this study will be to obtain a larger more divers cohort of patients with are more verity of kidney disorder (i.e. nephrotoxic mediated rejection, acute kidney disease, and pre-clinical rejection). It is our goal as well to analyze smaller b-values and to confirm accuracy of both diagnosing and differentiating different types of graft dysfunction.

However, though this thesis focused on diagnosing disorders of the kidney [154-163], this work is not limited to diagnosing renal graft dysfunction. This work can be extended to apply to analyzing and diagnosing disorders of the prostate [164-176], heart [177-200], retina [201-207], lungs [208-249], and conditions of the brain such as Autism

and Dyslexia [250-286].

In America prostate cancer is the second cancer-associated cause of deaths among males. A study form 2015 found that there was about 220,800 new cases diagnosed that year. The study also found that the mortality rate for prostate cancer was estimated to be at 27,540. Luckily, if prostate cancer is detected early it can increase the rate of survival since doctors can provide better treatment at earlier stages of the disease. This fact has provided incentive for researchers to develop non-invasive diagnostic CAD systems to detect prostate cancer. Such works can be found in [164-176].

Another application CAD systems can be used for is assessing the heart. With CAD systems the heart can be assessed for myocardial perfusion. CAD systems can also aid in the diagnosis, prognosis, and management of ischemic heart disease in patients. Works on this subject can be found [177-200].

Retinal abnormalities is another application that is implementing the use of CAD systems. Many ophthalmologists utilize visual interpretation to identify diseases of the retina. This however, can prove inaccurate and cause the patent to be missed diagnosed and at times lead to fatality. Due to this fact, there is a great need for CAD systems in this field of study. Works on this CAD systems in retinal abnormalities can be found [201-207].

Disorders of the lungs can also be have also been researched using CAD systems. The main side effect of lung cancer treatment is lung injury caused by radiation therapy. However, higher doses of radiation increase the effectiveness of controlling the size of the cancer while at the same time injuring normal lung tissue. Almost 37% of patients who undergo radiation will develop some form of lung injury. CAD systems can provide early

detection of lung injury and improve management of radiation treatment. Studies in this subject can be found [208-249].

Finally, CAD systems can one day be used in diagnosing conditions of the brain such as Autism and Dyslexia. Autism is a neuro-development disorder with a multitude of symptoms. The most dormant of the symptoms being that of repetitive behavior and social impairments. Dyslexia on the other hand is a condition that causes the patient to not read, right, or spell at an age-appropriate level despite maintain a normal to even high intelligence in all other areas. By detecting these conditions early in life and schooling children and parents can be provided with the necessary resources to live a somewhat normal lifestyle with their disability. A CAD system that scans the brain can provide the patent with early diagnosis and provide a better understanding in how these conditions manifest in the brain. Such studies are included [250-286].

The field of medicine is ever changing and with these CAD systems we are entering a new frontier that will improve the way doctors practice medicine and prolong the life's' of patients.

REFERENCES

1. Kukla, A., M. Adulla, J. Pascual, M. Samaniego, L. Nanovic, B.N. Becker, and A. Djamali, *CKD stage-to-stage progression in native and transplant kidney disease.* Nephrol Dial Transplant, 2008. 23(2): p. 693-700.
2. *About Chronic Kidney Disease*. 2016 [cited 2016 May 2, 2016]; Available from: https://www.kidney.org/kidneydisease/aboutckd.
3. Foundation, N.K. *Organ Donation and Transplantion Statisitcs*. 2016 [cited 2016 May 25 2016]; Available from: https://www.kidney.org/news/newsroom/factsheets/Organ-Donation-and-Transplantation-Stats.
4. Myers, G.L., M.G. Miller, J. Coresh, J. Fleming, N. Greenberg, et al., *Recommendations for improving serum creatinine measurment: A Report from the labratory working group of the natonal kidney diesease education program*, in *Clinical Chemistry 52*. 2006. p. 1, 5-18.
5. Widmaier, E.P., H. Raff, K.T. Strang, and A.J. Vander, *Vander's human physiology: the mechanisms of body function*. 2008, Boston: McGraw-Hill Higher Education.
6. Mostapha, M., F. Khalifa, A. Alansary, A. Soliman, J. Suri, and A.S. El-Baz, *Computer-Aided Diagnosis Systems for Acute Renal Transplant Rejection: Challenges and Methodologies*, in *Abdomen and Thoracic Imaging: An Engineering & Clinical Perspective*, S.A. El-Baz, L. Saba, and J. Suri, Editors. 2014, Springer US: Boston, MA. p. 1-35.
7. Tortora, G.J. and N.P. Anagnostakos, *The Urinary System*, in *Princeiples of Anatomy and Physiology*, Third, Editor. 1981: New York, NY. p. 669-683.
8. Burwell, S.M., T.R. Frieden, and C.J. Rothwell, *Health, United States, 2015: With Special Feature on Racial and Ethnic Health Disparities.* U.S. Department of Health and Human Services: Centers for Disease Control and Prevention: National Center of Health Statistics, 2016.
9. Stanifer, J.W., E.L. Turner, J.R. Egger, N. Thielman, F. Karia, V. Maro, K. Kilonzo, U.D. Patel, and K. Yeates, *Knowledge, Attitudes, and Practices Associated with Chronic Kidney Disease in Northern Tanzania: A Community-Based Study.* PloS One, 2016. 11(6): p. e0156336.
10. Mendoza, S.A., *Nephrotoxic drugs.* Pediatric Nephrology, 1988. 2(4): p. 466-76.
11. Gregorio T Obrador, M., MPH; Brian JG Pereira MD, *Screening for chronic kidney disease*, in *UpToDate*. 2015, UpToDate: Waltham, MA.
12. Medical Education Institute, I. *10 Symptoms of Kidney Disease*. Life Options [Online] 2016 Febuary 5, 2016 [cited 2016 Febuary 5, 2016]; Online:[Available from: http://lifeoptions.org/kidneyinfo/ckdinfo.php?page=3.
13. Papadakis, M.A. and S.J. Mcphee, *Quick Medical Diagnosis & Treatment 2015*. 2015 ed. 2015, New York, NY: McGraw-Hill.

14. Stephen Textor, M. and M. Lionel U Mailoux, FACP, *Clinical manifestations and diagnosis of chronic kidney disease resulting from atherosclerotic renal artery stenosis*, in *UpToDate*. 2016, UpToDate: Online.
15. Sara N Davison, M., MHSc, FRCP (C), *Management of chronic pain in chronic kidney disease*. 2015, UpToDate: Online.
16. *Dialysis*. 2012 March 1, 2012 [cited 2016 May 3, 2016]; Available from: http://www.niddk.nih.gov/health-information/health-communication-programs/nkdep/learn/living/kidney-failure/dialysis/Pages/dialysis.aspx
17. Desai, M.M. and I.S. Gill, *Laparoscopic surgery in renal transplant recipients.* The Urologic clinics of North America, 2001. 28(4): p. 759-67.
18. Mobley, C.M. and S.J. Pelletier, *Current Procedures: Surgery*, in *Current Procedures: Surgery*, R.M. Minter and G.M. Doherty, Editors. 2010, McGraw-Hill: New York, NY.
19. Nadig, S.N. and J.D. Punch, *Organ Transplantation*, in *CURRENT Diagnosis & Treatment*, G.M. Doherty, Editor. 2015, McGraw-Hill: New York, NY.
20. Gruessner, A.C., *Schwartz's Principles of Surgery*, in *Schwartz's Principles of Surgery*, C. Brunicardi, Editor. 2014, Mcgraw-Hill: New York, NY.
21. *The National Waiting List*. [Web Page] 2016 December 2015 [cited 2016 April 14, 2016]; Available from: http://www.transplantliving.org/before-the-transplant/getting-on-the-list/the-national-waiting-list/.
22. Foundation, N.K. *NKF: CARE AFTER KIDNEY TRANSPLANT*. 2015 2015; Available from: http://www.kidney.org/atoz/content/immunosuppression.
23. Hospital, S.C.s. *Kidney: Clinic and Follow-Up Visits After Kidney Transplation*. 2016 [cited 2016 May 18, 2016]; Available from: http://www.seattlechildrens.org/clinics-programs/transplant/kidney/clinic-followup-visits-after-kidney-transplantation/.
24. Kasiske, B.L., M.G. Zeier, J.R. Chapman, J.C. Craig, H. Ekberg, et al., *KDIGO clinical practice guideline for the care of kidney transplant recipients: a summary.* Kidney International, 2010. 77(4): p. 299-311.
25. Streeter, E.H., D.M. Little, D.W. Cranston, and P.J. Morris, *The urological complications of renal transplantation: a series of 1535 patients.* BJU International, 2002. 90(7): p. 627-34.
26. Akbar, S.A., S.Z.H. Jafri, M.A. Amendola, B.L. Madrazo, R. Salem, and K.G. Bis, *Complications of Renal Transplantation.* Radiographics, 2005. 25(5): p. 1335-1356.
27. Park, S.B., J.K. Kim, and K.S. Cho, *Complications of renal transplantation: ultrasonographic evaluation.* Journal of Ultrasound in Medicine, 2007. 26(5): p. 615-33.
28. Richard, H.M., *Perirenal transplant fluid collections.* Semin Intervent Radiol, 2004. 21(4): p. 235-7.
29. Lutz, J. and U. Heemann, *Tumours after kidney transplantation.* Curr Opin Urol, 2003. 13(2): p. 105-9.
30. Wong, G. and J.R. Chapman, *Cancers after renal transplantation.* Transplantation Reviews (Orlando, Fla.), 2008. 22(2): p. 141-9.
31. Ramos, E.L. and C.C. Tisher, *Recurrent diseases in the kidney transplant.* American Journal of Kidney Diseases, 1994. 24(1): p. 142-54.
32. *Special Issue: KDIGO Clinical Practice Guideline for the Care of Kidney Transplant Recipients.* American Journal of Transplantation, 2009. 9: p. S33-S37.

33. Muglia, V.F., S.R. Teixeira, E.A. RomRomão, M.F. Cassini, M.F.d. Andrade, M. Kato, M.E.P. Nardin, and S.T. Jr, *Imaging in Kidney Transplantation*, in *Current Issues and Future Direction in Kidney Transplantation*, T. Rath, Editor. 2013.
34. Collins, A.J., R.N. Foley, B. Chavers, D. Gilbertson, C. Herzog, et al., *'United States Renal Data System 2011 Annual Data Report: Atlas of chronic kidney disease & end-stage renal disease in the United States.* American Journal of Kidney Diseases, 2012. 59(1 Suppl 1): p. A7, e1-420.
35. Abbas, A.K., A.H.H. Lichtman, and S. Pilai, *Transplantion Immunology*, in *Cellular and Molecular Immunology*. 2015. p. 359-382.
36. Flechner, S.M., *Renal Transplantation*, in *Smith and Tanagho's General Urology*, J.W. McAninch and T.F. Lue, Editors. 2013, McGraw-Hill: New York, NY. p. AcessMedicine.
37. Daniel C Brennan, M., FACP; Emilio Ramos, MD, FACP, *Management of BK virus-induced (polyomavirus-induced) nephropathy in kidney transplantation*. 2015, UpToDate: Waltham, MA.
38. Montgomery, R.A., A.A. Zachary, L.C. Racusen, M.S. Leffell, K.E. King, J. Burdick, W.R. Maley, and L.E. Ratner, *Plasmapheresis and intravenous immune globulin provides effective rescue therapy for refractory humoral rejection and allows kidneys to be successfully transplanted into cross-match-positive recipients.* Transplantation, 2000. 70(6): p. 887-95.
39. Pascual, M., S. Saidman, N. Tolkoff-Rubin, W.W. Williams, S. Mauiyyedi, et al., *Plasma exchange and tacrolimus-mycophenolate rescue for acute humoral rejection in kidney transplantation.* Transplantation, 1998. 66(11): p. 1460-4.
40. Abbas, A.K., A.H.H. Lichtman, and S. Pilai, *Lymphocyte Developemtn and Antigen Receptor Gene Rearrangment*, in *Cellular and Molecular Immunology*. 2015. p. 171-198.
41. W James Chon, M., FACP; Daniel C Brennan, MD, FACP, *Acute renal allograft rejection: Treatment*. 2014, UpToDate: Waltham, MA.
42. Jordan, M.L., R. Shapiro, C.A. Vivas, V.P. Scantlebury, P. Rhandhawa, et al., *FK506 "rescue" for resistant rejection of renal allografts under primary cyclosporine immunosuppression.* Transplantation, 1994. 57(6): p. 860-5.
43. Jordan, M.L., R. Naraghi, R. Shapiro, D. Smith, C.A. Vivas, et al., *Tacrolimus rescue therapy for renal allograft rejection--five-year experience.* Transplantation, 1997. 63(2): p. 223-8.
44. Burdmann, E.A., T.F. Andoh, L. Yu, and W.M. Bennett, *Cyclosporine nephrotoxicity.* Seminars in Nephrology, 2003. 23(5): p. 465-76.
45. William M Bennett, M., *Cyclosporine and tacrolimus nephrotoxicity*. 2015, UpToDate: Waltham, MA.
46. de Mattos, A.M., A.J. Olyaei, and W.M. Bennett, *Nephrotoxicity of immunosuppressive drugs: long-term consequences and challenges for the future.* American Journal of Kidney Diseases, 2000. 35(2): p. 333-46.
47. Weikert, B.C. and E.A. Blumberg, *Viral infection after renal transplantation: surveillance and management.* Clinical Journal of the American Society of Nephrology, 2008. 3 Suppl 2: p. S76-86.

48. Ursula C. Brewster, M. and M. Mark Perazella, FACP, FASN, *Chronic Kidney Disease and Dialysis* in *Principles and Practice of Hospital Medicine*, S.C. McKean and E. al., Editors. 2012, McGraw-Hill: New York, NY. p. AccessMedicine.
49. Diseases, T.N.I.o.D.a.D.a.K. *Estimating Glomerular Filtration Rate (GFR)*. 2015 [cited 2015 October 4, 2015]; Available from: http://www.niddk.nih.gov/health-information/health-communication-programs/nkdep/lab-evaluation/gfr/estimating/Pages/estimating.aspx.
50. Kathleen Deska Pagana, P., RN and M. Timothy J. Pagana, FACS, *Diagnostic & Laboratory Test Reference*, in *Diagnostic & Laboratory Test Reference*. 2013, Elsevier Inc.: Riverport Lane St. Louis,Missouri 63043. p. 278 and 794.
51. *Blood Smear*. 2014 Febuary 24, 2014 [cited 2015 Octobeer 16, 2015]; Available from: http://www.pennmedicine.org/encyclopedia/em_PrintArticle.aspx?gcid=003665.
52. Adamson, J.W. and D.L. Longo, *Anemia and Polycythemia*, in *Harrison's Principles of Internal Medcine*, D. Kasper, Editor. 2015, McGraw-Hill: New York, NY. p. AcessMedicine.
53. Fogo, A.B. and E.G. Nelison, *Atlas of Urinary Sediments and Renal Biopsies*, in *Harrison's Principles of Internal Medicine*, D. Kasper and E. al., Editors. 2015, McGraw-Hill: New York, NY.
54. Jha, V., *Post-transplant infections: An ounce of prevention.* Indian Journal of Nephrology, 2010. 20(4): p. 171-8.
55. Staff, M.C. *Test and Procedures: Kidney biopsy: Results*. Test and Procedures: Kidney biopsy 2016 [cited 2016 April 22, 2016]; Available from: http://www.mayoclinic.org/tests-procedures/kidney-biopsy/basics/results/prc-20018979.
56. Chesney, D.S., B.H. Brouhard, and R.J. Cunningham, *Safety and cost effectiveness of pediatric percutaneous renal biopsy.* Pediatric nephrology (Berlin, Germany), 1996. 10(4): p. 493-5.
57. Brown, E.D., M.Y. Chen, N.T. Wolfman, D.J. Ott, and N.E. Watson, Jr., *Complications of renal transplantation: evaluation with US and radionuclide imaging.* Radiographics, 2000. 20(3): p. 607-22.
58. Giele, E.L.W., *Computer methods for semi-automatic MR rengram dtermination.* Technishe Universiteit Eindhoven, 2002.
59. Taylor, A., Jr. and J.V. Nally, *Clinical applications of renal scintigraphy.* AJR: American Journal of Roentgenology, 1995. 164(1): p. 31-41.
60. Heaf, J.G. and J. Iversen, *Uses and limitations of renal scintigraphy in renal transplantation monitoring.* European Journal of Nuclear Medicine, 2000. 27(7): p. 871-9.
61. Sebastia, C., S. Quiroga, R. Boye, C. Cantarell, M. Fernandez-Planas, and A. Alvarez, *Helical CT in renal transplantation: normal findings and early and late complications.* Radiographics, 2001. 21(5): p. 1103-17.
62. Grabner, A., D. Kentrup, U. Schnockel, M. Schafers, and S. Reuter, *Non-invasive diagnosis of acute renal allograft rejection- Special focus on gamma scintigraph and positron emission tomography.* Current Issues and Future Direction in Kidney Transplantation, 2013.
63. Mostapha, M., F. Khalifa, A. Alansary, A. Soliman, J. Suri, and A.S. El-Baz, *Computer-Aided Diagnosis Systems for Acute Renal Transplant Rejection: Challenges*

and Methodologies, in *Abdomen and Thoracic Imaging: An Engineering & Clinical Perspective*, S.A. El-Baz, L. Saba, and J. Suri, Editors. 2014, Springer US: Boston, MA. p. 1-35.
64. Chudek, J., A. Kolonko, R. Krol, J. Ziaja, L. Cierpka, and A. Wiecek, *The intrarenal vascular resistance parameters measured by duplex Doppler ultrasound shortly after kidney transplantation in patients with immediate, slow, and delayed graft function.* Transplantation Proceedings, 2006. 38(1): p. 42-5.
65. Saracino, A., G. Santarsia, A. Latorraca, and V. Gaudiano, *Early assessment of renal resistance index after kidney transplant can help predict long-term renal function.* Nephrology, Dialysis, Transplantation, 2006. 21(10): p. 2916-20.
66. Kramann, R., D. Frank, V.M. Brandenburg, N. Heussen, J. Takahama, T. Kruger, J. Riehl, and J. Floege, *Prognostic impact of renal arterial resistance index upon renal allograft survival: the time point matters.* Nephrology, Dialysis, Transplantation, 2012. 27(10): p. 3958-63.
67. Krejci, K., J. Zadrazil, T. Tichy, S. Al-Jabry, V. Horcicka, P. Strebl, and P. Bachleda, *Sonographic findings in borderline changes and subclinical acute renal allograft rejection.* European Journal of Radiology, 2009. 71(2): p. 288-95.
68. Damasio, M.B., G. Cittadini, D. Rolla, F. Massarino, N. Stagnaro, M. Gherzi, E. Paoletti, and L.E. Derchi, *Ultrasound findings in dual kidney transplantation.* La Radiologia Medica, 2013. 118(1): p. 14-22.
69. Shebel, H.M., A. Akl, A. Dawood, T.A. El-Diasty, A.A. Shokeir, and M.A. Ghoneim, *Power doppler sonography in early renal transplantation: does it differentiate acute graft rejection from acute tubular necrosis?* Saudi Journal of Kidney Diseases and Transplantation, 2014. 25(4): p. 733-40.
70. Fischer, T., S. Filimonow, J. Dieckhofer, T. Slowinski, M. Muhler, et al., *Improved diagnosis of early kidney allograft dysfunction by ultrasound with echo enhancer--a new method for the diagnosis of renal perfusion.* Nephrology, Dialysis, Transplantation, 2006. 21(10): p. 2921-9.
71. Benozzi, L., G. Cappelli, M. Granito, D. Davoli, D. Favali, M.G. Montecchi, A. Grossi, P. Torricelli, and A. Albertazzi, *Contrast-enhanced sonography in early kidney graft dysfunction.* Transplantation Proceedings, 2009. 41(4): p. 1214-5.
72. Schwenger, V., V. Hankel, J. Seckinger, S. Macher-Goppinger, C. Morath, M. Zeisbrich, M. Zeier, and L.P. Kihm, *Contrast-enhanced ultrasonography in the early period after kidney transplantation predicts long-term allograft function.* Transplantation Proceedings, 2014. 46(10): p. 3352-7.
73. Gocze, I., P. Renner, B.M. Graf, H.J. Schlitt, T. Bein, and K. Pfister, *Simplified approach for the assessment of kidney perfusion and acute kidney injury at the bedside using contrast-enhanced ultrasound.* Intensive Care Medicine, 2015. 41(2): p. 362-3.
74. Jin, Y., C. Yang, S. Wu, S. Zhou, Z. Ji, T. Zhu, and W. He, *A novel simple noninvasive index to predict renal transplant acute rejection by contrast-enhanced ultrasonography*. Transplantation, 2015. 99(3): p. 636-41.
75. Kirkpantur, A., R. Yilmaz, D.E. Baydar, T. Aki, B. Cil, et al., *Utility of the Doppler ultrasound parameter, resistive index, in renal transplant histopathology.* Transplantation Proceedings, 2008. 40(1): p. 104-6.
76. Seiler, S., S.M. Colbus, G. Lucisano, K.S. Rogacev, M.K. Gerhart, M. Ziegler, D. Fliser, and G.H. Heine, *Ultrasound renal resistive index is not an organ-specific*

predictor of allograft outcome. Nephrology, Dialysis, Transplantation, 2012. 27(8): p. 3315-20.
77. Cosgrove, D.O. and K.E. Chan, *Renal transplants: What ultrasound can and cannot do.* Ultrasound Quarterly, 2008. 24(2): p. 77-78.
78. Mansfield, P., *Snapshot magnetic resonance imaging (Nobel lecture).* Angewandte Chemie. International Ed. In English, 2004. 43(41): p. 5456-64.
79. de Priester, J.A., J.A. den Boer, M.H. Christiaans, A.G. Kessels, E.L. Giele, A. Hasman, H.P. van Hooff, and J.M. van Engelshoven, *Automated quantitative evaluation of diseased and nondiseased renal transplants with MR renography.* Journal of Magnetic Resonance Imaging, 2003. 17(1): p. 95-103.
80. Yuksel, S.E., A. El-Baz, A.A. Farag, M.A. El-Ghar, T.A. Eldiasty, and M.A. Ghoneim, *Automatic detection of renal rejection after kidney transplantation.* International Congress Series, 2005. 1281(Elsevier): p. 773-778.
81. Farag, A.A., A. El-Baz, S. Yuksel, M.A. El-Ghar, and T. Eldiasty, *A framework for the detection of acute rejection with Dynamic Contrast Enhanced Magnetic Resonance Imaging.* Arlinton, Virginia, USA, 2006(April 6-9): p. 418–421.
82. El-Baz, A., A. Farag, R. Fahmi, S. Yuksel, M.A. El-Ghar, and T. Eldiasty, *Image analysis of renal DCE MRI for the detection of acute renal rejection.* Hong Kong, 2006: p. 822-825.
83. El-Baz, A., A. Farag, R. Fahmi, S. Yuksel, W. Miller, M.A. El-Ghar, T. El-Diasty, and M. Ghoneim, *A new CAD system for the evaluation of kidney diseases using DCE-MRI.* Copenhagen, Denmark, 2006: p. 446-453.
84. El-Baz, A., A.A. Farag, S.E. Yuksel, M.E.A. El-Ghar, T.A. Eldiasty, and M.A. Ghoneim, *Application of deformable models for the detection of acute renal rejection.* In Farag, A.A., Suri, J.S., eds.: Deformable Models, 2007. 1(293-333): p. 293.
85. El-Baz, A., G. Gimel'farb, and M.A. El-Ghar, *New motion correction models for automatic identification of renal transplant rejection.* Medical Image Computing and Computer-Assisted Intervention, 2007. 10(Pt 2): p. 235-43.
86. El-Baz, A., G. Gimel'farb, and M.A. El-Ghar, *A novel image analysis approach for accurate identification of acute renal rejection.* San Diego, California, USA, 2008.
87. El-Baz, A., G. Gimel'farb, and M.A. El-Ghar, *Image analysis approach for identification of renal transplant rejection.* Tampa, Florida, USA, 2008: p. 1-4.
88. Rusinek, H., Y. Boykov, M. Kaur, S. Wong, L. Bokacheva, J.B. Sajous, A.J. Huang, S. Heller, and V.S. Lee, *Performance of an automated segmentation algorithm for 3D MR renography.* Magnetic Resonance in Medicine, 2007. 57(6): p. 1159-67.
89. Zikic, D., S. Sourbron, X. Feng, H.J. Michaely, A. Khamene, and N. Navab, *Automatic alignment of renal DCE-MRI image series for improvement of quantitative tracer kinetic studies.* Proc. of SPIE, Medical Imaging: Image Processing, 2008. 6914(International Society for Optics and Photonics): p. 1-8.
90. de Senneville, B.D., I.A. Mendichovszky, S. Roujol, I. Gordon, C. Moonen, and N. Grenier, *Improvement of MRI-functional measurement with automatic movement correction in native and transplanted kidneys.* Journal of Magnetic Resonance Imaging, 2008. 28(4): p. 970-8.
91. Aslan, M.S., H.A. El Munim, A.A. Farag, and M.A. El-Ghar, *Assessment of kidney function using dynamic contrast enhanced mri techniques.* Biomedical Image Analysis

and Machine Learning Technologies: Applications and Techniques: Applications and Techniques, 2009: p. 214.
92. Anderlik, A., A. Munthe-Kaas, O. Oye, E. Eikefjord, J. Rorvik, D. Ulvang, F. Zollner, and A. Lundervold, *Quantitative assessment of kidney function using dynamic contrast enhanced MRI-Steps towards an integrated software prototype.* Proceedings of the 6th International Symposium on Image and Signal Processing and Analysis (ISPA'09), 2009. Salzburg, Austria: p. 575–581.
93. Sourbron, S.P., H.J. Michaely, M.F. Reiser, and S.O. Schoenberg, *MRI-measurement of perfusion and glomerular filtration in the human kidney with a separable compartment model.* Investigative Radiology, 2008. 43(1): p. 40-8.
94. Zollner, F.G., R. Sance, P. Rogelj, M.J. Ledesma-Carbayo, J. Rorvik, A. Santos, and A. Lundervold, *Assessment of 3D DCE-MRI of the kidneys using non-rigid image registration and segmentation of voxel time courses.* Computerized Medical Imaging and Graphics, 2009. 33(3): p. 171-81.
95. MacQueen, J.B., *Some methods for classification and analysis of multivariate observations*. Some methods for classification and analysis of multivariate observations , University of California Press, 1967: p. 281–297.
96. Wentland, A.L., E.A. Sadowski, A. Djamali, T.M. Grist, B.N. Becker, and S.B. Fain, *Quantitative MR measures of intrarenal perfusion in the assessment of transplanted kidneys: initial experience.* Academic Radiology, 2009. 16(9): p. 1077-85.
97. El-Ghar, M.A., A. Farag, T. El-Diasty, A. Shokeir, H. Refaie, Y. Osman, T. Mohsen, and M. Ghoneim, *Computer aided detection of acute renal allograft dysfunction using dynamic contrast enhanced MRI.* The Egyptian Journal of Radiology and Nuclear Medicine, 2011. 42(3): p. 443-449.
98. Yamamoto, A., J.L. Zhang, H. Rusinek, H. Chandarana, P.H. Vivier, et al., *Quantitative evaluation of acute renal transplant dysfunction with low-dose three-dimensional MR renography.* Radiology, 2011. 260(3): p. 781-9.
99. Hodneland, E., A. Kjorstad, E. Andersen, J. Monssen, A. Lundervold, J. Rorvik, and A. Munthe-Kaas, *In vivo estimation of glomerular filtration in the kidney using DCE-MRI.* Proceedings of the 7th International Symposium on Image and Signal Processing Analysis (ISPA'11), Dubrovnik, Croatia, 2011: p. 755-761.
100. Positano, V., I. Bernardeschi, V. Zampa, M. Marinelli, L. Landini, and M.F. Santarelli, *Automatic 2D registration of renal perfusion image sequences by mutual information and adaptive prediction.* MAGMA, 2013. 26(3): p. 325-35.
101. Khalifa, F., A. El-Baz, G. Gimel'farb, and M. Abu El-Ghar, *Non-invasive image-based approach for early detection of acute renal rejection.* Medical Image Computing and Computer-Assisted Intervention, 2010. 13(Pt 1): p. 10-8.
102. Khalifa, F., G.M. Beache, M.A. El-Ghar, T. El-Diasty, G. Gimel'farb, M. Kong, and A. El-Baz, *Dynamic contrast-enhanced MRI-based early detection of acute renal transplant rejection.* IEEE Transactions on Medical Imaging, 2013. 32(10): p. 1910-27.
103. Khalifa, F., G.M. Beache, G. Gimel'farb, G.A. Giridharan, and A. El-Baz, *Accurate automatic analysis of cardiac cine images.* IEEE Transactions on Biomedical Engineering, 2012. 59(2): p. 445-55.

104. Khalifa, F., G.M. Beache, M. Nitzken, G. Gimel'farb, G.A. Giridharan, and A. El-Baz, *Automatic analysis of left ventricle wall thickness using short-axis cine CMR images.* Chicago, Illinois, USA, 2011: p. 1306–1309.
105. Elbeltagi, E., T. Hegazy, and D. Grierson, *Comparison among five evolutionary-based optimization algorithms.* Adv. Eng. Informat, 2005. 19(1): p. 43–53.
106. Khalifa, F., M. Abou El-Ghar, B. Abdollahi, H.B. Frieboes, T. El-Diasty, and A. El-Baz, *A comprehensive non-invasive framework for automated evaluation of acute renal transplant rejection using DCE-MRI.* NMR in Biomedicine, 2013. 26(11): p. 1460-70.
107. Liu, G., F. Han, W. Xiao, Q. Wang, Y. Xu, and J. Chen, *Detection of renal allograft rejection using blood oxygen level-dependent and diffusion weighted magnetic resonance imaging: a retrospective study.* BMC Nephrology, 2014. 15: p. 158.
108. Djamali, A., E.A. Sadowski, M. Samaniego-Picota, S.B. Fain, R.J. Muehrer, S.K. Alford, T.M. Grist, and B.N. Becker, *Noninvasive assessment of early kidney allograft dysfunction by blood oxygen level-dependent magnetic resonance imaging.* Transplantation, 2006. 82(5): p. 621-8.
109. Han, F., W. Xiao, Y. Xu, J. Wu, Q. Wang, H. Wang, M. Zhang, and J. Chen, *The significance of BOLD MRI in differentiation between renal transplant rejection and acute tubular necrosis.* Nephrology, Dialysis, Transplantation, 2008. 23(8): p. 2666-72.
110. Sadowski, E.A., A. Djamali, A.L. Wentland, R. Muehrer, B.N. Becker, T.M. Grist, and S.B. Fain, *Blood oxygen level-dependent and perfusion magnetic resonance imaging: detecting differences in oxygen bioavailability and blood flow in transplanted kidneys.* Magnetic Resonance Imaging, 2010. 28(1): p. 56-64.
111. Yablonskiy, D.A. and E.M. Haacke, *Theory of NMR signal behavior in magnetically inhomogeneous tissues: the static dephasing regime.* Magnetic Resonance in Medicine, 1994. 32(6): p. 749-63.
112. Michaely, H.J., K.A. Herrmann, K. Nael, N. Oesingmann, M.F. Reiser, and S.O. Schoenberg, *Functional renal imaging: nonvascular renal disease.* Abdominal Imaging, 2007. 32(1): p. 1-16.
113. Eisenberger, U., H.C. Thoeny, T. Binser, M. Gugger, F.J. Frey, C. Boesch, and P. Vermathen, *Evaluation of renal allograft function early after transplantation with diffusion-weighted MR imaging.* European Radiology, 2010. 20(6): p. 1374-83.
114. Hueper, K., A.A. Khalifa, J.H. Brasen, V.D. Vo Chieu, M. Gutberlet, et al., *Diffusion-Weighted imaging and diffusion tensor imaging detect delayed graft function and correlate with allograft fibrosis in patients early after kidney transplantation.* Journal of Magnetic Resonance Imaging, 2016.
115. Xu, J.J., W.B. Xiao, L. Zhang, and M.M. Zhang, *[Value of diffusion-weighted MR imaging in diagnosis of acute rejection after renal transplantation]*. Zhejiang Da Xue Xue Bao. Yi Xue Ban. Journal of Zhejiang University. Medical Sciences, 2010. 39(2): p. 163-7.
116. Palmucci, S., L.A. Mauro, P. Veroux, G. Failla, P. Milone, et al., *Magnetic resonance with diffusion-weighted imaging in the evaluation of transplanted kidneys: preliminary findings.* Transplantation Proceedings, 2011. 43(4): p. 960-6.

117. Palmucci, S., L.A. Mauro, G. Failla, P.V. Foti, P. Milone, et al., *Magnetic resonance with diffusion-weighted imaging in the evaluation of transplanted kidneys: updating results in 35 patients.* Transplantation Proceedings, 2012. 44(7): p. 1884-8.
118. Vermathen, P., T. Binser, C. Boesch, U. Eisenberger, and H.C. Thoeny, *Three-year follow-up of human transplanted kidneys by diffusion-weighted MRI and blood oxygenation level-dependent imaging.* Journal of Magnetic Resonance Imaging, 2012. 35(5): p. 1133-8.
119. Wypych-Klunder, K., A. Adamowicz, A. Lemanowicz, W. Szczesny, Z. Wlodarczyk, and Z. Serafin, *Diffusion-weighted MR imaging of transplanted kidneys: Preliminary report.* Pol J Radiol, 2014. 79: p. 94-8.
120. Provenzale, J.M., S.T. Engelter, J.R. Petrella, J.S. Smith, and J.R. MacFall, *Use of MR exponential diffusion-weighted images to eradicate T2 "shine-through" effect.* AJR: American Journal of Roentgenology, 1999. 172(2): p. 537-9.
121. Kaul, A., R.K. Sharma, R.K. Gupta, H. Lal, A. Yadav, D. Bhadhuria, N. Prasad, and A. Gupta, *Assessment of allograft function using diffusion-weighted magnetic resonance imaging in kidney transplant patients.* Saudi Journal of Kidney Diseases and Transplantation, 2014. 25(6): p. 1143-7.
122. Abou-El-Ghar, M.E., T.A. El-Diasty, A.M. El-Assmy, H.F. Refaie, A.F. Refaie, and M.A. Ghoneim, *Role of diffusion-weighted MRI in diagnosis of acute renal allograft dysfunction: a prospective preliminary study.* British Journal of Radiology, 2012. 85(1014): p. e206-11.
123. Thoeny, H.C., D. Zumstein, S. Simon-Zoula, U. Eisenberger, F. De Keyzer, et al., *Functional evaluation of transplanted kidneys with diffusion-weighted and BOLD MR imaging: initial experience.* Radiology, 2006. 241(3): p. 812-21.
124. Shehata, M., F. Khalifa, A. Soliman, A. Takieldeen, M.A. El-Ghar, et al., *3D diffusion MRI-based CAD system for early diagnosis of acute renal rejection.* Proc. IEEE 13th International Symposium on Biomedical Imaging, (ISBI'16), IEEE, 2016: p. 1177–1180.
125. Shehata, M., F. Khalifa, E. Hollis, A. Soliman, E. Hosseini-Asl, et al., *A New Non-Invasive Approach for Early Classification of Renal Rejetion Types Using Diffusion-Weighted MRI.* IEEE International Conference on Image Processing, 2016.
126. Beckmann, N., C. Cannet, M. Fringeli-Tanner, D. Baumann, C. Pally, C. Bruns, H.G. Zerwes, E. Andriambeloson, and M. Bigaud, *Macrophage labeling by SPIO as an early marker of allograft chronic rejection in a rat model of kidney transplantation.* Magnetic Resonance in Medicine, 2003. 49(3): p. 459-67.
127. Yang, D., Q. Ye, M. Williams, Y. Sun, T.C. Hu, D.S. Williams, J.M. Moura, and C. Ho, *USPIO-enhanced dynamic MRI: evaluation of normal and transplanted rat kidneys.* Magnetic Resonance in Medicine, 2001. 46(6): p. 1152-63.
128. Hanssen, O., P. Erpicum, P. Lovinfosse, P. Meunier, L. Weekers, L. Tshibanda, J.-M. Krzesinski, R. Hustinx, and F. Jouret, *Non-invasive approaches in the diagnosis of acute rejection in kidney transplant recipients. Part I. In vivo imaging methods.* Clinical Kidney Journal, 2016.
129. Zhang, Y., S.J. Dodd, K.S. Hendrich, M. Williams, and C. Ho, *Magnetic resonance imaging detection of rat renal transplant rejection by monitoring macrophage infiltration.* Kidney International, 2000. 58(3): p. 1300-10.

130. Erpicum, P., O. Detry, L. Weekers, C. Bonvoisin, C. Lechanteur, A. Briquet, Y. Beguin, J.M. Krzesinski, and F. Jouret, *Mesenchymal stromal cell therapy in conditions of renal ischaemia/reperfusion.* Nephrology, Dialysis, Transplantation, 2014. 29(8): p. 1487-93.
131. Ye, Q., D. Yang, M. Williams, D.S. Williams, C. Pluempitiwiriyawej, J.M. Moura, and C. Ho, *In vivo detection of acute rat renal allograft rejection by MRI with USPIO particles.* Kidney International, 2002. 61(3): p. 1124-35.
132. Hitchens, T.K., Q. Ye, D.F. Eytan, J.M. Janjic, E.T. Ahrens, and C. Ho, *19F MRI detection of acute allograft rejection with in vivo perfluorocarbon labeling of immune cells.* Magnetic Resonance in Medicine, 2011. 65(4): p. 1144-53.
133. E. Hollis et al., "Towards non-invasive diagnostic techniques for early detection of acute renal transplant rejection: A review," Egy. J. Radiol. Nucl. Med., http://dx.doi.org/10.1016/j.ejrnm.2016.11.005, 2016.
134. M. Shehata et al., "A promising non-invasive cad system for kidney function assessment," in Med. Image Comput. Comput.- Assist. Interv., 2016, vol. 9902, pp. 611–621.
135. Nicholas J Tustison, Brian B Avants, Philip A Cook, Yuanjie Zheng, Alexander Egan, Paul A Yushkevich, and James C Gee, "N4ITK: Improved N3 bias correction," IEEE Transactions on Medical Imaging, vol. 29, no. 6, pp. 1310–1320, 2010.
136. Ben Glocker, Nikos Komodakis, Nikos Paragios, and Nassir Navab, "Non-rigid registration using discrete MRFs: Application to thoracic CT images," in Proc. MICCAI Workshop on Evaluation of Methods for Pulmonary Image Registration, (MICCAI'10), 2010, pp. 147–154.
137. Mohamed Shehata, Fahmi Khalifa, Ahmed Soliman, Rahaf Alrefai, Mohamed A El-Ghar, Amy C Dwyer, Rosemary Ouseph, and Ayman El-Baz, "A novel framework for automatic segmentation of kidney from DW-MRI," in IEEE 12th Proc. International Symposuim on Biomedical Imaging (ISBI'15). IEEE, 2015, pp. 951–954.
138. Mohamed Shehata, Fahmi Khalifa, Ahmed Soliman, Rahaf Alrefai, Mohamed Abou El-Ghar, Amy C Dwyer, Rosemary Ouseph, and Ayman El-Baz, "A level set-based framework for 3D kidney segmentation from diffusion MR images," in IEEE 22nd Proc. International Conference on Image Processing, (ICIP'15). IEEE, 2015, pp. 4441–4445.
139. A. El-Baz, X. Jiang, and S. Jasjit, Biomedical Image Segmentation: Advances & Trends, CRC Press, 2016.
140. Denis Le Bihan and E Breton, "Imagerie de diffusion invivo par resonance magn ´ etique nucl ´ eaire," ´ Comptes-Rendus de l'Academie des Sciences ´ , vol. 93, no. 5, pp. 27–34, 1985.
141. Fahmi Khalifa, Ahmed Soliman, Ayman El-Baz, Mohamed Abou El-Ghar, Tarek El-Diasty, Georgy Gimel'farb, Rosemary Ouseph, and Amy C Dwyer, "Models and methods for analyzing DCE-MRI: A review," Medical Physics, vol. 41, no. 12, pp. 124301, 2014.
142. Steven M Gieser and Andrew Z Fenves, "Chronic kidney disease, dialysis, & transplantation, edited by Brian JG Pereira, MD, DM, Mohamed H. Sayegh, MD, and Peter Blake, MD," Proceedings (Baylor University. Medical Center), vol. 19, no. 1, pp. 69, 2006.

143. WJ Chon, DC Brennan, et al., "Clinical manifestations and diagnosis of acute renal allograft rejection," UpToDate version, vol. 21, 2014
144. Guangyi Liu, Fei Han, Wenbo Xiao, Qidong Wang, Ying Xu, and Jianghua Chen, "Detection of renal allograft rejection using blood oxygen level-dependent and diffusion weighted magnetic resonance imaging: A retrospective study," BMC Nephrology, vol. 15, no. 1, pp. 158, 2014.
145. L Nilsson, H Ekberg, K Falt, H L ¨ ofberg, and G Sterner, "Renal ¨ arteriovenous shunting in rejecting allograft, hydronephrosis, or haemorrhagic hypotension in the rat," Nephrology Dialysis Transplantation, vol. 9, no. 11, pp. 1634–1639, 1994.
146. Aly A Farag, Ayman S El-Baz, and Georgy Gimel'farb, "Precise segmentation of multimodal images," IEEE Transactions on Image Processing, vol. 15, no. 4, pp. 952–968, 2006.
147. A. El-Baz, A. Elnakib, F. Khalifa, M. Abou El-Ghar, P. McClure, A. Soliman, and G. Gimel'farb, "Precise segmentation of 3-D magnetic resonance angiography," IEEE Transtions on Biomedical Engineering, vol. 59, no. 7, pp. 2019–2029, 2012.
148. A. El-Baz and G. Gimel'farb, "EM–based approximation of empirical distributions with linear combinations of discrete Gaussians," in IEEE International Conference on Image Processing, (ICIP'07), San Antonio, Texas, USA, September 16– 19, 2007.
149. Y. Bengio, P. Lamblin, D. Popovici, H. Larochelle, et al., "Greedy layer-wise training of deep networks," Advances in Neural Information Processing Systems, vol. 19, pp. 153, 2007.
150. E. Hosseini-Asl, J.M. Zurada, and O. Nasraoui, "Deep learning of part-based representation of data using sparse autoencoders with nonnegativity constraints," IEEE Transactions on Neural Networks and Learning Systems, pp. 1–13, 2015, e-publication ahead of print.
151. Kelly H Zou, Simon K Warfield, Aditya Bharatha, Clare MC Tempany, Michael R Kaus, Steven J Haker, William M Wells, Ferenc A Jolesz, and Ron Kikinis, "Statistical validation of image segmentation quality based on a spatial overlap index 1: Scientific reports," Acadimic Radiology, vol. 11, no. 2, pp. 178–189, 2004.
152. Guido Gerig, Matthieu Jomier, and Miranda Chakos, "Valmet: A new validation tool for assessing and improving 3D object segmentation," in Proc. Medical Image Computing and Computer-Assisted Intervention (MICCAI'01), 2001, pp. 516– 523.
153. Mark Hall, Eibe Frank, Geoffrey Holmes, Bernhard Pfahringer, Peter Reutemann, and Ian H Witten, "The weka data mining software: An update," ACM SIGKDD explorations newsletter, vol. 11, no. 1, pp. 10–18, 2009.
154. Fahmi Khalifa, Ayman El-Baz, Georgy Gimel'farb, and Mohammed Abu El-Ghar. Non-invasive image-based approach for early detection of acute renal rejection. In Proc. Int. Conf. Med. Image Comput. Computer-Assisted Intervention (MICCAI'10), Beijing, China, Sept. 20–24, pages 10–18, 2010.
155. Mohamed Shehata, Fahmi Khalifa, Ahmed Soliman, Mohamed Abou El-Ghar, Amy Dwyer, Rosemary Ouseph, and Ayman El-Baz. Early assessment of acute renal rejection. In 12th Annual Scientific Meeting of American Society for Diagnosticsand Interventional Nephrology (ASDIN), Phoenix, Arizona, USA, Feb 19–21, 2016.
156. Mohamed Shehata, Fahmi Khalifa, Ahmed Soliman, Ali Taki Eldeen, Mohamed Abou El-Ghar, Tarek Eldiasty, Ayman El-Baz, and Robert Keynton. An appearanceguided deformable model for 4D kidney segmentation using diffusion MRI.

In X. Jiang A. El-Baz and Taylor & Francis J. Suri, Eds, editors, Biomedical Image Segmentation: Advances and Trends, page (In Press). CRC, 2016.

157. M Shehata, F Khalifa, A Soliman, M Abou El-Ghar, A Dwyer, G Gimelfarb, R Keynton, and A El-Baz. A promising non-invasive cad system for kidney function assessment. In International Conference on Medical Image Computing and Computer-Assisted Intervention, pages 613–621. Springer, 2016.
158. Fahmi Khalifa, Ahmed Soliman, Amy C Dwyer, Georgy Gimel'farb, and Ayman El- Baz. A random forest-based framework for 3d kidney segmentation from dynamic contrast-enhanced ct images. In Image Processing (ICIP), 2016 IEEE International Conference on, pages 3399–3403. IEEE, 2016.
159. F. Khalifa, A. Soliman, G. Gimel'farb, R. Ouseph, A. Dwyer, T. El-Diasty, and A. El- Baz. Models and methods for analyzing DCE-MRI: A review. Medical Physics, 41(12):1–32, 2014.
160. Mahmoud Mostapha, Fahmi Khalifa, Amir Alansary, Ahmed Soliman, Georgy Gimel'farb, and Ayman El-Baz. Dynamic MRI-based computer aided diagnostic systems for early detection of kidney transplant rejection: A survey. In Proceedings of of Computational Models for Life Science, Sydney, Australia (CMLS), volume 1559, pages 297–306. AIP Publishing, 2013.
161. Fahmi Khalifa, Ahmed Soliman, Ali Takieldeen, Mohamed Shehata, Mahmoud Mostapha, Ahmed Shaffie, Rosemary Ouseph, Adel Elmaghraby, and Ayman El- Baz. Kidney segmentation from CT images using a 3D NMF-guided active contour model. In Proceedings of IEEE 13th International Symposium on Biomedical Imaging, (ISBI'16), pages 432–435. IEEE, 2016.
162. M. Shehata, F. Khalifa, A. Soliman, M. Abou El-Ghar, A. C. Dwyer, and A. El-Baz, "Assessment of Renal Transplant Using Image and Clinical-based Biomarkers," In: Proceedings of 13th Annual Scientific Meeting of American Society for Diagnostics and Interventional Nephrology (ASDIN'17), New Orleans, Louisiana, USA, February 10–12, 2017.
163. F. Khalifa, M. Shehata, A. Soliman, M. Abou El-Ghar, T. El-Diasty, A. C. Dwyer, M. El-Melegy, R. Keynton, **A. El-Baz**, " A GENERALIZED MRI-BASED CAD SYSTEM FOR FUNCTIONAL ASSESSMENT OF RENAL TRANSPLANT," *In: Proceedings of International Symposium on Biomedical Imaging: From Nano to Macro (ISBI'17)*, Melbourne, Australia, April 18–21, 2017, (in press).
164. A. Firjani, A. Elmaghraby, and A. El-Baz. MRI-based diagnostic system for early detection of prostate cancer. In *Biomedical Sciences and Engineering Conference (BSEC), 2013*, pages 1–4, 2013.
165. Ahmad Firjani, Ahmed Elnakib, Fahmi Khalifa, Ayman El-Baz, Georgy Gimel'farb, Mohamed Abou El-Ghar, and Adel Elmaghraby. A novel 3D segmentation approach for segmenting the prostate from dynamic contrast enhanced MRI using current appearance and learned shape prior. In *Proceedings of IEEE International Symposium on Signal Processing and Information Technology, (ISSPIT'10)*, pages 137–143, Luxor, Egypt, December 15–18, 2010.
166. Ahmad Firjani, Ahmed Elnakib, Fahmi Khalifa, Georgy Gimelfarb, Mohamed Abou El-Ghar, Adel Elmaghraby, and Ayman El-Baz. A diffusion-weighted imaging based diagnostic system for early detection of prostate cancer. *Journal of Biomedical Science and Engineering*, 6(03):346, 2013.

167. A. Firjani, A. Elnakib, F. Khalifa, G. Gimel'farb, M. Abou El-Ghar, J. Suri, A. Elmaghraby, and A. El-Baz. A new 3D automatic segmentation framework for accurate extraction of prostate from DCE-MRI. In *Proceedings of IEEE International Symposium on Biomedical Imaging: From Nano to Macro, (ISBI'11)*, pages 1476–1479, Chicago, Illinois, March 30–April 2, 2011.
168. A. Firjani, A. Elnakib, F. Khalifa, G. Gimelfarb, M. Abou El-Ghar, A. Elmaghraby, and A. El-Baz. A diffusion-weighted imaging based diagnostic system for early detection of prostate cancer. *Journal of Biomedical Science and Engineering*, 6(3A):346–356, 2013.
169. A. Firjani, F. Khalifa, A. Elnakib, G. Gimel'farb, M. Abou El-Ghar, A. Elmaghraby, and A. El-Baz. 3D automatic approach for precise segmentation of the prostate from diffusion-weighted magnetic resonance imaging. In *Proceedings of IEEE International Conference on Image Processing, (ICIP'11)*, pages 2285–2288, Brussels, Belgium, September 11–14, 2011.
170. A. Firjani, F. Khalifa, A. Elnakib, G. Gimel'farb, M. Abou El-Ghar, A. Elmaghraby, and A. El-Baz. A novel image-based approach for early detection of prostate cancer using DCE-MRI. In Kenji Suzuki, editor, *Computational Intelligence in Biomedical Imaging*, pages 55–82. Springer New York, 2014.
171. A. Firjani, F. Khalifa, A. Elnakib, G. Gimel'farb, A. Elmaghraby, and A. El-Baz. A novel image-based approach for early detection of prostate cancer. In *Proceedings of IEEE International Conference on Image Processing, (ICIP'12)*, pages 2849–2852, Lake Buena Vista, Florida, September 30–October 3, 2012.
172. Islam Reda, Ahmed Shalaby, Mohamed Abou El-Ghar, Fahmi Khalifa, Mohammed Elmogy, Ahmed Aboulfotouh, Ehsan Hosseini-Asl, Ayman El-Baz, and Robert Keynton. A new NMF-autoencoder based CAD system for early diagnosis of prostate cancer. In *Proceedings of IEEE 13th International Symposium on Biomedical Imaging (ISBI'16)*, pages 1237–1240. IEEE, 2016.
173. Ahmad Firjany, Ahmed Elnakib, Ayman El-Baz, Georgy Gimelfarb, Mohamed Abou El-Ghar, and Adel Elmagharby. Novel stochastic framework for accurate segemntation of prostate in dynamic contrast-enhanced MRI. In *Proceedings of the International Wokshop on Prostate Cancer Imaging: Computer-Aided Diagnosis, Prognosis, and Intervention*, pages 121–130, Beijing, China, Sptember 24, 2010.
174. P. McClure, F. Khalifa, A Soliman, M Abou El-Ghar, G Gimelfarb, A Elmagraby, and A El-Baz. A novel nmf guided level-set for dwi prostate segmentation. *Journal of Computer Science and Systems Biology*, 7:209–216, 2014.
175. A. Firjani, A. Elnakib, F. Khalifa, G. Gimel'farb, M. Abou El-Ghar, A. Elmaghraby, and A. El-Baz. A new 3D automatic segmentation framework for accurate extraction of prostate from diffusion imaging. In *Proceedings of Biomedical Science and Engineering Conference–Image Informatics and Analytics in Biomedicine, (BSEC'11)*, pages 1306–1309, 2011.
176. A. Firjani, F. Khalifa, A. Elnakib, G. Gimel'farb, M. Abou El-Ghar, A. Elmaghraby, and A. El-Baz. Non-invasive image-based approach for early detection of prostate cancer. In *Proceedings of Fourth International Conference on Developments in eSystems Engineering, (DeSE'11)*, pages 172–177, Dubai, UAE, December 6–8, 2011.

177. A. Elnakib, G. M. Beache, G. Gimelfarb, and A. El-Baz. Intramyocardial strain estimation from cardiac cine mri. *International journal of computer assisted radiology and surgery*, 10(8):1299–1312, 2015.
178. G. M. Beache, F. Khalifa, G. Gimel'farb, and A. El-Baz. Fully automated framework for the analysis of myocardial first-pass perfusion MR images. *Medical Physics*, 41(10):1–18, 2014.
179. A. Elnakib, G. M. Beache, G. Gimelfarb, and A. El-Baz. New automated Markov–Gibbs random field based framework for myocardial wall viability quantification on agent enhanced cardiac magnetic resonance images. *Int. J. Cardiovasc. Imaging*, 28(7):1683–1698, 2012.
180. A. Elnakib, G. M. Beache, G. Gimel'farb, and A. El-Baz. A new framework for automated segmentation of left ventricle wall from contrast enhanced cardiac magnetic resonance images. In *Proc. IEEE Intern. Conf. on Image Processing (ICIP'2011)*, pages 2289–2292, 2011.
181. A. Elnakib, G. M. Beache, T. I. G. Gimel'farb, and A. El-Baz. Validating a new methodology for strain estimation from cardiac cine MRI. In *Proc. Intern. Symp. On Computational Models for Life Science (CMLS'13)*, pages 277–286, 2013.
182. H. Sliman, F. Khalifa, A. Elnakib, A. Soliman, G. Beache, G. Gimel'farb, A. Emam, A. Elmaghraby, and A. El-Baz. Accurate segmentation framework for the left ventricle wall from cardiac cine mri. In *2013 INTERNATIONAL SYMPOSIUM ON COMPUTATIONAL MODELS FOR LIFE SCIENCES*, volume 1559, pages 287–296. AIP Publishing, 2013.
183. A. Elnakib, G. M. Beache, M. Nitzken, G. Gimel'farb, and A. El-Baz. A new framework for automated identification of pathological tissues in contrast enhanced cardiac magnetic resonance images. In *Proc. IEEE Intern. Symp. on Biomedical Imaging: From Nano to Macro (ISBI'2011)*, pages 1272–1275, 2011.
184. A. Elnakib, G. Beache, H. Sliman, G. Gimel'farb, T. Inanc, and A. El-Baz. A novel Laplace-based method to estimate the strain from cine cardiac magnetic resonance images. In *Proceedings of IEEE International Conference on Image Processing (ICIP'2013)*. IEEE, 2013.
185. F. Khalifa, G. Beache, A. El-Baz, and G. Gimel'farb. Deformable model guided by stochastic speed with application in cine images segmentation. In *Proc. IEEE Intern. Conf. on Image Processing (ICIP'2010)*, pages 1725–1728, Hong Kong, September 26–29, 2010.
186. F. Khalifa, G. M. Beache, A. Elnakib, H. Sliman, G. Gimel'farb, K. C. Welch, and A. El-Baz. A new shape-based framework for the left ventricle wall segmentation from cardiac first-pass perfusion MRI. In *Proc. IEEE Int. Symp. Biomed. Imaging: From Nano to Macro, (ISBI'13)*, pages 41–44, 2013.
187. F. Khalifa, G. M. Beache, A. Elnakib, H. Sliman, G. Gimel'farb, K. C. Welch, and A. El-Baz. A new nonrigid registration framework for improved visualization of transmural perfusion gradients on cardiac first-pass perfusion MRI. In *Proc. IEEE Int. Symp. Biomed. Imaging: From Nano to Macro, (ISBI'12)*, pages 828–831, 2012.
188. F. Khalifa, G. M. Beache, A. Firjani, K. C. Welch, G. Gimel'farb, and A. El-Baz. A new nonrigid registration approach for motion correction of cardiac first-pass perfusion MRI. In *Proc. IEEE Int. Conf. Image Process., (ICIP'12)*, pages 1665–1668, 2012.

189. F. Khalifa, G. M. Beache, G. Gimel'farb, and A. El-Baz. A novel CAD system for analyzing cardiac first-pass MRI images. In *Proc. IEEE Int. Conf. Pattern Recogni., (ICPR'12)*, pages 77–80, 2012.
190. F. Khalifa, G. M. Beache, G. Gimel'farb, and A. El-Baz. A novel approach for accurate estimation of left ventricle global indexes from short-axis cine MRI. In *Proc. IEEE Intern. Conf. on Image Processing (ICIP'2011)*, pages 2645–2649, Brussels, Belgium, September 11–14, 2011.
191. F. Khalifa, G. M. Beache, G. Gimel'farb, G. A. Giridharan, and A. El-Baz. A new image-based framework for analyzing cine images. In A. El-Baz, U. R. Acharya,M. Mirmedhdi, and J. S. Suri, editors, *Handbook of Multi Modality State-of-the-Art Medical Image Segmentation and Registration Methodologies*, volume 2, chapter 3, pages 69–98. Springer, 2011.
192. F. Khalifa, G. M. Beache, G. Gimel'farb, G. A. Giridharan, and A. El-Baz. Accurate automatic analysis of cardiac cine images. *IEEE Trans. Biomed. Eng.*, 59(2):445–455, 2012.
193. F. Khalifa, G. M. Beache, M. Nitzken, G. Gimel'farb, G. A. Giridharan, and A. El-Baz. Automatic analysis of left ventricle wall thickness using short-axis cine CMR images. In *Proc. IEEE Int. Symp. Biomed. Imaging: From Nano to Macro, (ISBI'11)*, pages 1306–1309, 2011.
194. M. Nitzken, G. Beache, A. Elnakib, F. Khalifa, G. Gimel'farb, and A. El-Baz. Accurate modeling of tagged CMR 3D image appearance characteristics to improve cardiac cycle strain estimation. In *Proc. 19th IEEE Intern. Conf. on Image Processing (ICIP 2012)*, pages 521–524, Orlando, FL, USA, Sept. 30 – Oct. 3, 2012. IEEE Press.
195. M. J. Nitzken, A. S. El-Baz, and G. M. Beache. Markov-Gibbs random field model for improved full-cardiac cycle strain estimation from tagged CMR. *J. CardiovascularMagnetic Resonance*, 14(1):1–2, 2012.
196. H. Sliman, A. Elnakib, G. M.Beache, A. Elmaghraby, and A. El-Baz. Assessment of myocardial function from cine cardiac MRI using a novel 4D tracking approach. *J. Computer Science & Systems Biology*, 7:169–173, 2014.
197. H. Sliman, A. Elnakib, G. M. Beache, A. Soliman, F. Khalifa, G. Gimel'farb, A. Elmaghraby, and A. El-Baz. A novel 4D PDE-based approach for accurate assessment of myocardium function using cine cardiac magnetic resonance images. In *Proc. 21st IEEE Intern. Conf. on Image Processing (ICIP 2014)*, pages 3537–3541, Paris, France, October 27–30, 2014.
198. H. Sliman, F. Khalifa, A. Elnakib, A. Soliman, G. M. Beache, A. Elmaghraby, G. Gimel'farb, and A. El-Baz. Myocardial borders segmentation from cine MR images using bi-directional coupled parametric deformable models. *Medical Physics*, 40(9):1–13, 2013.
199. H. Sliman, F. Khalifa, A. Elnakib, G. Beache, A. Elmaghraby, and A. El-Baz. A new segmentation-based tracking framework for extracting the left ventricle cavity from cine cardiac MRI. In *Proceedings of IEEE International Conference on Image Processing, (ICIP'13)*, pages 685–689, Melbourne, Australia, September 15–18, 2013.
200. H. Sliman, F. Khalifa, A. Elnakib, A. Soliman, G. M. Beache, G. Gimel'farb, A. Emam, A. Elmaghraby, and A. El-Baz. Accurate segmentation framework for the left ventricle wall from cardiac cine MRI. In *AIP Proc.: Intern. Symp. on Computational*

Models for Life Science, (CMLS'13), volume 1559, pages 287–296, Sydney, Australia, Nov. 27–29, 2013.

201. Shlomit Schaal, Marwa Ismail, Agustina C Palacio, Ahmed ElTanboly, Andy Switala, Ahmed Soliman, Thomas Neyer, Amir Hajrasouliha, Amir Hadayer, Douglas Kenneth Sigford, et al. Subtle early changes in diabetic retinas revealed by a novel method that automatically quantifies spectral domain optical coherence tomography (sd-oct) images. *Investigative Ophthalmology & Visual Science*, 57(12):6324–6324, 2016.
202. Thomas Neyer, Ahmed ElTanboly, Agustina C Palacio, Marwa Ismail, Andy Switala, Ahmed Soliman, Amir Hajrasouliha, Amir Hadayer, Douglas Kenneth Sigford, Ayman El-Baz, et al. A novel automated method for the objective quantification of retinal layers based on spectral domain optical coherence tomography (sd-oct) imaging reveals sequential changes in the normal retina with age. *Investigative Ophthalmology & Visual Science*, 57(12):5943–5943, 2016.
203. A El Tanboly, M Ismail, A Switala, M Mahmoud, A Soliman, T Neyer, A Palacio, A Hadayer, M El-Azab, S Schaal, et al. A novel automated method for the objective quantication of retinal layers reveals sequential changes that occur in the normal retina with age. In *Image Processing (ICIP), 2016 IEEE International Conference on*, pages 116–120. IEEE, 2016.
204. S Schaal, A El Tanboly,MIsmail, A Switala, A Shalaby, A Hadayer, O Abdelmegid, and A El-Baz. A novel automatic segmentation of healthy and diseased retinal layers from oct scans. In *Frontiers in Nanoscience and Nanotechnology*, 2016.
205. Ahmed ElTanboly, Marwa Ismail, Ahmed Shalaby, Andy Switala, Shlomit Schaal, Georgy Gimel'farb, Magdi El- Azab, and Ayman El- Baz." A computer aided diagnostic system for detecting diabetic retinopathy in optical coherence tomography images.", Medical Physics. 2016 Dec 1
206. Schaal, Shlomit, Ahmed ElTanboly, Marwa Ismail, Andy Switala, Ahmed Shalaby, Amir Hadayer, Omar Abdelmegid, and Ayman El-Baz. "A novel automated method for the objective quantification of Retinal layers reveals sequential changes that occur in the Normal retina with age."
207. Ahmed ElTanboly, Agustin Palacio, Ahmed Shalaby , Andy E. Switala, Omar Helmy, Shlomit Schaal, and Ayman El-Baz, An automated approach for early detection of diabetics retinopathy, Frontier in Bioscience.
208. A. El-Baz, A. Elnakib, F. Khalifa, M. A. El-Ghar, P. McClure, A. Soliman, and G. Gimelrfarb, "Precise segmentation of 3-d magnetic resonance angiography," IEEE Transactions on Biomedical Engineering, vol. 59, no. 7, pp. 2019–2029, 2012.
209. A. El-Baz, F. Khalifa, A. Elnakib, M. Nitzken, A. Soliman, P. McClure, M. El-Ghar, and G. Gimelfarb, "A novel approach for global lung registration using 3d markov-gibbs appearance model," Medical Image Computing and Computer-Assisted Intervention–MICCAI 2012, pp. 114–121, 2012.
210. B. Abdollahi, A. Soliman, A. Civelek, X.-F. Li, G. Gimelfarb, and A. El-Baz, "A novel 3d joint mgrf framework for precise lung segmentation," in International Workshop on Machine Learning in Medical Imaging, pp. 86–93, Springer Berlin Heidelberg, 2012.
211. A. El-Baz, A. Soliman, P. McClure, G. Gimel'farb, M. A. El-Ghar, and R. Falk, "Early assessment of malignant lung nodules based on the spatial analysis of detected

lung nodules," in Biomedical Imaging (ISBI), 2012 9th IEEE International Symposium on, pp. 1463–1466, IEEE, 2012.
212. A. El-Baz, G. M. Beache, G. Gimel'farb, K. Suzuki, K. Okada, A. Elnakib, A. Soliman, and B. Abdollahi, "Computer-aided diagnosis systems for lung cancer: challenges and methodologies," International journal of biomedical imaging, vol. 2013, 2013.
213. A. Soliman, F. Khalifa, A. Alansary, G. Gimel'farb, and A. El-Baz, "Segmentation of lung region based on using parallel implementation of joint mgrf: Validation on 3d realistic lung phantoms," in Biomedical Imaging (ISBI), 2013 IEEE 10th International Symposium on, pp. 864–867, IEEE, 2013.
214. A. Soliman, F. Khalifa, A. Alansary, G. Gimel'farb, A. El-Baz, C. Sun, T. Bednarz, T. D. Pham, P. Vallotton, and D. Wang, "Performance evaluation of an automatic mgrf-based lung segmentation approach," in AIP Conference Proceedings, vol. 1559, pp. 323–332, AIP, 2013.
215. N. Liu, A. Soliman, G. Gimelfarb, and A. El-Baz, "Segmenting kidney dce-mri using 1st-order shape and 5th-order appearance priors," in International Conference on Medical Image Computing and Computer-Assisted Intervention, pp. 77–84, Springer International Publishing, 2015.
216. A. Soliman, A. Elnakib, F. Khalifa, M. A. El-Ghar, and A. El-Baz, "Segmentationof pathological lungs from ct chest images," in Image Processing (ICIP), 2015 IEEE International Conference on, pp. 3655–3659, IEEE, 2015.
217. A. Soliman, F. Khalifa, N. Dunlap, B. Wang, M. A. El-Ghar, and A. El-Baz, "An iso-surfaces based local deformation handling framework of lung tissues," in Biomedical Imaging (ISBI), 2016 IEEE 13th International Symposium on, pp. 1253–1259, IEEE, 2016.
218. A. Soliman, F. Khalifa, A. Shaffie, N. Dunlap, B. Wang, A. Elmaghraby, and A. El-Baz, "Detection of lung injury using 4d-ct chest images," in Biomedical Imaging (ISBI), 2016 IEEE 13th International Symposium on, pp. 1274–1277, IEEE, 2016.
219. A. Soliman, F. Khalifa, A. Elnakib, M. A. El-Ghar, N. Dunlap, B. Wang, G. Gimelfarb, R. Keynton, and A. El-Baz, "Accurate lungs segmentation on ct chest images by adaptive appearance-guided shape modeling," IEEE Transactions on Medical Imaging, vol. 36, no. 1, pp. 263–276, 2017.
220. A. Soliman, F. Khalifa, A. Shaffie, N. Liu, N. Dunlap, B. Wang, A. Elmaghraby, G. Gimel'farb, and A. El-Baz, "Image-based cad system for accurate identification of lung injury," in Image Processing (ICIP), 2016 IEEE International Conference on, pp. 121–125, IEEE, 2016.
221. A. El-Baz, G. Gimelfarb, R. Falk, and M. A. El-Ghar, "3D MGRF-based appearance modeling for robust segmentation of pulmonary nodules in 3D LDCT chest images," in Lung Imaging and Computer Aided Diagnosis, ch. 3, pp. 51–63, chapter, 2011.
222. A. El-Baz, G. Gimel'farb, M. Abou El-Ghar, and R. Falk, "Appearance-based diagnostic system for early assessment of malignant lung nodules," in Proceedings of IEEE International Conference on Image Processing, (ICIP'12), pp. 533–536, IEEE, 2012.
223. A. El-Baz, P. Sethu, G. Gimel'farb, F. Khalifa, A. Elnakib, R. Falk, and M. A. El-Ghar, "Elastic phantoms generated by microfluidics technology: Validation of an

imaged-based approach for accurate measurement of the growth rate of lung nodules," Biotechnology journal, vol. 6, no. 2, pp. 195–203, 2011.
224. A. S. El-Baz and J. S. Suri, Lung Imaging and Computer Aided Diagnosis. CRC Press, 2011.
225. A. El-Baz, G. Gimelfarb, R. Falk, M. A. El-Ghar, and J. Suri, "Appearance analysis for the early assessment of detected lung nodules," in Lung Imaging and Computer Aided Diagnosis, ch. 17, pp. 395–404, chapter, 2011.
226. A. El-Baz, P. Sethu, G. Gimelfarb, F. Khalifa, A. Elnakib, R. Falk, M. A. El-Ghar, and J. Suri, "Validation of a new imaged-based approach for the accurate estimating of the growth rate of detected lung nodules using real computed tomography images and elastic phantoms generated by state-of-theart microfluidics technology," in Lung Imaging and Computer Aided Diagnosis, ch. 18, pp. 405–420, chapter, 2011.
227. A. El-Baz, M. Nitzken, G. Gimelfarb, E. Van Bogaert, R. Falk, M. A. El-Ghar, and J. Suri, "Three-dimensional shape analysis using spherical harmonics for early assessment of detected lung nodules," in Lung Imaging and Computer Aided Diagnosis, ch. 19, pp. 421–438, chapter, 2011.
228. M. Kondapaneni, M. Nitzken, E. Bogaert, G. Gimelfarb, R. Falk, M. A. El-Ghar, and A. ElBaz, "A novel shape-based diagnostic approach for early diagnosis of lung nodules," CHEST Journal, vol. 140, no. 4 MeetingAbstracts, pp. 655A–655A, 2011.
229. A. El-Baz, G. Gimel'farb, R. Falk, and M. El-Ghar, "Appearance analysis for diagnosing malignant lung nodules," in Proceedings of IEEE International Symposium on Biomedical Imaging: From Nano to Macro (ISBI'10), pp. 193–196, IEEE, 2010.
230. "Automatic analysis of 3D low dose CT images for early diagnosis of lung cancer, author=ElBaz, Ayman and Gimelfarb, G and Falk, Robert and Abo El-Ghar, M, journal=Pattern Recognition, volume=42, number=6, pages=1041–1051, year=2009, publisher=Elsevier,"
231. A. El-Baz, G. Gimelfarb, R. Falk, M. A. El-Ghar, S. Rainey, D. Heredia, and T. Shaffer, "Toward early diagnosis of lung cancer," in Proceedings of Medical Image Computing and Computer-Assisted Intervention, (MICCAI'09), pp. 682–689, Springer, 2009.
232. A. M. Ali and A. A. Farag, "Automatic lung segmentation of volumetric low-dose CT scans using graph cuts," in Advances in Visual Computing, pp. 258–267, Springer, 2008.
233. A. El-Baz, G. L. Gimel'farb, R. Falk, M. Abou El-Ghar, T. Holland, and T. Shaffer, "A new stochastic framework for accurate lung segmentation," in Proceedings of Medical Image Computing and Computer-Assisted Intervention, (MICCAI'08), pp. 322–330, 2008.
234. A. El-Baz, G. L. Gimel'farb, R. Falk, D. Heredis, and M. Abou El-Ghar, "A novel approach for accurate estimation of the growth rate of the detected lung nodules," in Proceedings of International Workshop on Pulmonary Image Analysis, pp. 33–42, 2008.
235. A. El-Baz, G. L. Gimel'farb, R. Falk, T. Holland, and T. Shaffer, "A framework for unsupervised segmentation of lung tissues from low dose computed tomography images," in Proceedings of British Machine Vision, (BMVC'08), pp. 1–10, 2008.
236. A. El-Baz, G. Gimel'farb, R. Falk, and M. A. El-Ghar, "A new approach for automatic analysis of 3D low dose CT images for accurate monitoring the detected lung

nodules," in Proceedings of International Conference on Pattern Recognition, (ICPR'08), pp. 1–4, IEEE, 2008.
237. A. El-Baz, G. Gimel'farb, R. Falk, M. A. El-Ghar, and H. Refaie, "Promising results for early diagnosis of lung cancer," in Proceedings of IEEE International Symposium on Biomedical Imaging: From Nano to Macro, (ISBI'08), pp. 1151–1154, IEEE, 2008.
238. A. M. Ali, A. S. El-Baz, and A. A. Farag, "A novel framework for accurate lung segmentation using graph cuts," in Proceedings of IEEE International Symposium on Biomedical Imaging: From Nano to Macro, (ISBI'07), pp. 908–911, IEEE, 2007.
239. A. El-Baz, G. Gimel'farb, R. Falk, and M. A. El-Ghar, "A novel approach for automatic follow-up of detected lung nodules," in Proceedings of IEEE International Conference on Image Processing, (ICIP'07), vol. 5, pp. V–501, IEEE, 2007.
240. "A new CAD system for early diagnosis of detected lung nodules,"
241. A. El-Baz, A. Farag, G. Gimel'farb, R. Falk, M. A. El-Ghar, and T. Eldiasty, "A framework for automatic segmentation of lung nodules from low dose chest CT scans," in Proceedings of International Conference on Pattern Recognition, (ICPR'06), vol. 3, pp. 611–614, IEEE, 2006.
242. A. A. Farag, A. El-Baz, G. Gimelfarb, R. Falk, M. A. El-Ghar, T. Eldiasty, and S. Elshazly, "Appearance models for robust segmentation of pulmonary nodules in 3d ldct chest images," in Proceedings of Medical Image Computing and Computer-Assisted Intervention–MICCAI 2006, pp. 662–670, Springer, 2006.
243. A. El-Baz, S. E. Yuksel, S. Elshazly, and A. A. Farag, "Non-rigid registration techniques for automatic follow-up of lung nodules," in Proceedings of Computer Assisted Radiology and Surgery, (CARS'05), vol. 1281, pp. 1115–1120, Elsevier, 2005.
244. A. A. Farag, A. El-Baz, G. Gimelfarb, M. A. El-Ghar, and T. Eldiasty, "Quantitative nodule detection in low dose chest ct scans: new template modeling and evaluation for cad system design," in roceedings of Medical Image Computing and Computer-Assisted Intervention, (MICCAI'05), pp. 720–728, Springer, 2005.
245. A. A. Farag, A. El-Baz, G. Gimel'farb, and R. Falk, "Detection and recognition of lung abnormalities using deformable templates," in Proceedings of the 17th International Conference on Pattern Recognition, (ICPR'04), vol. 3, pp. 738–741, IEEE, 2004.
246. A. A. Farag, A. El-Baz, G. G. Gimelfarb, R. Falk, and S. G. Hushek, "Automatic detection and recognition of lung abnormalities in helical CT images using deformable templates," in Proceedings of Medical Image Computing and Computer-Assisted Intervention, (MICCAI'04), pp. 856–864, Springer, 2004.
247. A. El-Bazl, A. A. Farag, R. Falk, and R. La Rocca, "Automatic identification of lung abnormalities in chest spiral CT scans," in Proceedings of IEEE International Conference on Acoustics, Speech, and Signal Processing, (ICASSP'03), vol. 2, pp. II–261, IEEE, 2003.
248. A. El-Baz, A. A. Farag, R. Falk, and R. La Rocca, "A unified approach for detection, visualization, and identification of lung abnormalities in chest spiral CT scans," in International Congress Series, vol. 1256, pp. 998–1004, Elsevier, 2003.

249. A. El-Baz, A. A. Farag, R. Falk, and R. La Rocca, "Detection, visualization and identification of lung abnormalities in chest spiral CT scan: Phase-I," in Proceedings of International conference on Biomedical Engineering, Cairo, Egypt, vol. 12, 2002.
250. A. Elnakib, M. F. Casanova, A. Soliman, G. Gimelfarb, and A. El-Baz. Analysis of 3d corpus callosum images in the brains of autistic individuals. *Handbook of Research on Trends in the Diagnosis and Treatment of Chronic Conditions*, page 159, 2015.
251. A. Elnakib, A. Soliman, M. Nitzken, M. F. Casanova, G. Gimel'farb, and A. El-Baz. Magnetic resonance imaging findings for dyslexia: A review. *J. Biomedical Nanotechnology*, 10(10):2778–2805, 2014.
252. M. Ismail, R. Keynton, M. Mostapha, A. ElTanboly, M. Casanova, G. Gimel'farb, and A. El-Baz. Studying autism spectrum disorder with structural and diffusion magnetic resonance imaging: A survey. *Frontiers in Human Neuroscience*, 10, 2016.
253. M. Ismail, A. Soliman, A. ElTanboly, A. Switala, M. Mahmoud, F. Khalifa, G. Gimel'farb, M. F. Casanova, R. Keynton, and A. El-Baz. Detection of white matter abnormalities in mr brain images for diagnosis of autism in children. In *Proceedings of IEEE 13th International Symposium on Biomedical Imaging (ISBI'16)*, pages 6–9. IEEE, 2016.
254. A. Alansary, M. Ismail, A. Soliman, F. Khalifa, M. Nitzken, et al. Infant brain extraction in t1-weighted mr images using bet and refinement using lcdg and mgrf models. *IEEE journal of biomedical and health informatics*, 20(3):925–935, 2016.
255. M. F. Casanova, A. E.-B. S, S. S. Kamat, B. A. Dombroski, F. Khalifa, A. Elnakib, A. Soliman, A. Allison-McNutt, and A. E. Switala. Focal cortical dysplasias in autism spectrum disorders. *Acta Neuropathologica Communications*, 1(1):67, 2013.
256. A. Alansary, A. Soliman, F. Khalifa, A. Elnakib, M. Mostapha, M. Nitzken, M. Casanova, and A. El-Baz. MAP-based framework for segmentation of mr brain images based on visual appearance and prior shape. *MIDAS J*, 1:1, 2013.
257. M. Ismail, M. Mostapha, A. Soliman, M. Nitzken, F. Khalifa, A. Elnakib, G. Gimel'farb, M. Casanova, and A. El-Baz. Segmentation of infant brain mr images based on adaptive shape prior and higher-order mgrf. In *Image Processing (ICIP), 2015 IEEE International Conference on*, pages 4327–4331. IEEE, 2015.
258. A. Alansary, A. Soliman, M. Nitzken, F. Khalifa, A. Elnakib, M. Mostapha, M. F. Casanova, and A. El-Baz. An integrated geometrical and stochastic approach for accurate infant brain extraction. In *Proc. 2014 IEEE Intern. Conf. on Image Processing (ICIP 2014)*, pages 3542–3546. IEEE Press, 2014.
259. B. A. Dombroski, A. E. Switala, A. S. El-Baz, and M. F. Casanova. Gyral window mapping of typical cortical folding using MRI. *Translational Neuroscience*, 2(2):142–147, 2011.
260. B. Dombroski, M. Nitzken, A. Elnakib, F. Khalifa, A. El-Baz, and M. F. Casanova. Cortical surface complexity in a population-based normative sample. *Translational Neuroscience*, 5(1):17–24, 2014.
261. A. El-Baz, M. Casanova, G. Gimel'farb, M. Mott, and A. Switala. An MRI-based diagnostic framework for early diagnosis of dyslexia. *Intern. J. Computer Assisted Radiology and Surgery*, 3(3-4):181–189, 2008.
262. A. El-Baz, M. Casanova, G. Gimel'farb, M. Mott, A. Switala, E. V. Bogaert, and R. McCracken. A new CAD system for early diagnosis of dyslexic brains. In *Proc. IEEE Intern. Conf. on Image Processing (ICIP'2008)*, pages 1820–1823, 2008.

263. A. El-Baz, M. F. Casanova, G. Gimel'farb, M. Mott, and A. E. Switala. Autism diagnostics by 3D texture analysis of cerebral white matter gyrifications. In *Proc. Intern. Conf. on Medical Image Computing and Computer-Assisted Intervention (MICCAI'2007)*, pages 882–890. Springer, 2007.
264. A. El-Baz, M. F. Casanova, G. Gimel'farb, M. Mott, and A. E. Switala. A new image analysis approach for automatic classification of autistic brains. In *Proc. IEEE Intern. Symp. on Biomedical Imaging: From Nano to Macro (ISBI'2007)*, pages 352–355. IEEE Press, 2007.
265. A. El-Baz, A. A. Farag, G. L. Gimel'farb, M. A. El-Ghar, and T. Eldiasty. Probabilistic modeling of blood vessels for segmenting MRA images. In *Proc. 18th IAPR Intern. Conf. on Pattern Recognition (ICPR'06)*, volume 3, pages 917–920, Hong Kong, China, Aug. 20–24, 2006. IEEE Press.
266. A. El-Baz, A. A. Farag, G. Gimel'farb, M. A. El-Ghar, and T. Eldiasty. A new adaptive probabilistic model of blood vessels for segmenting MRA images. In *Proc. Intern Conf. on Medical Image Computing and Computer-Assisted Intervention (MICCAI 2006)*, volume 4191, pages 799–806. Springer, 2006.
267. A. El-Baz, A. Farag, G. Gimelfarb, and S. Hushek. Automatic cerebrovascular segmentation by accurate probabilistic modeling of tof-mra images. In *Medical Image Computing and Computer-Assisted Intervention (MICCAI'05)*, pages 34–42.Springer, 2005.
268. A. El-Baz, A. Elnakib, M. F. Casanova, G. Gimel'farb, A. E. Switala, D. Jordan, and S. Rainey. Accurate automated detection of autism related Corpus Callosum abnormalities. *J. Medical Systems*, 35(5):929–939, 2011
269. A. El-Baz, M. Casanova, G. Gimel'farb, M. Mott, A. Switala, E. V. Bogaert, and R. McCracken. Dyslexia diagnostics by 3D texture analysis of cerebral white matter gyrifications. In *Proc. IAPR Intern. Conf. on Pattern Recognition (ICPR'2008)*,pages 1–4, 2008.
270. A. El-Baz, M. Casanova, G. Gimel'farb, M. Mott, and A. Switala. A new imagebased diagnostic framework for early diagnosis of dyslexic brains. In *Proc. 22nd Intern. Congress and Exhibition on Computer Assisted Radiology and Surgery (CARS'08)*, pages 46–47, Barcelona, Spain, June 25–28, 2008.
271. A. Elnakib, A. El-Baz, M. F. Casanova, G. Gimel'farb, and A. E. Switala. Imagebased detection of corpus callosum variability for more accurate discrimination between dyslexic and normal brains. In *Proc. IEEE Intern. Symp. on Biomedical Imaging: From Nano to Macro (ISBI'2010)*, pages 109–112, 2010.
272. A. Elnakib, A. El-Baz, M. F. Casanova, G. Gimel'farb, and A. E. Switala. Imagebased detection of Corpus Callosum variability for more accurate discrimination between autistic and normal brains. In *Proc. IEEE Intern. Conf. on Image Processing (ICIP2010)*, pages 4337–4340, 2010.
273. A. Elnakib, A. El-Baz, M. F. Casanova, and A. E. Switala. Dyslexia diagnostics by centerline-based shape analysis of the corpus callosum. In *Proc. IAPR Intern. Conf. on Pattern Recognition (ICPR'2010)*, pages 261–264, 2010.
274. A. Elnakib, M. F. Casanova, G. Gimel'farb, A. E. Switala, and A. El-Baz. Dyslexia diagnostics by 3-D shape analysis of the corpus callosum. *IEEE Trans. Information Technology in Biomedicine*, 16(4):700–708, 2012.

275. A. Elnakib, M. F. Casanova, G. Gimel'farb, A. E. Switala, and A. El-Baz. Autism diagnostics by centerline-based shape analysis of the Corpus Callosum. In *Proc. IEEE Intern. Symp. on Biomedical Imaging: From Nano to Macro (ISBI'2011)*, pages 1843–1846, 2011.
276. A. Elnakib, M. F. Casanova, G. Gimel'farb, and A. El-Baz. Autism diagnostics by 3D shape analysis of the Corpus Callosum. In K. Suzuki, editor, *Machine Learning in Computer-aided Diagnosis: Medical Imaging Intelligence and Analysis*, chapter 15, pages 315–335. IGI Global, 2012.
277. R. Fahmi, A. El-Baz, H. Hassan, A. A. Farag, and M. F. Casanova. Structural MRIbased discrimination between autistic and typically developing brain. In *Proc. Computer Assisted Radiology and Surgery (CARS'2007)*, pages 24–26, 2007.
278. M. Mostapha, A. Alansary, A. Soliman, F. Khalifa, M. Nitzken, R. Khodeir, M. F. Casanova, and A. El-Baz. Atlas-based approach for the segmentation of infant DTI MR brain images. In *Proc. 11th IEEE Intern. Symp. on Biomedical Imaging (ISBI 2014)*, pages 1255–1258. IEEE Press, 2014.
279. M. Mostapha, A. Soliman, F. Khalifa, A. Elnakib, A. Alansary, M. Nitzken, M. F. Casanova, and A. El-Baz. A statistical framework for the classification of infant DT images. In *Proc. 21st IEEE Intern. Conf. on Image Processing (ICIP 2014)*, pages 2222–2226, Paris, France, Oct. 27–30, 2014. IEEE Press.
280. M. Nitzken, M. F. Casanova, G. Gimel'farb, A. Elnakib, F. Khalifa, A. Switala, and A. El-Baz. 3D shape analysis of the brain cortex with application to dyslexia. In *Proc. 18th IEEE Intern. Conf. on Image Processing (ICIP 2011)*, pages 2657–2660,Brussels, Belgium, Sept. 11–14, 2011. IEEE Press.
281. M. Nitzken, M. F. Casanova, G. Gimel'farb, F. Khalifa, A. Elnakib, A. E. Switala, and A. El-Baz. 3D shape analysis of the brain cortex with application to autism. In *Proc. 8th IEEE Intern. Symp. on Biomedical Imaging: From Nano to Macro (ISBI 2011)*, pages 1847–1850, Chicago, IL, USA, March 30 – April 2, 2011. IEEE Press.
282. M. Nitzken, M. F. Casanova, F. Khalifa, G. Sokhadze, and A. El-Baz. Shape-based detection of cortex variability for more accurate discrimination between autistic and normal brains. In A. El-Baz., R. Acharya, A. Laine, and J. Suri, editors, *Handbook of Multi-Modality State-of-the-Art Medical Image Segmentation and Registration Methodologies*, volume 2, chapter 7, pages 161–185. Springer, New York, 2011.
283. M. J. Nitzken, M. F. Casanova, and A. El-Baz. SPHARM analysis of the brain cortex for diagnosing dyslexia. In *Proc. IEEE 11th Intern. Symp. on Biomedical Imaging (ISBI 2014)*, Beijing, China, April 29 – May 2, 2014.
284. M. J. Nitzken, M. F. Casanova, G. Gimelfarb, T. Inanc, J. M. Zurada, and A. El-Baz. Shape analysis of the human brain: A brief survey. *IEEE J. Biomedical and Health Informatics*, 18(4):1337–1354, 2014.
285. El-Baz, Ayman, Georgy Gimel'farb, and Jasjit S. Suri. Stochastic modeling for medical image analysis. CRC Press, 2015.
286. Ismail, Marwa Maher Tawfik, "A CAD system for early diagnosis of autism using different imaging modalities." (2016). Electronic Theses and Dissertations. Paper 2599.

CURRICULUM VITA

NAME: Elizabeth Marie Hollis

ADDRESS: 6980 Big Bend Rd
Battletown, KY 40104

DOB: New Albany, Indiana – September 25, 1991

EDUCATION
& TRAINING:

B.A. Chemistry
Hanover College
2010-2014

M.S. Pharmacology and Toxicology
University of Louisville
2015-2017

AWARDS Hanvoer College President Honors the Arts: For Work In Costume Design
2014

Meade County High School Departmental Scince Award
2010

PROFESSIONAL SOCIETIES: Alpha Delta Pi: Historian of Phi Chapter for 2 terms

PUBICATIONS:

M. Shehata, F. Khalifa, Elizabeth Hollis, A. Soliman, E. Hosseini-Asl, M.A. El-Baz, A.C. Dwyer, A. El-Baz, and R. Keynton, "A New Non-Invasive Approach for Early Classification of Renal Rejection Types Using Diffusion-Weighted MRI" *In: Proc. IEEE International Conference on Image Processing: (ICIP'16),* Phoenix, Arizona, USA, September 25-28, 2016

E.Hollis, M. Shehata, F. Khalifa, M Abou El-Ghar, T. El-Diasty, El-Baz Ayman., "Towards non-invasive diagnostic techniques for early detection of acute renal transplant reection: A review, : *Egyption Journal of*

Radiology Nuclear Medicine, http://dx.doi.org/10.106/j.ejrnm.2016.11.005,2016.

Hollis, M. Shehata, M. Abou El-Ghar, M. Ghazal, T. Eldiasty, M. Merchant, A. Switala, and A. El-Baz, " Statistical Analysis of ADCs and Clinical Biomarkers in., "Investigating Possible Significant Differences Between Rejection and Non-Rejected RenalAllografts Using Diffusion-Weighted MRI : *British Journal of Radiology*, *(*Under review*)*

ABSTRACT:

Elizabeth Hollis, Mohamed Shehata, Fahmi Khalifa, Andy Switala, Mohamed Abou El-Ghar, Amy Dwyer, and Ayman El-Baz; "Investigating Possible Significant Differences between Rejected and NonRejected Allografts Using Diffusion-Weighted MRI". 2nd Annual Kidney Congress; Philadelphia, Pennsylvania; August 28-30, 2017."